Università degli studi di Trieste
Facoltà di Scienze Matematiche, Fisiche e Naturali
Dottorato di Ricerca in Fisica - XX Ciclo

Evolution of chemical abundances in active and quiescent spiral bulges

Settore scientifico-disciplinare: FIS/05 ASTRONOMIA E ASTROFISICA

Dottorando
Silvia Kuna Ballero

Coordinatore del Collegio dei Docenti
Prof. Gaetano Senatore, Università di Trieste

Tutore
Prof. Francesca Matteucci, Università di Trieste

Relatore
Prof. Francesca Matteucci, Università di Trieste

A.A. 2006/2007

This is dedicated to Dero

Contents

1 Introduction **1**

1.1 Galactic bulges: definition and properties 1

1.2 Scenarios of bulge formation and evolution 5

1.3 Bulges and Seyfert galaxies 10

1.4 Aims and plan of the thesis 12

2 The chemical evolution model for bulges **15**

2.1 The stellar birthrate 15

2.2 The equation of chemical evolution 16

2.3 The starting model 17

2.4 The new chemical evolution model 19

2.4.1 Implementation of the wind 21

3 Formation and evolution of the Milky Way bulge **23**

3.1 Model parameters 23

3.2 Observations of abundances in the Galactic bulge 24

3.2.1 Metallicity distribution 25

3.2.2 α-elements and carbon 27

3.2.3 Nitrogen 29

3.3 Results 33

3.3.1 The supernova rates 33

3.3.2 The metallicity distribution of the bulge giants 35

3.3.3 Evolution of the abundance ratios 40

3.4 Summary and conclusions 51

4 O and Mg evolution in the Galactic bulge and solar neighbourhood **55**

4.1 Mass loss and stellar yields 55

4.2 Evidence for metallicity-dependent O yields . . . 57
4.3 The chemical evolution models . . . 61
4.4 Results . . . 62
4.4.1 [O/Mg] *vs.* [O,Mg/H] . . . 62
4.4.2 [O/Fe] *vs.* [Fe/H] . . . 67
4.5 Summary and conclusions . . . 69

5 Universal or environment-dependent IMF? 71
5.1 The issue of the IMF . . . 71
5.2 Model results . . . 73
5.2.1 Constraining yields for very massive stars . . . 75
5.2.2 The effect of other evolutionary parameters . . . 78
5.2.3 Results for M31 . . . 78
5.2.4 Discussion . . . 80
5.3 Summary and conclusions . . . 81

6 Chemical evolution of Seyfert galaxies and bulge photometry 83
6.1 The co-evolution of AGNs and spheroids . . . 83
6.2 Observations of abundances in QSOs and Seyfert galaxies . . . 85
6.3 Building models for other bulges . . . 88
6.4 Photometry of bulges . . . 89
6.5 Energetics of the interstellar medium . . . 90
6.5.1 The binding energy . . . 90
6.5.2 Black hole accretion and feedback . . . 94
6.6 Results . . . 95
6.6.1 Mass loss and energetics . . . 95
6.6.2 Star formation rate . . . 98
6.6.3 Black hole masses and luminosities . . . 100
6.6.4 Metallicity and elemental abundances . . . 104
6.6.5 Bulge colours and colour-magnitude relation . . . 114
6.7 Summary and conclusions . . . 120

7 Concluding remarks 123
7.1 Summary . . . 123
7.2 Future perspectives . . . 126

A The disk gravitational energy contributions **127**

Bibliography **129**

Acknowledgements **147**

Chapter 1

Introduction

"In the beginning the Universe was created. This has made a lot of people very angry and been widely regarded as a bad move."
(Douglas Adams)

1.1 Galactic bulges: definition and properties

There is not a general consensus on what is meant for a bulge in astronomy. According to the most general definition, any spheroidal stellar system is a bulge, i.e. this definition includes both elliptical galaxies and the spheroidal stellar components located at the centre of spiral galaxies. To further confuse the reader, the latter show a bimodality of properties, therefore spiral bulges are divided accordingly into *true* (or *classical*) *bulges* and *pseudobulges* (Kormendy & Kennicutt 2004). These two subclasses have very different evolutionary histories. While the former are thought to form very rapidly and almost independently of the disk, the latter are most probably built slowly by disk material; this is suggested by the similarity of their features to those of the disk, contrarily to classical bulges. Our work will only concern classical bulges of spiral galaxies.

Spiral bulges usually possess metallicity[1], photometric and kinematic properties that separate them from all the other components (thin disk, thick disk and halo) of spirals, whereas they show a broad similarity to elliptical galaxies and among themselves. Their stellar angular momentum distribution clearly separates them from the disk components, which are fully rotationally supported, and suggests that the halo and bulge are kine-

[1]We define as metallicity Z the abundance fraction by mass of all the chemical species heavier than ^{4}He.

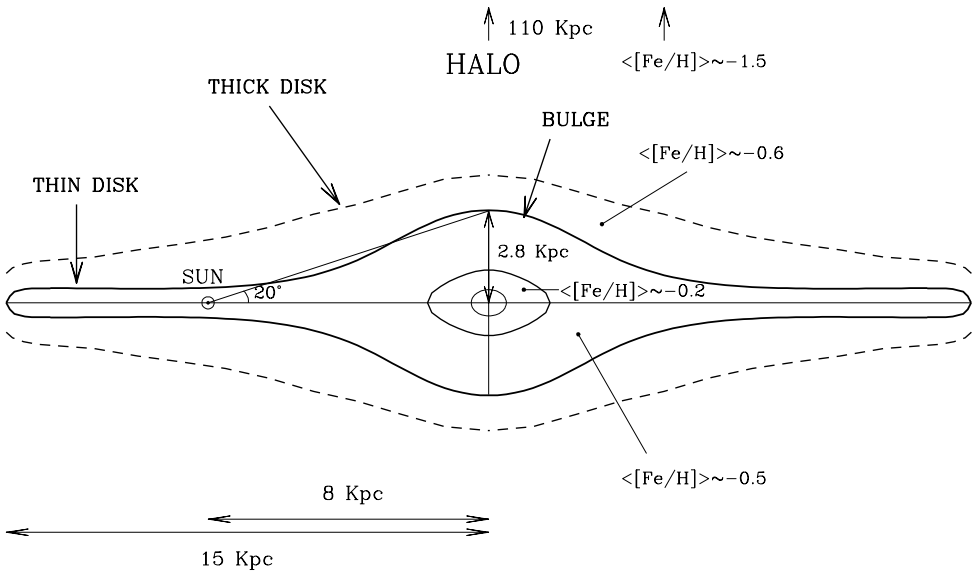

Figure 1.1: A sketch of the structure of the Milky Way: the stellar halo, bulge, thick and thin disk are indicated together with the mean metallicity of the stars in each galactic component. The galactocentric distance of the Sun and the dimension of the optical disk are shown at the bottom.

matically linked as different parts of the same spheroid. Whitford (1978) and Maraston et al. (2003) found a significant similarity of the integrated light of the Galactic bulge to that of elliptical galaxies and other spiral bulges. Moreover, bulges and ellipticals are located in the same region of the Fundamental Plane (Falcon-Barroso et al. 2002), i.e. a plane in the space defined by the effective radius R_e, the mean surface brightness within R_e (Σ_e) and the central velocity dispersion σ (Djorgovski & Davies 1987; Bender et al. 1992; Burstein et al. 1997). The scaling relation represented by the Fundamental Plane is very tight. The small scatter shown by ellipticals around the Fundamental Plane is interpreted as an evidence of a highly synchronised formation of this type of galaxies, and is naturally explained by a scenario where ellipticals are formed at high redshift. Given these analogies, this is a first evidence that bulges are old systems which formed on a quite short timescale.

More direct evidence of the age of bulges comes from photometrical studies of our own bulge. The presence of RR Lyrae variables (Lee 1992; Alard 1996) shows that there is at least one component of age comparable to that of the oldest known stars (i.e. those in the globular clusters of the halo). Terndrup (1988) first argued for a

globular cluster-like nature of the bulge population. From colour-magnitude diagrams of M giants, he derived old ages ($\tau_{turn-off} = 11 \pm 3$ Gyr) and concluded that bulge stars formed almost simultaneously and that there has not been star formation for the last 5 Gyrs. From the analysis of the bulge horizontal branch stars, Lee (1992) found that the oldest stars in the bulge are older than the oldest halo stars by ~ 1 Gyr, and an analogous conclusion was reached also by Ortolani et al. (1995). Recently, Kuijken & Rich (2002) showed that when the bulge field is decontaminated from disk foreground stars by proper motion cleaning or statistical subtraction, the remaining population of stars is indistinguishable from that of an old metal rich globular cluster.

This seems to be at variance with the discovery of a sub-population confined to the most central regions of the bulge, whose age is estimated to be a few Gyrs (e.g. Harmon & Gilmore 1988, Holtzman et al. 1993; van Loon et al. 2003). However, we must consider that bulges are not isolated systems, and that many of them are influenced by the presence of a bar which can drive disk gas to the centre and give rise to secondary episodes of star formation extending out to a few parsecs from the centre. In any case, the younger population will contribute a minor fraction of the bulge stellar population ($\sim 10 - 20\%$).

Chemical abundances provide an independent way to estimate the formation history of bulges. Before discussing the abundances in the gas or in stars, we define the bracket notation for abundance ratios. If A and B are two chemical elements and X_A, X_B their respective abundance fractions by mass, then

$$[A/B] = \log(X_A/X_B)_{gas,star} - \log(X_A/X_B)_{\odot} \tag{1.1}$$

where the subscript $\odot$ refers to the Sun. These abundances are measured in units of dex (decimal exponential).

Deriving accurate and detailed chemical abundances for stars in the Galactic bulge is not an easy task, since the observations along the line-of-sight to the bulge are hampered by dust extinction and reddening which, on the Galactic plane, are very large. However, it is possible to perform successful observations in some low-extinction windows, among which the so-called Baade's Window, a region with $l = 1^{\circ}$, $b = -4^{\circ}$.

By observing K giants in the Baade's window with low-resolution spectroscopy, Rich (1988) measured a wide range of [Fe/H] (from -1.5 to $+1.0$ dex) with a mean value of $+0.3$ dex. Later, McWilliam & Rich (1994) re-calibrated these data with higher-resolution measurements and found values for [Fe/H] systematically lower by $0.25 - 0.3$ dex. This result was confirmed by Sadler et al. (1996) for a sample of M and K giants

in the bulge, and more recently by Ramírez et al. (2000). The overestimation of Rich (1988) was partly due to blending of lines, and partly to the assumption [Mg/Fe] = 0.0 employed to derive [Fe/H] values from the magnesium index M_{g_2}, whereas the ratios of α-elements (O, Ne, Mg, Si, S, Ca, Ti) over Fe in the bulge are enhanced with respect to the sun. The α-enhancement is a signature of fast star formation history, since α-elements are produced by Type II supernovae, contrarily to Fe, whose main contributors are Type Ia supernovae. The difference in the timescales for the occurrence of Type Ia and Type II supernovae produces a time delay in the Fe production relative to the α-elements (*time delay model*: Tinsley 1979; Greggio & Renzini 1983; Matteucci & Greggio 1986). McWilliam & Rich (1994) and Sadler et al. (1996) found a certain degree of α-enhancement, but the situation remained unclear until Barbuy (1999) showed overabundances for most of the α-elements observed in stars belonging to the bulge globular clusters NGC 6553 and NGC 6528. Subsequent high-resolution ($R \sim 45000 - 60000$) spectroscopic works, both in in low-extinction optical windows (e.g. McWilliam & Rich 2004; Zoccali et al. 2006; Lecureur et al. 2007; Fulbright et al. 2007), or in the infrared (Origlia et al. 2005; Rich & Origlia 2005) firmly established this trend for α-elements. These recent data were the basis for the development of our bulge chemical evolution model and will be extensively discussed in §3.2.

Another way to obtain an estimate of the metallicity distribution of bulge giants other than spectroscopy is by means of photometry, and namely by the analysis of specific features of the colour-magnitude diagram. The mean de-reddened colour and colour dispersion of the red giant branch can be matched with empirical red giant branch templates to determine the global metal abundance and its dispersion, and to set constraints on the bulge age as well. Thus, Zoccali et al. (2003) essentially confirmed a wide range in [Fe/H] and an age of $\sim$ 10 Gyr for the stellar population residing in the bulge, whereas Sarajedini & Jablonka (2005) suggest that, since the differences in the metallicity distributions of the Milky Way and M31 halos find no correspondence in those of their bulges, the bulk of the stars in the bulges of both galaxies must have been in place before any accretion event, that might have occurred in the halo, could have any influence on them. This conclusion supports a common scenario for the formation of bulges.

It is not clear whether there is a metallicity gradient in the Galactic bulge. Minniti et al. (1995) measured a gradient within the inner 2 kiloparsecs of the Galaxy, although the spread in metal abundances at any given galactocentric distance is large. If con-

firmed, the presence of a metallicity gradient together with a correlation between stellar abundances and kinematics would be a strong signature of a fast dissipative collapse, as opposed to dissipationless stellar merging or formation through inflow of material expelled from the disk.

1.2 Scenarios of bulge formation and evolution

The first modern model for the formation of the Milky Way was proposed by Eggen, Lynden-Bell & Sandage (1962). In their scenario, the halo and the bulge form through a rapid "monolithic" collapse within only 10^8 years, approximately 10^{10} years ago, when extended and nearly spherical protogalactic gas clouds cooled and condensed out of the dark matter halo. This collapse initiated the formation of the Galaxy as a whole. The lowest angular momentum gas fell into the centre and formed the bulge; fast star formation in an initial burst and subsequent enrichment can explain the bulge metallicity. The high angular momentum gas collapsed later and formed the disk. In this context, the bulge is essentially the oldest component of a spiral galaxy ("old-bulge" scenario), and is treated as a miniature elliptical. Eggen et al. (1962) also argued that the observed highly non-circular motions of halo stars can be understood only if the collapse was rapid and lasted no longer than 2×10^8 years.

As a cause of the rapid collapse in this simple scenario a correlation among metallicity, age and kinematics and a metallicity gradient in the halo is expected. When investigating the metallicity of globular clusters of the outer halo, Searle & Zinn (1978) did not find any significant gradient. Motivated through these observations, they proposed a more chaotic origin of the Galactic halo, in which the central regions form first. In their scenario, the outer halo is formed by inhomogeneous coalescence of transient extant protogalactic stellar systems during an extended period of time after the collapse of the central region is completed. Within this scenario, the bulge is again formed early in the history of the Galaxy. The idea of a bulge consisting of material coming from satellite galaxies was further adopted by Schweizer & Seitzer (1988) who observed sharped-edge ripples in disk galaxies and concluded that they consisted of extraneous matter acquired through mass transfer from neighbour galaxies. They also suggested that such intruders would end up in the bulge, thus giving rise to episodic growth. More recent models of bulge formation were developed who assumed accretion of stellar satellites (e.g. Aguerri et al. 2001). However, Wyse (1998) showed that the metallicity

distribution in our Galaxy is not consistent with a picture where the bulge is formed via accretion of satellites. There is now additional evidence that the bulge is not formed by satellites similar to those observed at the present day in the halos of the Milky Way and M31: McWilliam et al. (2003) find a systematically decreased abundance of Mn in the Galactic bulge, compared to stars in the Sgr dwarf spheroidal. So, even though Sgr does in principle reach high metallicities, its detailed chemistry is different (see also Venn et al. 2004, Monaco et al. 2007).

In the framework of the Eggen, Lynden-Bell and Sandage (1962) scenario, early numerical one-zone, closed-box[2] models for ellipticals, adopting the instantaneous recycling approximation[3] (Arimoto & Yoshii 1986), were able to produce the observed wide abundance range. The incorporation of yields from Type Ia and Type II supernovae and detailed stellar lifetimes into these models allowed to make more extensive predictions. In this way, Matteucci & Brocato (1990) predicted that the [α/Fe] ratio for some elements (O, Si and Mg) should be supersolar over almost the whole metallicity range, in analogy with the halo stars, as a consequence of assuming a fast bulge evolution which involved rapid gas enrichment in Fe mainly by Type II supernovae. At that time, no data were available for detailed chemical abundances; the predictions of Matteucci & Brocato (1990) were later confirmed for a few α-elements (Mg, Ti) by the observations of McWilliam & Rich (1994), whereas for other elements (e.g. O, Ca, Si) the observed trend looked different. Other discrepancies regarding the Mg overabundance came from the observations of Sadler et al. (1996).

In order to better assess these points, Matteucci, Romano & Molaro (1999) modelled the behaviour of a larger set of abundance ratios, by means of a detailed chemical evolution model whose parameters were calibrated so that the metallicity distribution observed by McWilliam & Rich (1994) could be fitted. They predicted the evolution of several abundance ratios that were meant to be confirmed or disproved by subsequent observations, namely that α-elements should in general be overabundant with respect to Fe, but some (e.g. Si, Ca) less than others (e.g. O, Mg), due to the fact that they are partly synthesised in Type Ia supernovae, and that the [^{12}C/Fe] ratio should be solar at

[2]In a closed-box galactic model, all the gas is present at the beginning; no infall or outflow occur.

[3]The instantaneous recycling approximation consists in the assumptions that all stars with $M < 1M_{\odot}$ live forever, whereas all stars with $M > 1M_{\odot}$ die immediately. This approximation allows to neglect stellar lifetimes and simplify the equations of chemical evolution. However, while the first assumption is reasonable, the second one leads to model incorrectly the evolution of elements which contribute to the enrichment of the interstellar medium at later times (e.g. Fe).

all metallicities. They concluded that an initial mass function flatter ($x = 1.1 - 1.35$; see §2.1) than that of the solar neighbourhood is needed for the metallicity distribution of McWilliam & Rich (1994) to be reproduced, and that a much faster evolution than in the solar neighbourhood and faster than in the halo (see also Renzini, 1993) is necessary as well.

Mollá et al. (2000) proposed a multiphase model in the context of the dissipative collapse scenario of the Eggen, Lynden-Bell & Sandage (1962) picture. They suppose that the bulge formation occurred in two main infall episodes, the first from the halo to the bulge, on a timescale $\tau_H = 0.7$ Gyr (longer than that proposed by Matteucci et al. 1999), and the second from the bulge to a so-called core population in the very nuclear region of the Galaxy, on a timescale $\tau_B \gg \tau_H$. The three zones (halo, bulge, core) interact via supernova winds and gas infall. They concluded that there is no need for accretion of external material to reproduce the main properties of bulges and that the analogy to ellipticals is not justified. Because of their rather long timescale for the bulge formation, these authors did not predict a noticeable difference in the trend of the [α/Fe] ratios but rather suggested that they behave more likely as in the solar neighbourhood (contrary to the first indications of α-enhancement by McWilliam & Rich 1994).

Ferreras, Wyse & Silk (2003) tried to fit the stellar metallicity distributions of K giants measured by Sadler et al. (1996), Ibata & Gilmore (1995) and Zoccali et al. (2003), which are pertinent to different bulge fields, by means of a model of star formation and chemical evolution. Their model assumes a Schmidt law similar to that of the disk, and simple recipes with a few parameters controlling infall and continuous outflow of gas. They explored a large range in the parameter space and conclude that timescales longer than ~ 1 Gyr must be excluded at the 90% confidence level, regardless of which field is being considered.

A more recent model was proposed by Costa et al. (2005), in which the best fit to the observations relative to planetary nebulae is achieved by means of a double infall model. An initial fast (0.1 Gyr) collapse of primordial gas is followed by a supernova-driven mass loss and then by a second, slower (2 Gyr) infall episode, enriched by the material ejected by the bulge during the first collapse. Costa et al. (2005) claim that the mass loss is necessary to reproduce the abundance distribution observed in planetary nebulae, and because the predicted abundances would otherwise be higher than observed. With their model, they are able to reproduce the trend of [O/Fe] abundance ratio observed by Pompéia et al. (2003) and the data of nitrogen versus oxygen abundance observed

by Escudero & Costa (2001) and Escudero et al. (2004). It must be noted however that Pompéia et al. (2003) obtained abundances for "bulge-like" dwarf stars. This "bulge-like" population consists of old ($\sim 10 - 11$ Gyr), metal-rich nearby dwarfs with kinematics and metallicity suggesting an inner disk or bulge origin and a mechanism of radial migration, perhaps caused by the action of a Galactic bar. However, the birthplace of these stars is not certain (and in the discussion of our model we shall omit these data from our model, and only consider those stars for which membership in the present day bulge is secure). Moreover, as we shall see, the use of nitrogen abundance from planetary nebulae is questionable, since N is known to be also synthesised by their progenitors and therefore it might not be the pristine one.

A short formation timescale for the bulge is also suggested on theoretical grounds by Elmegreen (1999), who argued that the potential well of the Galactic bulge is too deep to allow self-regulation and that most of the gas must have been converted into stars within a few dynamical timescales.

Not all models of the bulge support the conclusions of a fast formation and evolution. In the hierarchical clustering scenario (Kauffmann 1996) the bulges form through violent relaxation and destruction of disks in major mergers. The stars of the destroyed disk build the bulge, and subsequently the disk has to be rebuilt. This implies that late type spirals should have older bulges than early types, since the build-up of a large disk needs time during which the galaxy is allowed to evolve undisturbed. This is not confirmed by observations, as well as the high metallicity and the narrow age distribution observed in bulges of local spirals are not compatible with a merger origin of these objects (see Wyse 1999, and references therein).

Samland et al. (1997) developed a self-consistent chemo-dynamical model for the evolution of the Milky Way components starting from a rotating protogalactic gas cloud in virial equilibrium, that collapses owing to dissipative cloud-cloud collisions. They found that self-regulation due to a bursting star formation and subsequent injection of energy from Type II supernovae lead to the development of "contrary flows", i.e. alternate collapse and outflow episodes in the bulge. This causes a prolonged star formation episode lasting over $\sim 4 \times 10^9$ yr. They included stellar nucleosynthesis of O, N and Fe, but claim that gas outflows prevent any clear correlation between local star formation rate and chemical enrichment. With their model, they could reproduce the oxygen gradient of H II regions in the equatorial plane of the Galactic disk and the metallicity distribution of K giants in the bulge (Rich 1988), field stars in the halo and G

dwarfs in the disk, but they did not make predictions about the evolution of abundance ratios in the bulge.

Finally, there is another class of scenarios for the bulge formation, which investigate the outcome of the secular evolution of disks. In this context, bulges are assumed to be the result of instabilities that either drive gas to the galactic centre, e.g. through the action of a stellar bar or due to gravitational instabilities of the spiral structure, or lead to the fragmentation and partial disruption of the internal disk with subsequent rebuildup. Indications of bulges unaccounted for by the "old-bulge" scenario include: the existence of box-shaped or peanut-shaped bulges and triaxiality (Bertola et al. 1991); observations of bulges with velocity dispersions (Kormendy 1982) and colours (Balcells & Peletier 1994) close to those of disks; and deviations from the de Vaucouleur's $r^{1/4}$ profile (Wainscoat et al. 1989).

The idea of secular evolution developed in the 80's, and was prompted by N-body simulations; Combes & Sanders (1981) first demonstrated that the vertical thickening of a stellar bar can produce a bulge-like object in the centre of the disk. This conclusion was later confirmed and refined by Pfenniger & Norman (1990) and Hasan et al. (1993): a barred potential in a flat disk can lead to heating of the stellar component in the centre, with the formation of a bulge-like structure. However, the bulges produced by means of this mechanism are small compared to the disk, and multiple minor accretion events have to be invoked to account for the big bulges of early-type spirals. Other examples of models assuming secular evolution of disks are those of Friedly & Benz (1993, 1995), where dissipation can lead to the destruction of the stellar bar producing a bulge component. The gravitational torque induced by the bar causes an angular momentum redistribution in the gas phase leading to inflow to the centre. The fuelling results in an intermediate starburst episode of duration $\approx 10^8$ years. The central mass accumulation then weakens or destroys the bar, possibly leading to a bulge (Norman et al. 1996). On the other side, Noguchi (1999) proposed a model of unstable disk which forms clumps. These clumps then merge, fall to the centre and build a massive bulge.

Immeli et al. (2004) investigated the rôle of cloud dissipation in the formation and dynamical evolution of star-forming gas-rich disks by means of a 3-D chemo-dynamical model including a dark matter halo, stars and a two-phase interstellar medium with stellar feedback. They found that the galaxy evolution proceeds very differently depending on whether the gas disk or the stellar disk first becomes unstable. This in turn depends on how efficiently the cold cloud medium can dissipate its kinetic energy. If

the cold gas cools efficiently and drives the instability, the disk fragments and develops a number of massive clumps of gas and stars which spiral to the centre, where they merge, thus forming the bulge at relatively early times. A starburst takes place which gives rise to enhanced [α/Fe] values. This picture corresponds to the model of Noguchi (1999). On the other hand, if dissipation occurs at a lower rate, stars form in the disk in a more quiescent fashion and the instability occurs at a much later time, when the stellar surface density has become sufficiently high. A stellar bar forms which funnels gas into the centre, then evolves into a bulge at late times. The stars of a bulge formed in this way keep trace of a more extended star formation history and thus show lower [α/Fe]. This scenario resembles those of Combes & Sanders (1981) and Pfenniger & Norman (1990), and seems to be excluded by the recent measurements of Zoccali et al. (2006) and Lecureur et al. (2007).

We do not exclude that such mechanisms actually occur; however, in our view, structures fully resulting from the secular evolution of disks must be considered as pseudo-bulges and not classical bulges. Secular processes can also account for the minority of young stars found in the very centre of our galaxy; but the chemistry and stellar ages require that the bulk of bulge stars formed early and self-enriched rapidly (see also Renzini 1999).

1.3 Bulges and Seyfert galaxies

Active Galactic Nuclei (AGNs) are a class of astrophysical objects of peculiar interest. They produce extremely high luminosities (up to 10^4 times the luminosity of a typical galaxy), and their continuum emission can emerge over up to 13 orders of magnitude, i.e. they have a rather flat broadband continuum spectrum. So, contrarily to normal galaxies, for active galaxies (i.e. the galaxies which host an AGN) the emitted radiation is not approximately the sum of the energy radiated by the stars which form them; there must be a non-thermal component. Many of them show strong and fast variability, which points to an energy source confined in tiny volumes ($\ll 1$ pc^3). The most popular scenario to explain these features is accretion onto a relativistically deep gravitational potential; the characteristics of AGN emission make black holes the most probable candidate (Salpeter 1964). This hypothesis is supported by the detection of supermassive black holes at the centre of the majority of spheroids (ellipticals and bulges), with masses $M_{BH} \gtrsim 10^6 M_\odot$

Because their high luminosities and distinctive spectra make them relatively easy to pick out, AGNs are disproportionately represented among the known high-redshift sources. Most of them show very prominent emission lines; this makes AGN spectra stand in great contrast to the spectra of most stars and galaxies, where lines are generally relatively weak and predominantly in absorption. The emission lines that we see show a broad similarity among different objects (mainly Lyα, Balmer lines, the C IV 1549 doublet, [O III] 5007, the Fe Kα X-ray line and others). However, there is a split in the line width distribution: In some objects many lines have broad wings extending out several thousand km/s (broad emission lines), whereas in others the line width never exceeds a few hundred km/s (narrow emission lines). The forbidden lines are only found within the latter. The mechanism which produces emission lines is photoionization by the AGN continuum, and the sharp bimodality of emission lines indicates the existence of two distinct regions with specific cloud properties. The broad line region basically consists of clumps of gas with density higher than the environmental medium, whose distance from the ionising source ranges from $\sim$0.01 to a few pc; their line width is mainly ascribed to orbital motions. The narrow line region is instead a lower-density medium located much farther out (several hundred pc).

It is also apparent that AGNs often have absorption features which in general are much narrower than the emission lines. While broad absorption lines are strongly associated to the nuclear region and are thought to be produced by resonance line scattering in outflowing gas, many of the narrow absorption lines arise from material unassociated with the AGN, and which lies along the line of sight. However, the detection of intrinsic narrow absorption lines can be particularly helpful to infer AGN chemical abundances, since the atomic physics of absorption lines are much simpler than emission lines, and because the reduced blending allows to resolve correctly a number of features which would otherwise be mixed up.

Since subgroups of AGNs share common properties, they were divided into several classes (Seyfert galaxies, quasars, radio galaxies, LINERs, blazars), although sometimes the taxonomy is rather fuzzy and the nomenclature is not properly used; therefore, we need to define the class of objects we are dealing with, i.e. Seyfert galaxies.

Seyfert galaxies are named after the astronomer Carl Keenan Seyfert, who identified and described these objects in the 1940s (Seyfert 1943). They are the low-luminosity counterpart of AGNs, with a visual magnitude $M_B > -21.5$ for the active nucleus as a general criterion established by Schmidt & Green (1983) to distinguish them from

quasars (QSOs). A Seyfert galaxy has a QSO nucleus but the host galaxy is clearly detectable. When observed directly, it looks like a normal distant spiral with a bright nucleus superimposed on it. The definition has evolved so that Seyfert galaxies are now identified spectroscopically by the presence of strong high-ionisation emission lines. Morphological studies indicate that most if not all Seyferts occur in spiral galaxies (Adams 1977, Yee 1983, MacKenty 1990, Ho et al. 1997). There are two subclasses of Seyfert galaxies: Type 1 Seyferts show the two superimposed sets of emission lines (broad and narrow emission lines), while Type 2 Seyferts only show the narrow emission lines in their spectra. According to the unification scheme (Antonucci 1993) Type 2 Seyferts are intrinsically Type 1 Seyferts where the broad line region, which lies close to the central ionising source, is hidden from our view by an obscuring medium, typically a torus of dust.

In our study, we make no difference between the two types of Seyfert galaxies, because we are investigating properties which should not depend on orientation effects (i.e. star formation rates, bolometric luminosities, bulge mass to black hole mass relation), and we assume that the interstellar medium in the spiral bulge which hosts the Seyfert nucleus is well mixed with both the broad and narrow line region, so that the chemical abundances measured in one of them should not differ much from the other. This assumption is observationally justified (see e.g. Hamann et al. 2004).

1.4 Aims and plan of the thesis

This thesis is aimed at investigating the formation and evolution of spiral bulges, and the rôle played by the supernova feedback, infall timescale, star formation efficiency, initial mass function and stellar nucleosynthesis in driving the evolution of a number of chemical abundance ratios and determining the metal content of the bulge interstellar medium and stars. In particular, we want to show that abundance ratios can provide an independent constraint for the bulge formation scenario, since they can show noticeable differences depending on the star formation history (Matteucci 2000).

Some fundamental concepts of chemical evolution, as well as the baseline model on which we implemented the novelties described in this thesis, are presented in Chapter 2. The features of the new model are discussed in the same Chapter.

The applications of the updated model on the chemical evolution of the Galactic bulge and of other quiescent bulges are presented in Chapters 3, 4 and 5. In Chapter 3,

the most recent measurements of abundances of Fe and α-elements in giant stars of the Galactic bulge are reviewed, and they are interpreted and employed to make constraints on the assembly and star formation history of the bulge. In Chapter 4, the issue of the [O/Mg] ratio in the solar neighbourhood and bulge was analysed, and the rôle of stellar mass loss in driving the evolution of abundance ratios involving oxygen was investigated. In Chapter 5, the hypothesis of a universal stellar initial mass function was tested against the recent observations of metallicity distributions in the bulges of the Milky Way and M31.

Chapter 6 introduces new modifications in the calculation of the Galactic potential and of the binding energy of the bulge gas, and the treatment of accretion and feedback from the central supermassive black hole was implemented in order to investigate the evolution of Seyfert galaxies. Bulge photometry was also calculated and compared to observations of local bulges.

Finally, in Chapter 7 the original results of this work are summarised, and a brief review of plans for future work is also presented.

Chapter 2

The chemical evolution model for bulges

2.1 The stellar birthrate

Many parameters are involved in the process of chemical evolution, such as the initial conditions, star formation, stellar evolution and nucleosynthesis and possible gas flows. We need to give a specification for each of them. In particular, it is necessary to define the *stellar birthrate function* $B(m,t)$, i.e. the number of stars formed in the mass interval m, $m+dm$ and in the time interval t, $t+dt$. Due to the lack of a clear knowledge of the star formation processes, the stellar birthrate is usually assumed to be the product of two independent functions:

$$B(m,t) = \varphi(m)\psi(t)dmdt \tag{2.1}$$

The function $\psi(t)$ is the star formation rate (SFR), and represents how many solar masses of interstellar medium are converted into stars per unit area per unit time; in other words, it describes the rate at which gas is turned into stars. Several parametrizations were proposed for this function, but they all share the dependence upon gas density. The most widely adopted formulation is the Schmidt (1959) law, which assumes that the SFR is proportional to some power of the gas density σ_{gas}, via a coefficient ν, called star formation efficiency, representing the inverse of the timescale of star formation:

$$\psi(t) = \nu\sigma^k_{gas}(t) \tag{2.2}$$

A more complex formulation was suggested by Dopita & Ryder (1994), to include a

dependence on the total surface mass density σ_{tot}, induced by the supernova feedback:

$$\psi(t) = \nu \sigma_{tot}^{k_1}(t) \sigma_{gas}^{k_2}(t) \tag{2.3}$$

The function $\varphi(m)$ is the initial mass function (IMF) which is the number of stars formed per unit mass. It is basically a probability distribution function, and it is usually normalized to unity:

$$\int_0^\infty m\varphi(m)dm = 1 \tag{2.4}$$

The most popular parametrization of the IMF is the power law (Salpeter 1955) with one slope over the whole mass range:

$$\varphi(m) = Am^{-(1+x)} \tag{2.5}$$

where A is fixed by the normalization condition (Eq. 2.4). However, multiple-slope IMFs are more suitable to describe the luminosity function of main-sequence stars in the solar neighbourhood. For example, the IMF commonly adopted for the solar neighbourhood is the one from Scalo (1986), with $x = 1.35$ for $M < 2M_\odot$ and $x = 1.7$ for $M \geq 2M_\odot$. A further flattening below $0.5 - 1M_\odot$ seems necessary to avoid overproducing brown dwarfs (see e.g. Kroupa et al. 1993).

2.2 The equation of chemical evolution

If we call G_i the gas mass surface density in the form of an element i and X_i the mass fraction of that element in the bulge interstellar medium, then the evolution of the elemental abundances is calculated by means of the equation of chemical evolution:

$$\begin{aligned}
\frac{dG_i(t)}{dt} &= -\psi(t)X_i(t) + X_{iF}\mathcal{F}(t) - X_i\mathcal{W}(t) + \\
&+ \int_{M_L}^{M_{B_m}} \psi(t-\tau_m)Q_{mij}X_j(t-\tau_m)\varphi(m)dm + \\
&+ \mathcal{A}\int_{M_{B_m}}^{M_{B_M}} \varphi(m)\left[\int_{\mu_{min}}^{0.5} f(\mu)\psi(t-\tau_m)Q_{mij}X_j(t-\tau_{m2})d\mu\right]dm + \\
&+ (1-\mathcal{A})\int_{M_{B_m}}^{M_{B_M}} \psi(t-\tau_m)Q_{mij}X_j(t-\tau_m)\varphi(m)dm + \\
&+ \int_{M_{B_M}}^{M_U} \psi(t-\tau_m)Q_{mij}X_j(t-\tau_m)\varphi(m)dm
\end{aligned} \tag{2.6}$$

In this equation, τ_m is the stellar lifetime of a star of mass m, X_j is the is the abundance of the element j originally present in the star and later transformed into the

element i and ejected, and Q_{mij} is the production matrix, whose elements represent the fraction of the stellar mass originally present in the form of the element j and eventually ejected by the star in the form of the element i. The quantity $Q_{mij}X_j(t-\tau_m)$ contains all the information about stellar nucleosynthesis. The total contribution of a star of mass m to the ejected mass of the element i is called the *stellar yield* and is given by:

$$(M_{ej})_i = \sum_j Q_{ij}(m)X_j m \tag{2.7}$$

The various terms at the right hand side of Eq. 2.6 represent the physical processes acting on the bulge interstellar medium. The first term stands for the SFR, which subtracts gas and turns it into stars; the second term represents the infall of gas that forms the bulge; the third term expresses the loss of gas to the intergalactic medium through a galactic wind; finally, the integrals represent the rate of restitution of matter from stars, and they include the contributions from low-mass stars, Type Ia and Type II supernovae.

The first, third and fourth integral represent the contribution of single stars in the mass range from $M_L = 0.1M_\odot$ to $M_U = 80M_\odot$, which end up as white dwarfs plus planetary nebula ($m < 8M_\odot$) or Type II supernovae ($m > 8M_\odot$). The second integral describes the contribution from the binary systems which have the right properties to generate a Type Ia supernova. The single-degenerate model, i.e. a C-O white dwarf plus a red giant companion (Nomoto et al. 1984), is assumed. The extremes of the integral represent the minimum (M_{B_m}) and maximum (M_{B_M}) mass for binary systems suitable to give rise to a Type Ia supernova. M_{B_M} is fixed by the requirement that each component cannot exceed $8M_\odot$, the maximum mass giving rise to a C-O white dwarf, thus $M_{B_M} = 16M_\odot$. The minimum mass M_{B_m} is more uncertain; as a general criterion, $M_{B_M} = 3M_\odot$ so that both the primary and the secondary star are massive enough to allow the white dwarf to reach the Chandrasekhar mass after accreting from the companion. The function $f(\mu)$ describes the distribution of mass ratio of the secondary (i.e. the less massive star) of the binary systems. $\mathcal{A}$ is a parameter representing the fraction of binary systems with properties suitable to give birth to a Type Ia supernova, and is fixed by reproducing the present-day Type Ia supernova rate.

2.3 The starting model

We adopted the one-zone model of Matteucci, Romano & Molaro (1999) as a starting point for our work. The main assumption is that the Galactic bulge formed with the fast

collapse of primordial gas (the same gas out of which the halo was formed) accumulating in the centre of our Galaxy. The ingredients of this model were the following:

- Instantaneous mixing approximation; the gas restored by dying stars is instantaneously mixed with the interstellar medium and is homogeneous at any time.

- SFR in the form of Eq. 2.3, with a star formation efficiency $\nu = 20$ Gyr^{-1} and exponents $k_1 = k - 1$, $k_2 = k$ and $k = 1.5$, which is the best value suggested for the solar neighbourhood by Chiappini, Matteucci & Gratton (1997).

- A gas collapse rate expressed as:

$$\mathcal{F}(t) \propto e^{-t/\tau} \tag{2.8}$$

  with $\tau = 0.1$ Gyr. The expression is normalized by the condition of reproducing the total surface mass density distribution in the bulge at the present time $t_G = 13.7$ Gyr.

- Various IMFs were tested in the model. Eventually, an index $x = 1.1$ was chosen to reproduce the metallicity distribution of McWilliam & Rich (1994).

- Stellar lifetimes from Maeder & Meynet (1989):

$$\tau_m(\mathrm{Gyr}) = \begin{cases} 10^{-0.6545\log m+1} & \text{for } m \leq 1.3\ M_\odot \\ 10^{-3.7\log m+1.35} & \text{for } 1.3 < m/M_\odot \leq 3 \\ 10^{-2.51\log m+0.77} & \text{for } 3 < m/M_\odot \leq 7 \\ 10^{-1.78\log m+0.17} & \text{for } 7 < m/M_\odot \leq 15 \\ 10^{-0.86\log m-0.94} & \text{for } 15 < m/M_\odot \leq 60 \\ 1.2\, m^{-1.85} + 0.003 & \text{for } m > 60\ M_\odot, \end{cases}$$

- Yields for low- and intermediate-mass stars ($0.1 \leq m/M_\odot < 8$), which produce ^{4}He, C, N and heavy elements with $A > 90$, are taken from the standard model of Van den Hoek & Groenewegen (1997), and are a function of initial stellar metallicity. For massive stars ($8 \leq m/M_\odot < 80$), which are the progenitors of Type II supernovae, the explosive nucleosynthesis of Woosley & Weaver (1995) was adopted. Type II supernovae mainly produce α-elements, some Fe and heavy elements with $A < 90$.

- The Type Ia supernova rate is calculated following Greggio & Renzini (1983) and Matteucci & Greggio (1986), and yields from Type Ia supernovae are taken from Thielemann et al. (1993). These supernovae are the main producers of Fe-peak elements and also contribute to some Si and Ca and, in minor amounts, C, Ne, Mg, S and Ni.

- The possibility of galactic winds was not taken into account since they seemed not to be appropriate for our Galaxy (Tosi et al. 1998), and because the potential well where the bulge lies was considered too deep to allow the development of a wind. The star formation was however assumed to stop at around 1 Gyr, as due to the low gas density.

2.4 The new chemical evolution model

Here we resume the main modifications implemented in the starting model in order to obtain a more updated chemical evolution model:

- For the SFR, we adopted a Schmidt (1959) law (Eq. 2.2) with $k = 1$. We chose this value to recover the star formation law of spheroids (e.g. Matteucci 1992). We also tested the value $k = 1.5$ and the results do not differ much. The main difference with the solar neighbourhood, as we shall see, resides in the higher ν parameter for the bulge.

- We did not adopt a threshold surface gas density for the onset of star formation such as that proposed by Kennicutt (1998) for the solar neighbourhood, since it is derived for self-regulated disks and there seems to be no reason for it to hold also in early galactic evolutionary conditions and in bulges. However, we also checked that adopting a threshold of 4 $M_{\odot}\mathrm{pc}^{-2}$ such as that proposed by Elmegreen (1999) does not change our results, since a wind (see below) develops much before such a low gas density is reached.

- Stellar lifetimes are taken into account following Kodama (1997):

$$\tau_m(\mathrm{Gyr}) = \begin{cases} 50 & \text{for } m \leq 0.56\ M_{\odot} \\ 10^{\left(0.334-\sqrt{1.790-0.2232\times(7.764-\log m)}\right)/0.1116} & \text{for } m \leq 6.6\ M_{\odot} \\ 1.2\, m^{-1.85} + 0.003 & \text{for } m > 6.6\ M_{\odot}, \end{cases}$$

This expression was found to be more suitable for environments with vigorous episodes of star formation, such as ellipticals.

- Detailed nucleosynthesis prescriptions for massive stars are taken from François et al. (2004), who made use of widely adopted stellar yields and compared the results obtained by including these yields in the model from Chiappini et al. (2003b) with the observational data, with the aim of constraining the stellar nucleosynthesis. In order to best fit the data in the solar neighbourhood, with the Woosley & Weaver (1995) yields, François et al. (2004) found that O yields should be adopted as a function of initial metallicity, Mg yields should be increased in stars with masses $11 - 20M_{\odot}$ and decreased in stars larger than $20M_{\odot}$, and that Si yields should be slightly increased in stars above $40M_{\odot}$; we use their constraints on the stellar nucleosynthesis to test whether the same prescriptions give good results for the Galactic bulge. Yields in the mass range $40-80M_{\odot}$ were not computed by Woosley and Weaver (1995), therefore one has to extrapolate them for chemical evolution purposes. We are aware that the extrapolation process is problematic. However, the behaviour above $40M_{\odot}$ is not clear, since a supernova explosion may occur with a large amount of fallback. Moreover, François et al. (2004) also showed that it is impossible to reproduce the observations at low metallicities in the solar neighbourhood if no contribution from stars in this mass range is considered.

- The Type Ia supernova rate was computed according to Greggio & Renzini (1983) and Matteucci & Recchi (2001). Yields are taken from Iwamoto et al. (1999) which is an updated version of model W7 (single degenerate) from Nomoto et al. (1984).

- Contrarily to Matteucci et al. (1999), we introduced the treatment of a supernova-driven galactic wind in analogy with ellipticals (e.g. Matteucci 1994). Although the occurrence of the wind did not seem suitable due to the depth of the potential well of the galactic disk and halo, as also theoretically sustained by Elmegreen (1999), this scenario needs to be tested quantitatively. To compute the gas binding energy $E_{b,gas}(t)$ and thermal energy $E_{th,SN}(t)$ we have followed Matteucci (1992). The details of this calculation are shown in the next subsection.

- We supposed, for a first investigation, that the feedback from the central supermassive black hole is negligible.

As a reference model, we adopt the one with the following reference parameters: $\nu = 20$ Gyr^{-1}, collapse timescale $\tau = 0.1$ Gyr and a two-slope IMF with index $x = 0.33$ for $M < 1M_{\odot}$ and $x = 0.95$ for $M > 1M_{\odot}$ (Matteucci & Tornambè 1987). The choice of such a flat IMF for the lowest-mass stars is motivated by the Zoccali et al. (2000) work, who measured the luminosity function of lower main-sequence bulge stars and derived the mass function, which was found to be consistent with a power-law of index 0.33 ± 0.07. The IMF index for intermediate-mass and massive stars is slightly flatter than that adopted by Matteucci et al. (1999) in order to reproduce the metallicity distribution of bulge stars from Zoccali et al. (2003) and Fulbright et al. (2006; see § 3.2.1 and § 3.3.2 for details) instead of that from McWilliam & Rich (1994).

2.4.1 Implementation of the wind

The binding energy of the bulge gas was calculated as if it was an elliptical, following Bertin, Saglia & Stiavelli (1992). They analysed the properties of a family of self-consistent spherical two-component models of elliptical galaxies, where the luminous mass is embedded in massive and diffuse dark halos, and in this context they computed the binding energy of the gas. A more refined treatment of the Galactic potential well would take into account the contribution of the disk as well; however, in the beginning we shall suppose that the main contributors to the bulge potential well are the bulge itself and the dark matter halo. The condition for the onset of the galactic wind is:

$$E_{th,SN}(t_{GW}) = E_{b,gas}(t_{GW}) \tag{2.9}$$

where $E_{th,SN}(t)$ is the thermal energy of the gas at the time t owing to the energy deposited by Type Ia and Type II supernovae. At the specific time t_{GW} (the time for the occurrence of a galactic wind), all the remaining gas is expelled from the bulge, and both star formation and gas infall cease.

The gas binding energy

We supposed that the bulge is bathed in a dark matter halo of mass 100 times greater than that of the bulge itself (i.e. $M_{dark} = 2 \times 10^{12} M_{\odot}$) and with an effective radius $r_{dark} = 100 r_e = 200$ kpc, where r_e is the effective radius of the bulge (Sérsic) mass distribution. In the case of a massive and diffuse dark halo, the binding energy of the gas is expressed as

$$E_{b,gas}(t) = W_L(t) + W_{LD}(t) \tag{2.10}$$

where $W_L(t)$ is the gravitational energy of the gas as due to the luminous matter and can be written as

$$W_L(t) = -\frac{q_L G M_{gas}(t) M_{lum}}{r_e} \tag{2.11}$$

where $q_L = 1/2$ if one wants to preserve the $r^{1/4}$ law.

$W_{LD}(t)$ is the gravitational energy of the gas due to the interaction of luminous and dark matter:

$$W_L(t) = -\frac{G M_{gas}(t) M_{dark}}{r_e}\, \widetilde{W}_{LD} \tag{2.12}$$

The interaction term $\widetilde{W}_{LD}$ is expressed as

$$\widetilde{W}_{LD} \simeq \frac{1}{2\pi}\frac{r_e}{r_{dark}}\left[1 + \left(\frac{r_e}{r_{dark}}\right)\right] \tag{2.13}$$

The gas thermal energy

The cumulative thermal energy injected by supernovae is calculated as in Pipino et al. (2002). Namely, if we call $R_{SNIa}(t)$ and $R_{SNII}(t)$ the rates of Type Ia and Type II supernova explosions, respectively:

$$R_{SNIa} = A \int_{M_{Bm}}^{M_{B_M}} \varphi(m) \left[\int_{\mu_{min}}^{0.5} f(\mu)\psi(t-\tau_m)d\mu\right] dm \tag{2.14}$$

$$R_{SNII} = (1-A)\int_{M_{Bm}}^{M_{B_M}} \psi(t-\tau_m)\varphi(m)dm + \int_{M_{B_M}}^{M_U} \psi(t-\tau_m)\varphi(m)dm \tag{2.15}$$

then we have

$$E_{th,SN}(t) = E_{th,SNIa}(t) + E_{th,SNII}(t), \tag{2.16}$$

where

$$E_{th,SNIa/II}(t) = \int_0^t \epsilon(t-t')R_{SNIa/II}(t')dt' \text{erg}. \tag{2.17}$$

The evolution with time of the thermal content ϵ of a supernova remnant, needed in equation above, is given by (Cox 1972):

$$\epsilon(t_{SN}) = \begin{cases} 7.2\times10^{50}\epsilon_0 & \text{erg for } 0 \le t_{SN} \le t_c, \\ 2.2\times10^{50}\epsilon_0(t_{SN}/t_c)^{-0.62} & \text{erg for } t_{SN} \ge t_c, \end{cases} \tag{2.18}$$

where ϵ_0 is the initial blast wave energy of a supernova in units of 10^{51} erg, assumed equal for all supernova types, t_{SN} is the time elapsed since explosion and t_c is the metallicity-dependent cooling time of a supernova remnant (Cioffi et al. 1988):

$$t_c = 1.49\times10^4 \epsilon_0^{3/14} n_0^{-4/7} \zeta^{-5/14} \text{ yr}. \tag{2.19}$$

In this expression $\zeta = Z/Z_\odot$ is the metallicity in solar units and n_0 is the hydrogen number density.

Chapter 3

Formation and evolution of the Milky Way bulge

"If the facts don't fit the theory, change the facts."
(Albert Einstein)

3.1 Model parameters

We explored (Ballero et al. 2007a) a number of possibilities regarding the formation and star formation history of the Galactic bulge by varying the model parameters in the following way:

- Star formation efficiency: ν from 2 to 200 Gyr^{-1};

- For the IMF above $1M_{\odot}$, we have considered the cases suggested by Zoccali et al. (2000) in their §8.3, i.e. their case 1 (hereafter Z00-1) with $x = 0.33$ in the whole range of masses, their case 3 (Z00-3) for which $x = 1.35$ for $m > 1M_{\odot}$ (Salpeter 1955) and their case 4 (Z00-4) in which $x = 1.35$ for $1 < m/M_{\odot} < 2$ and $x = 1.7$ for $m > 2M_{\odot}$ (Scalo 1986). Our reference model corresponds to their case 2 with $x = 0.95$ for $m > 1M_{\odot}$[1], therefore we call it Z00-2. We recall that the fraction of binary systems giving rise to Type Ia supernovae is a function of the adopted IMF (see Matteucci & Greggio 1986). Owing to the lack of information concerning the Type Ia supernova rate in the bulge, we calibrate such a fraction

[1]Actually, Zoccali et al. (2000) selected as "IMF 2" the one with $x = 1$ for $m > 1M_{\odot}$. We performed calculations with $x = 0.95$, which is very similar, for comparison to the IMF of Matteucci & Tornambè (1987).

Model name/specification	x ($m > 1M_\odot$)	ν (Gyr^{-1})	τ (Gyr)
Fiducial model (Z00-2)	0.95	20.0	0.1
Z00-1	0.33	20.0	0.1
Z00-3	1.35	20.0	0.1
Z00-4	1.35 ($m < 2M_\odot$)	20.0	0.1
	1.7 ($m \geq 2M_\odot$)		
$\nu = 2$ Gyr^{-1}	0.95	2.0	0.1
$\nu = 200$ Gyr^{-1}	0.95	200.0	0.1
$\tau = 0.01$ Gyr	0.95	20.0	0.01
$\tau = 0.7$ Gyr	0.95	20.0	0.7
S1	0.33	200.0	0.01
S2	0.95	200.0	0.01
S3	0.33	2.0	0.7
S4	0.95	2.0	0.7

Table 3.1: Features of the examined models: IMF index (second column), star formation efficiency (third column), infall timescale (fourth column).

in order to reproduce the Mannucci et al. (2005) estimate of the supernova rate of an elliptical galaxy of the same mass.

- Infall timescale: τ from 0.01 to 0.7 Gyr. The first case simulates a closed-box model, while the latest hypothesis follows the suggestion by Mollá et al. (2000) who assume a slower timescale for the formation of the bulge. We refer to the timescale τ_H which they chose for the gas collapse from halo to bulge.

Table 3.1 summarises the features of the examined models.

3.2 Observations of abundances in the Galactic bulge

The observations of abundances in the Galactic bulge taken from different datasets are re-normalised to the solar abundances of Grevesse & Sauval (1998) so that an artificial dispersion associated with the adoption of different solar abundance values is corrected for.

3.2.1 Metallicity distribution

Data for the [Fe/H] distribution of red giant branch and asymptotic giant branch stars in the bulge were taken from Zoccali et al. (2003), who provided photometric determination of metallicities for 503 bulge stars. By combining near-infrared data from the 2MASS survey, from the SOFI imager at ESO NTT and the NICMOS camera on Hubble Space Telescope, plus optical images taken with the Wide Field Imager at ESO/MPG 2.2m telescope within the EIS Pre-FLAMES survey, they constructed a disk-decontaminated (M_K,$V-K$) colour-magnitude diagram of the bulge stellar population with very large statistics and small photometric errors, which was compared to the analytical red giant branch templates in order to derive the metallicity distribution. The advantage of this approach is that it allows determinations of metallicities of a great number of stars, although the relationship between the position in the colour-magnitude diagram and the metallicity can be somewhat uncertain.

Since the template red giant branches are on the [M/H] scale (where M stands for the total metal abundance), in order to obtain the [Fe/H] distribution the α-enhancement contribution was subtracted in the following way (Zoccali, private communication):

$$[\mathrm{Fe/H}] = \begin{cases} [\mathrm{M/H}] - 0.14 & \text{if } [\mathrm{M/H}] > -0.86 \\ [\mathrm{M/H}] - 0.21 & \text{if } [\mathrm{M/H}] < -0.86 \end{cases} \tag{3.1}$$

This relation assumes that the α-elements in the bulge follow the abundance trends of globular clusters in the halo. The resulting metallicity distribution contains somewhat less metal-poor stars relative to a closed-box gas exhaustion model and suggests that the G-dwarf problem (i.e. the deficit of metal-poor stars relative to a simple model) may affect the Galactic bulge even though less severely than in the solar neighbourhood (see e.g. Hou et al. 1998).

In figure 3.1 we compare the photometric metallicity distribution derived by Zoccali et al. (2003) to the spectroscopic one of McWilliam & Rich (1994). The two distributions are broadly consistent, with a somewhat less pronounced supersolar [Fe/H] tail and a slightly sharper peak in the photometric case. However, the position of the high [Fe/H] cutoff for the photometric metallicity distribution is wholly dependent on the metallicity assigned to the only two template clusters, namely NGC 6528 and NGC 6553 available in the high-metallicity domain. Nevertheless, there are also indications (Zoccali, private communication) that the metallicity distribution of the bulge stars, when achieved with high-resolution spectroscopy, is comparable to or even narrower than the one showed

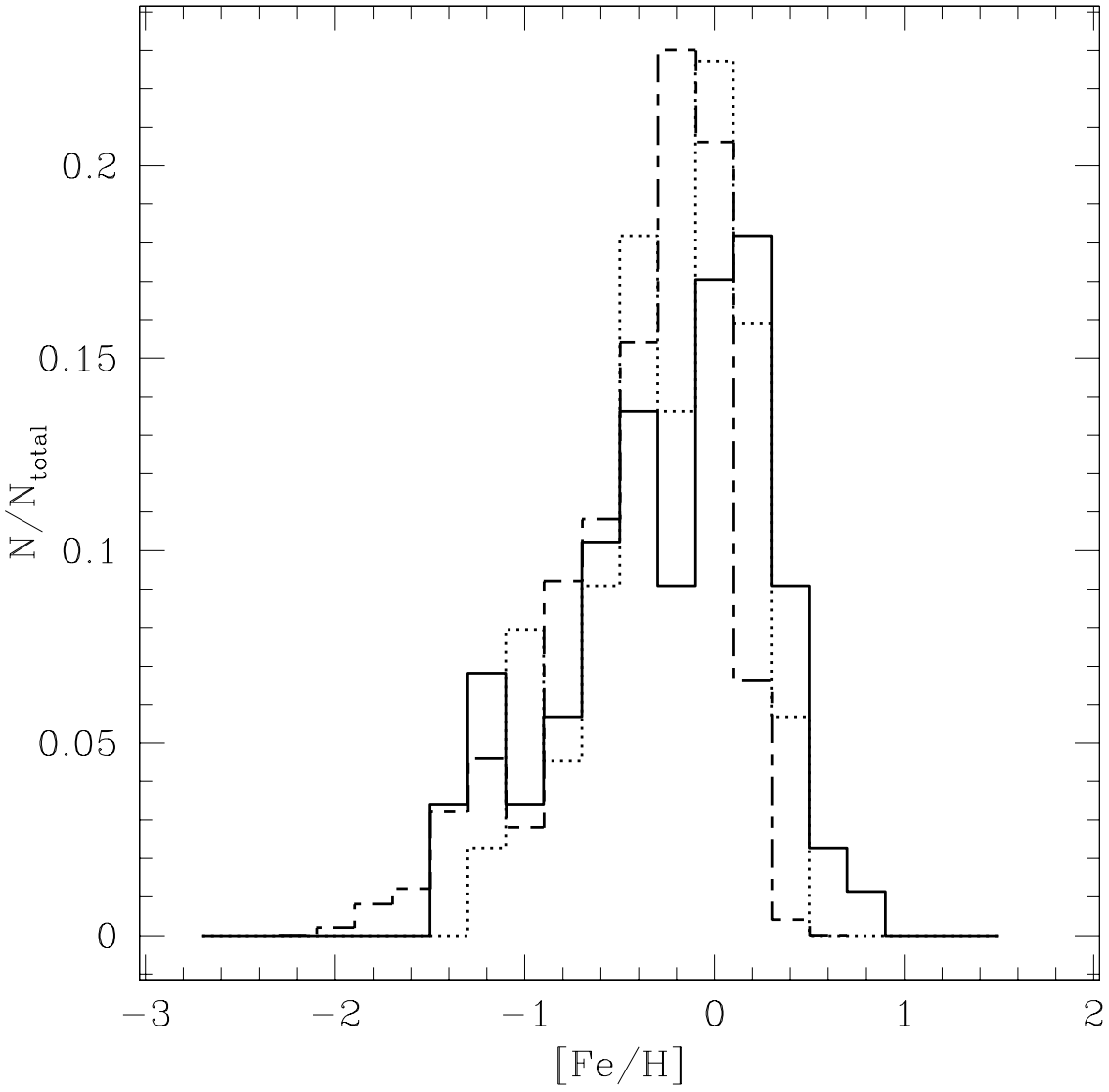

Figure 3.1: Comparison between the bulge metallicity distribution derived by Zoccali et al. (2003, solid histogram), Fulbright et al. (2006, dashed histogram) and the one derived with the spectroscopic survey of McWilliam & Rich (1994, dotted histogram).

here, and that there are a very few supersolar-metallicity stars. In the same figure we also show the data from Fulbright et al. (2006), who performed a new high-resolution ($R \sim 45000 - 60000$) analysis of 27 K-giants in the Baade's Window ($b = -4°$) sample with the HIRES spectrograph on the Keck I telescope and, after determining their Fe abundances, they used them as reference stars in order to re-calibrate the K-giant data from Rich (1988). They found that the derived metallicity distributions are slightly stretched towards both the metal-poor and metal-rich tails with respect to those derived in previous works (Rich 1988; McWilliam & Rich 1994; Sadler et al. 1996; Zoccali et al. 2003), although the overall consistency among these different metallicity distributions is reasonable.

3.2.2 α-elements and carbon

Abundances of O, Mg, Si, Ca, C and Fe for stars and clusters in the bulge are taken from Origlia et al. (2002), Origlia & Rich (2004), Origlia et al. (2005) and Rich & Origlia (2005). We refer to this set of abundances as the "IR spectroscopic database" hereafter. These datasets were obtained using the NIRSPEC spectrograph at Keck II, which allowed the determination of near-infrared, high-resolution ($R \sim 25000$), high signal-to-noise ratio (S/N > 40) échelle spectra. They used the 1.6μm region of the spectrum, corresponding to the H band. In all cases, abundance analysis was performed by means of full spectrum synthesis and equivalent width measurements of representative lines. Reliable oxygen abundances were derived from a number of OH lines; similarly, the C abundance was derived from CO molecular lines, whereas strong atomic lines were measured for Mg, Si, Ca, Ti and Fe. The data include observations of bright giants in the cores of the bulge globular clusters Liller 1 and NGC 6553 (Origlia et al. 2002, see also Melèndez et al. 2003), Terzan 4 and Terzan 5 (Origlia & Rich 2004), NGC 6342 and NGC 6528 (Origlia et al. 2005, see also Carretta et al. 2001, Zoccali et al. 2004) and measurements of abundances of M giants in Baade's window (Rich & Origlia 2005). The typical errors are of ± 0.1 dex. The main considerations that were drawn from these abundance analyses are that α-enhancement is safely determined in old stars with [Fe/H] as high as solar, pointing towards early formation and rapid enrichment in both clusters and field, which are likely to share a common formation history. The [C/Fe] abundance ratios can be depleted up to a factor of ≈ 3 with respect to the solar value, as expected because of the first dredge-up and possibly extra-mixing mechanisms

due to *cool bottom processing*[2], which are at work during the evolution along the red giant branch, as also indicated by the very low (< 10) $^{12}C/^{13}C$ abundance ratio (see also Origlia et al. 2003 and references therein). The analysis of M giants yielded abundances similar to those obtained with high-resolution optical spectroscopy of K giants; there is an apparent lack of supersolar-[Fe/H] stars, but the sample is too small to draw firm conclusions.

For O, Mg, Si and Ca we also included the abundance measurements of Fulbright et al. (2007), who used the same spectra as in Fulbright et al. (2006), i.e. obtained the spectra of 27 bulge K giant stars at the Keck I telescope using the HIRES échelle spectrograph with high resolution ($R \sim 45000 - 67000$) and high signal-to-noise ratio. The typical errorbars are of ~ 0.1 dex. The outcome of their analysis is that all elements produced from massive stars (i.e. α-elements, plus Na and Al) show enhancement in bulge stars relative to both Galactic thick and thin disk, although oxygen shows a sharply decreasing trend for supersolar [Fe/H], which can be attributed to a metallicity-dependent modulation of the oxygen yield from massive stars (McWilliam et al. 2007). These results suggest that massive stars contributed more to the chemical enrichment of the bulge than to the disk, and consequently that the timescale for bulge formation was shorter than that of the disk, although they did not exclude other possibilities (e.g. an IMF skewed to high masses).

Oxygen data from Zoccali et al. (2006) were also taken. In their paper, Fe and O abundances for 50 K giants in four fields ($b = -6$; Baade's Window; Blanco $b = -12$; NGC 6553) towards the Galactic bulge were derived; oxygen abundance was measured from the forbidden line at 6300 Å. A resolution of $R = 45000$ was achieved with the FLAMES-UVES spectrograph at the VLT. The typical errorbars are of ~ 0.1 dex. Also in this case, [O/Fe] is found to be higher in bulge stars than both in thick and thin disk, and supports a scenario where the bulge formed before the disk and more rapidly, with a formation history similar to that of old early-type galaxies. In the same four fields, Lecureur et al. (2007) analysed 53 stars observed with the red arm of the UVES spectrograph at a resolution $R \sim 47000$, in the range $4800 - 6800$ Å, obtaining Mg abundances from the 6319 Å triplet, with errorbars ranging from 0.06 to 0.21 dex. They found that the magnesium ratios relative to iron are higher than

[2]Deep circulation currents below the bottom of the standard convective envelope of stars can transport matter from the non-burning bottom of the convective envelope down to regions where some CNO processing can take place.

those in both galactic disks (thin and thick) for [Fe/H]> -0.5. This abundance pattern points towards a short formation timescale for the galactic bulge leading to a chemical enrichment dominated by massive stars at all metallicities, and perhaps also to a flatter IMF if the [α/Fe] ratios are really larger than in the disk. The [O/Mg] ratios are also similar to those of the galactic disk stars of the same metallicity, thus confirming that the enrichment of these elements is dominated by massive stars in all three populations (bulge, thin disk and thick disk). They also derived C and N abundances by an iterative procedure: to start with, the oxygen abundance was determined from the [O I] line with [C/Fe]$= -0.5$ and [N/Fe]$= +0.5$ for each star (appropriate values for mixed giants); then the C abundance was deduced from synthetic spectrum comparison of the C2 bandhead at 5635 Å (assuming this O abundance); given C and O, nitrogen was then constrained from the strong CN line at 6498.5 Å. The associated uncertainties for the resulting [C/Fe] and [N/Fe] ratios were about ± 0.2 dex. In search for probes of internal mixing for their bulge stars, a C-N anticorrelation was checked for. Within the uncertainties, they find no anticorrelation of [C/Fe] with [N/Fe], but merely a scatter entirely accounted for by measurement uncertainties, with the mean [C/Fe] and [N/Fe] values (-0.04 and $+0.43$, respectively) compatible with mildly mixed giants above the red giant branch bump. The mixing seems less efficient than in metal-poor field giants.

In Fig. 3.2 are resumed the observations for α-elements in the bulge, while in the upper panel of Fig. 3.3 the available data for carbon are shown.

3.2.3 Nitrogen

Nitrogen abundances for subsolar metallicities in the bulge are derived from planetary nebulae. This may represent a problem, since while the measured oxygen abundance represents the true value of the interstellar medium out of which the planetary nebula progenitor was formed, the observed N abundance has contributions both from the pre-existent nitrogen and from that produced by the star itself during its lifetime and dredged-up to the stellar surface. Moreover, these data come from emission lines which have a very complicated dependence upon several parameters (such as temperature, density and metal content) and assumptions (e.g. the photoionization model, where the largest uncertainties arise). Therefore it might be dangerous to employ these measurements to trace galactic chemical evolution. In principle, it would be possible to discriminate between enriched and primordial N by means of the C/N ratio (which is very different in the two cases, being much lower in the case of nitrogen-enriched stars).

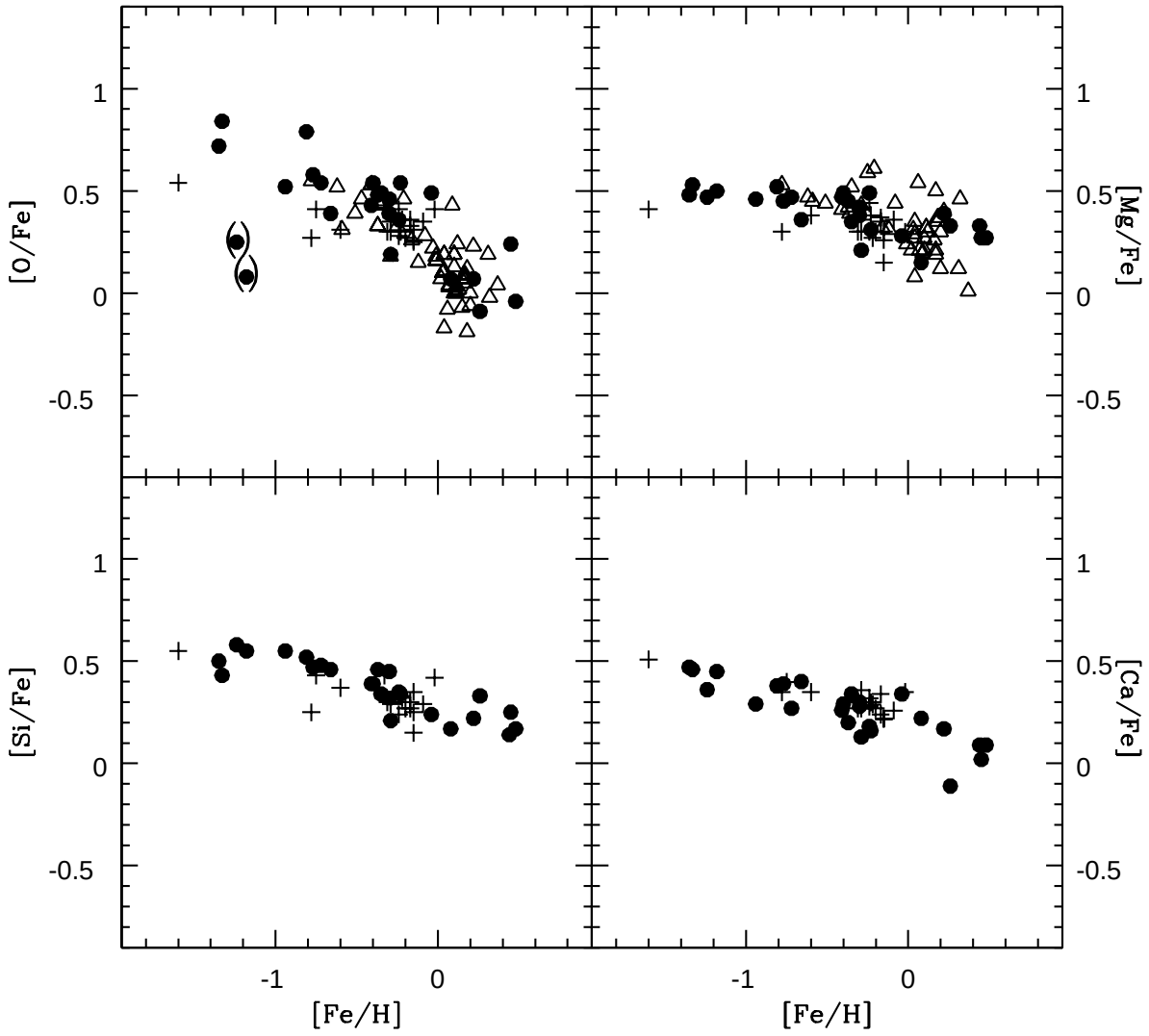

Figure 3.2: Observations of [α/Fe] ratios in the Galactic bulge for O, Mg, Si and Ca. Plus signs represent data taken from the IR spectroscopic database (see §3.2.2 for specific references). The filled circles represent the data from Fulbright et al. (2007). The two bulge stars in parentheses show the effects of proton burning products in their atmospheres. Therefore, they have probably suffered a reduction in the envelope oxygen abundances via stellar evolution, so their oxygen abundances do not reflect the bulge composition. Finally, triangles represent the observations of Zoccali et al. (2006) for oxygen and Lecureur et al. (2007) for magnesium.

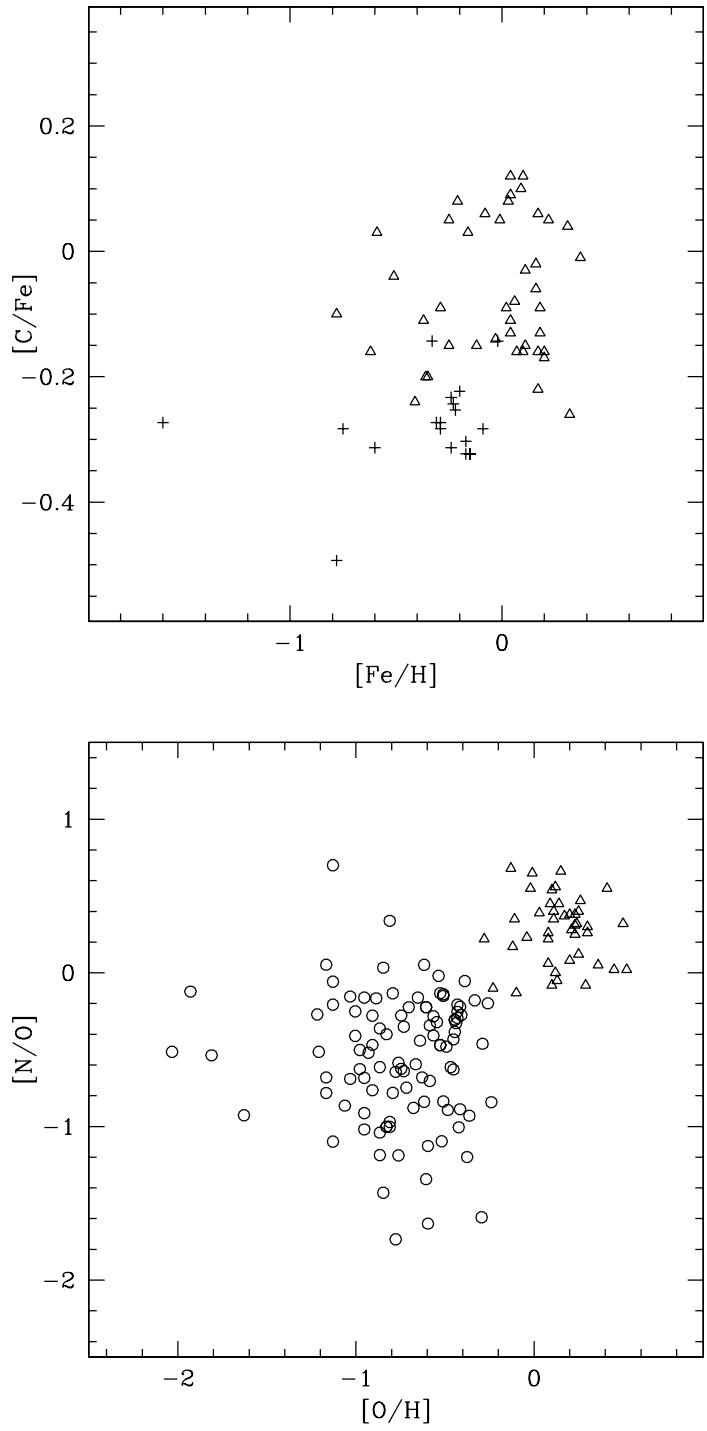

Figure 3.3: *Upper panel*: observations of [C/Fe] ratios in the bulge giants from the IR spectroscopic database (plus signs; see §3.2.2 for details) and Lecureur et al. (2007, triangles). *Lower panel*: observations of [N/O] ratios in bulge planetary nebulae from Górny et al. (2004, circles) and in bulge giants from Lecureur et al. (2007, triangles).

Unfortunately, measurements for carbon in bulge planetary nebulae are available to date only for a very limited set of objects (Webster 1984; Walton et al. 1993; Liu et al. 2001). Another possibility is to make use of symbiotic stars, i.e. presumably M giants in binary systems with a white dwarf or another hot companion. The envelope of the symbiotic star is photoionised from the hard UV radiation, leading to recombination line emission. Since the envelope has being observed, the abundances may be less evolved than in the planetary nebulae (Nussbaumer et al. 1988).

It is possible that the N enrichment is not very dramatic especially in non-Type I planetary nebulae, which constitute about 80% of the planetary nebula population in the Galaxy (Peimbert & Serrano 1980). Moreover, since the bulge presumably has not formed stars for a long time, Type I planetary nebulae (which have high-mass progenitors and are the most nitrogen-enriched) are not expected to be frequent. This is also confirmed by Cuisinier et al. (2000) who found quite low [N/O] ratios in their sample if compared to that resulting from self-enrichment. Moreover, Luna & Costa (2005) measured the N/O ratio of 43 symbiotic stars towards the Galactic bulge and, as it can be seen in their Figure 5, the values of log(N/O) are consistent with those coming from studies of planetary nebulae.

We employed the compilation of Górny et al. (2004), who observed 44 planetary nebulae in the direction of the Galactic bulge with the aim of discovering Wolf-Rayet stars at their centre. The spectra were obtained with the 1.9-m telescope at the South African Astronomical Observatory, with an average resolution of 1000. Furthermore, Górny et al. (2004) also merged their data with other published ones. Namely, they included the samples observed by Cuisinier et al. (2000), Escudero & Costa (2001) and Escudero et al. (2004). They obtained a total of 164 objects, among which a clear segregation of the subsamples is seen, due to the different selection criteria adopted to define each sample, and therefore none of them is truly representative of the bulge planetary nebula population. By merging the datasets, a more complete view of this population is achieved. Updated reddening corrections were applied to the objects from Escudero & Costa (2001) and Escudero et al. (2004). The merged sample was divided into two classes (according to the criteria listed in Stasińska et al. 1991), the first including those objects which are likely to be physically related to the Galactic bulge and the second containing the remaining objects which most probably belong to the disk. We only selected objects belonging to the bulge which had a clear detection of oxygen and nitrogen emission features; the resulting sample includes 103 objects.

Errors in abundance derivations from both observational and theoretical uncertainties are typically $0.2 - 0.3$ dex for [O/H] and can be even larger for [N/O].

Data for N are shown in the lower panel of Fig. 3.3: a large spread is evident. The [N/O] ratios derived by the Zoccali et al. (2006) and Lecureur et al. (2007) measurements are also added for comparison; they integrate the planetary nebula measurements at high metallicities. The two sets of measurements are consistent with an overall growth of the [N/O] ratio with metallicity.

In the future, when very high resolution IR spectroscopy ($R \approx 100,000$) becomes possible, N estimates could be also derived in giant stars from the faint CN lines that are de-blended from stronger the CO and OH lines at high resolution.

3.3 Results

3.3.1 The supernova rates

Fig. 3.4 shows the predicted time evolution of the rate of Type II and Type Ia supernovae in the Galactic bulge; the former die on short timescales and closely reflect the evolution of the SFR. The secondary peaks of the Type Ia supernova rates are mostly due to the discontinuities in the adopted stellar lifetimes (Kodama 1997) but do not affect the results concerning chemical abundances. The break in the Type II supernova rates corresponds to the suppression of the SFR due to the achievement of the condition expressed in Eq. 2.9, which quite intuitively occurs earlier for flatter IMFs, higher ν's and/or lower τ's. However, even without a galactic wind, the Type II supernova rate would become negligible at the same epoch, owing to the small amount of gas left in the bulge at that time.

In those cases where the star formation is "bursty" (e.g. high star formation efficiency and quick formation timescale), the peak of the Type Ia supernova rate (and therefore of Fe enrichment) can occur even before 1 Gyr, which is the timescale for Fe-enrichment in the solar neighbourhood. In fact, the time of occurrence of this peak is very sensitive to the underlying star formation history and can be as low as ~ 0.2 Gyr in the case of $\tau = 0.01$ Gyr or $\nu = 200$ Gyr^{-1} (see also Matteucci & Recchi 2001). Therefore, we expect that:

1. The down-turn (i.e. change of slope) of the [α/Fe] vs. [Fe/H] plots, corresponding to the beginning of a substantial Fe enrichment, will occur, in general, at higher

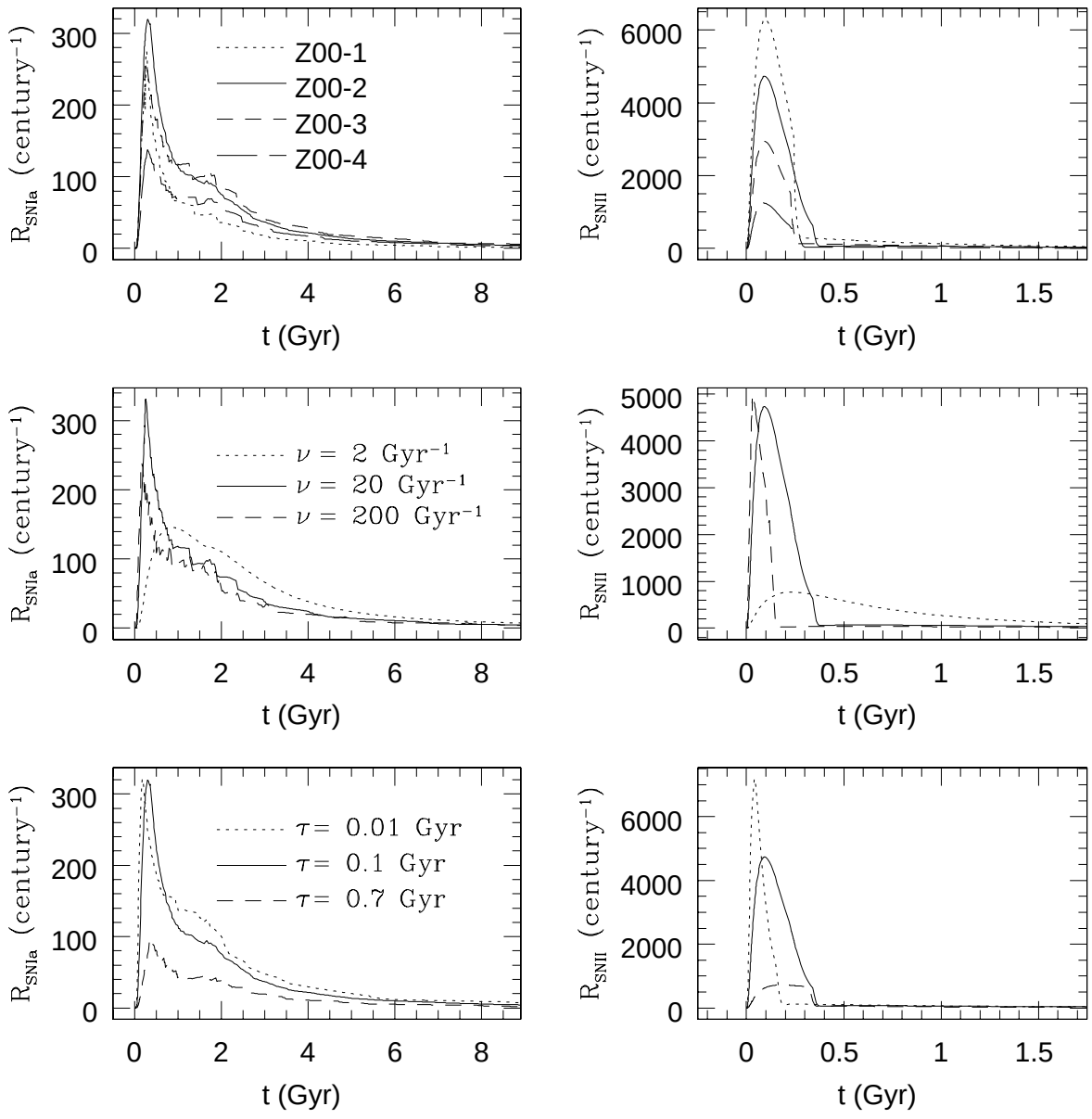

Figure 3.4: Evolution of the rates of Type Ia (left) and Type II (right) supernovae where different values of the IMF index (upper panel) star formation efficiency (middle panel) and infall timescale (lower panel) are considered. The break corresponds to the occurrence of the galactic wind.

[Fe/H] values relative to the change in slope in the solar vicinity. This is due to the high SFR and the short timescale for bulge formation. This fact was pointed out for the first time by Matteucci & Brocato (1990).

2. Where the IMF is flatter, the abundance trend of α-elements vs. Fe is flatter as well, because the ratio of Type Ia to Type II supernovae is smaller than in a Salpeter or steeper IMF. For the same reason, we expect that steeper IMFs will lead to overall lower [α/Fe] ratios.

3. For steeper IMFs (e.g. Scalo 1986, or Salpeter 1955), the nitrogen enrichment from low- and intermediate-mass stars is enhanced with respect to O, which mostly comes from massive stars. As a result, the [N/O] vs. [O/H] plot should lie above the one of our reference model. Moreover, N primary production from low- and intermediate-mass stars should be enhanced as well, and the flattening of the above mentioned plot towards the latest evolutionary stages should be prolonged. In general, any model that favours the contribution of massive rather than low- and intermediate-mass stars (e.g. high ν) should predict a suppressed [N/O] ratio if compared to our reference model, and vice versa.

3.3.2 The metallicity distribution of the bulge giants

Fig. 3.5 shows the predicted metallicity distribution for giant stars compared to the data from Zoccali et al. (2003) and Fulbright et al. (2006). We must remark that we did not make an attempt to convolve the predictions with uncertainties. Since the observed distributions are probably broader than the "true" distribution, due to random errors, and may be offset due to systematic errors, their comparison is likely to be affected. Moreover, the significance of a metallicity gradient in the bulge (Minniti & Zoccali 2007) is not taken into account, since it would require a multi-zone bulge model to be properly investigated.

The choice of a different IMF does not primarily influence the spread of the distribution but rather shifts its peak on the [Fe/H] scale: in general, flatter IMFs result into distributions peaked at higher values of [Fe/H]. Since the star-forming phase is relatively short, massive stars will be important in the Fe enrichment; if we adopt the Scalo (1986) exponent (model Z00-4) rather than the Salpeter (1955) one (model Z00-3) for stars more massive than $2M_{\odot}$, the resulting metallicity distribution will change dramatically, moving the peak towards significantly lower [Fe/H].

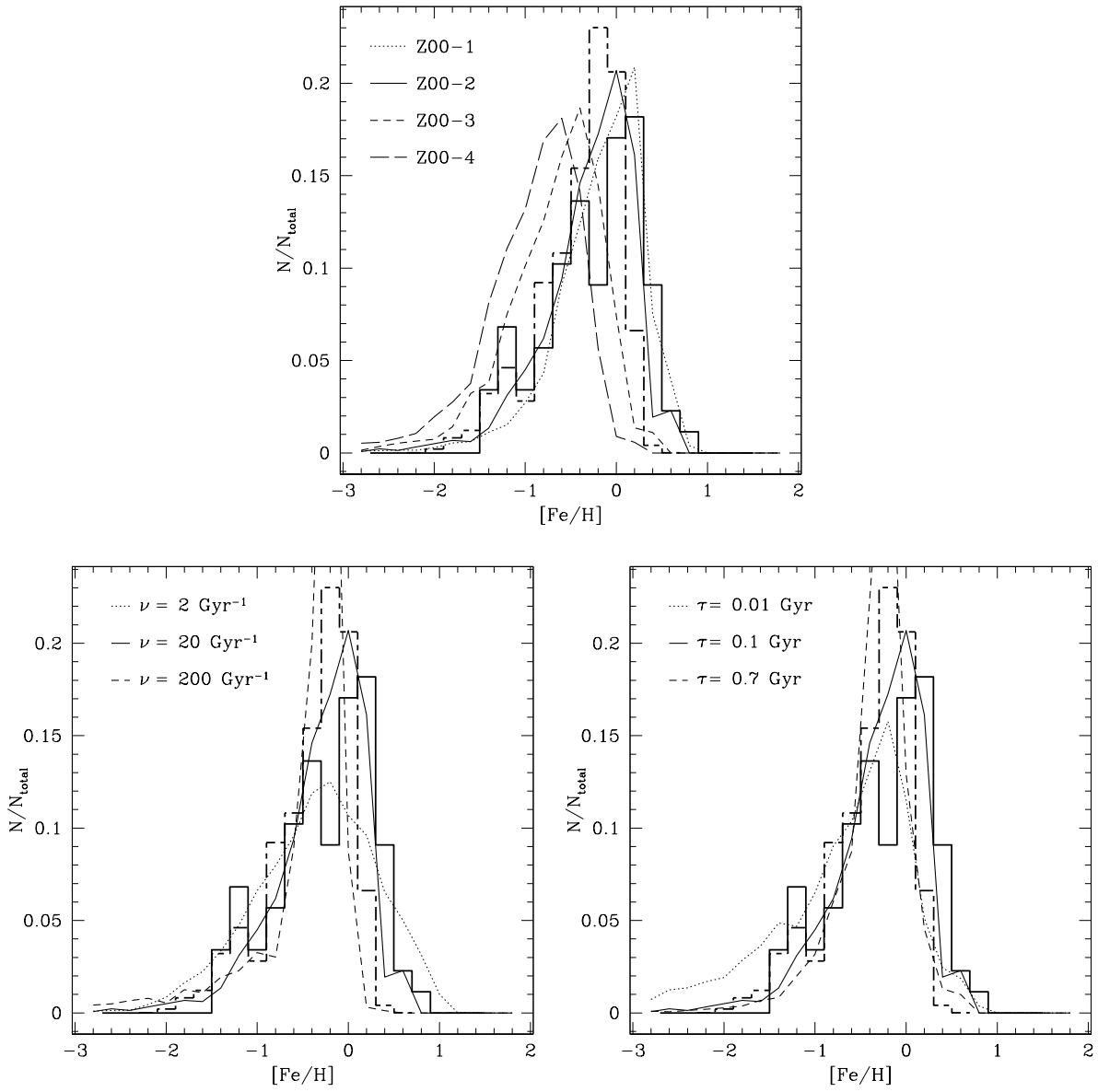

Figure 3.5: Predicted metallicity distributions in our bulge models for single parameter variations relative to the reference model, with different choices of the IMF index (upper panel; see text for details), star formation efficiency (lower left panel), and gas infall timescale (lower right panel). Our reference model is represented by the solid line. Data are from Zoccali et al. (2003, solid histogram) and Fulbright et al. (2006, dashed histogram).

Considerations on the metallicity distribution allow us to exclude IMFs much steeper than $x = 0.95$, whereas plots for flatter IMFs are all consistent with the observed distributions. In fact, the metallicity distribution obtained with the very flat ($x = 0.33$) IMF of case Z00-1 is almost indistinguishable from that calculated in case Z00-2, showing that the metallicity distribution progressively becomes almost insensitive to the flattening of the IMF under a certain value of the index. This is maybe suggestive of a "saturation effect" in the Fe enrichment from Type II supernovae. Namely, a flattening of the IMF below a certain value of the index x does not produce a sensible increase of the number of massive stars, and moreover, the Fe mass ejected is assumed to be the same (i.e. does not increase as a function of mass) for all masses above $40M_{\odot}$ (see §2.4).

If we choose a moderate star formation efficiency ($\nu = 2$ Gyr^{-1}, comparable to that of the galactic halo), the predicted metallicity distribution is broadened and the number of both high- and low-metallicity stars is somewhat overestimated. The observed peak is poorly reproduced (both in height and position) for all of the metallicity distributions considered. In contrast, the very high value of $\nu = 200$ Gyr^{-1} yields an extremely narrow distribution, with an excessive peak height (reaching 0.68, but is truncated in the figure to preserve clarity).

A change in the infall timescale affects mainly the spread of the distribution and only slightly the position of the peak. The low-metallicity wing is especially sensitive to the value of τ. The model with $\tau = 0.01$ Gyr approaches a closed-box model, i.e. a model where all the gas is already present from the beginning (which would correspond to the limit $\tau = 0$). The gas soon reaches high densities and is consumed very rapidly. Thus, the number of metal-poor stars is overestimated and the predicted distribution extends below the observed low-metallicity tail. This confirms the considerations of Zoccali et al. (2003), i.e. an equivalent (although less important) manifestation of the G-dwarf problem occurs also in the Galactic bulge. We also calculated the metallicity distribution resulting from the adoption of a slightly longer infall timescale, namely $\tau = 0.7$ Gyr, that corresponds to the timescale τ_H for collapse from halo to bulge in the model of Mollá et al. (2000). As the figure shows, the $\tau = 0.7$ Gyr metallicity distribution is at variance with observations, having a serious deficit of both metal-poor and metal-rich stars and too high a peak with respect to both measured distributions (again higher than 0.5 but truncated in the figure).

The main conclusions which can be drawn for variations of a single parameter are:

1. Changing the IMF slope has the general effect of shifting the peak of the metallicity

distribution towards lower metallicities for steeper IMFs, and vice versa. For $x \leq 0.95$ such variations become much less evident. We want to point out that a continuous wind such as that of the Samland et al. (1997) model cannot have the same effects of flattening the IMF, since outflows *lower* the effective yield, and thus if we had a continuous outflow we would need an even flatter IMF to reproduce the observed metallicity distribution and abundance ratios. This was shown i.e. for the galactic disk by Tosi et al. (1998, their Figure 7).

2. Lower star formation efficiencies give rise to broader metallicity distributions and vice versa. The same is true of shorter infall timescales, which additionally increase the number of low-metallicity stars.

3. The effect of both star formation efficiency and infall timescale on the position of the metallicity distribution peak is negligible.

We now explore whether any other combinations of parameters can fit the observed metallicity distribution. Since the position of the peak is essentially only determined by the IMF, combining IMFs other than those of models Z00-1 and Z00-2 with different values of the other parameters would not be useful to reproduce the required metallicity distribution. On the contrary, the effects of infall timescale and star formation efficiency might compensate each other; therefore, we also considered the following "supplementary" (S) models:

- *Model S1*: IMF like in model Z00-1, $\nu = 200$ Gyr^{-1}, $\tau = 0.01$ Gyr.

- *Model S2*: same as in S1, but with IMF like in model Z00-2.

- *Model S3*: IMF like in model Z00-1, $\nu = 2$ Gyr^{-1}, $\tau = 0.7$ Gyr.

- *Model S4*: same as in S3, but with IMF like in model Z00-2.

In Fig. 3.6 the resulting metallicity distributions for these supplementary models are shown. It is clear that while combining a high value of ν and a low value of τ exacerbates the bulge "G-dwarf problem", a longer formation timescale can combine with a milder star formation efficiency to give rise to a metallicity distribution compatible with observations, and this is what happened in some of the previous models (Samland et al. 1997; Mollá et al. 2000). However, such a degeneracy cannot be pushed above a certain range of values. We investigated longer timescales and found out that it becomes

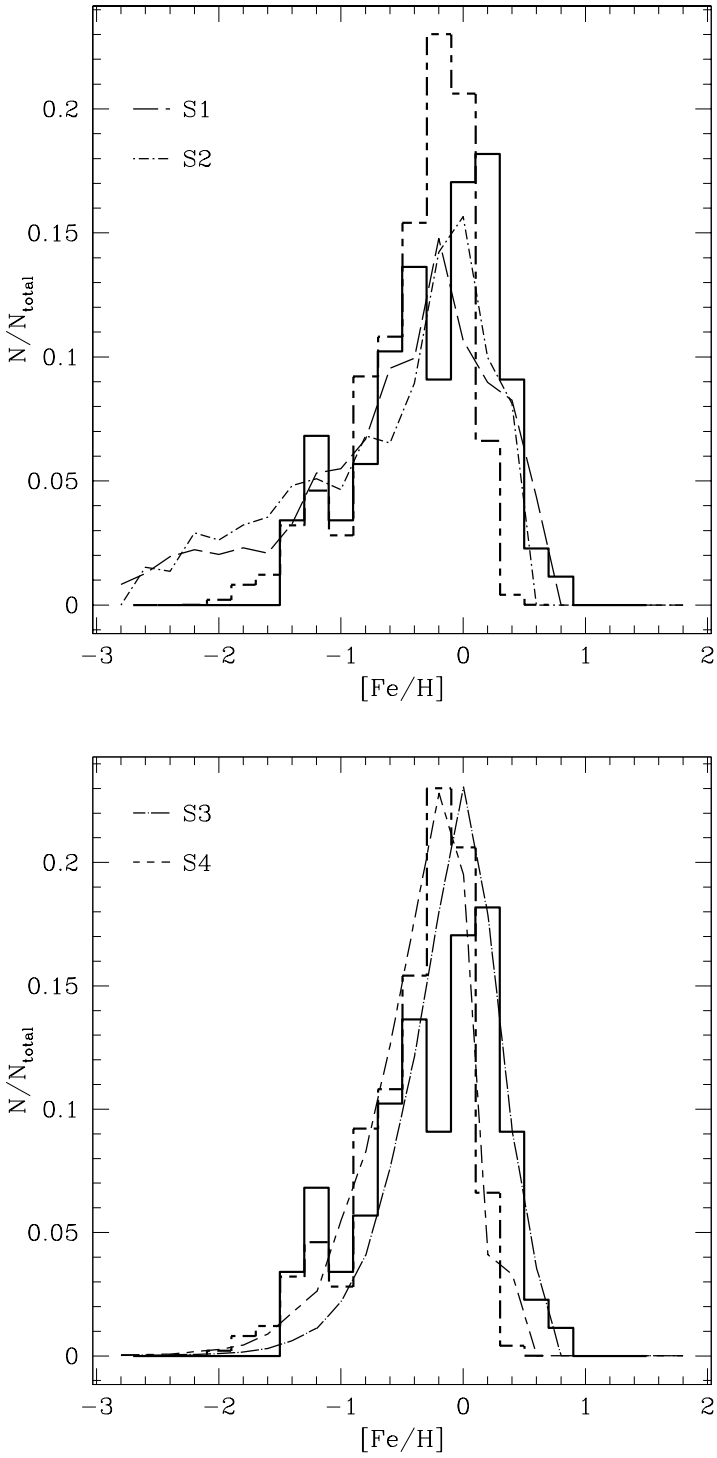

Figure 3.6: Predicted metallicity distributions in models with $\nu = 200$ Gyr^{-1} and $\tau = 0.01$ Gyr (upper panel) and in models with $\nu = 2$ Gyr^{-1} and $\tau = 0.7$ Gyr (lower panel), with the adoption of two different IMFs (see Table 3.1 for details). Data are from Zoccali et al. (2003, solid histogram) and Fulbright et al. (2006, dashed histogram).

progressively harder to maintain the required metallicity distribution both in height and position, since the result of combining much longer timescales with efficiencies suitable to keep the required shape is to shift the distribution towards lower metallicities, and vice versa, if we try to keep the predicted metallicity distribution at the right position, its shape becomes too narrow, somewhat in contrast with the observed metallicity distributions. In any case, as we shall see, such a degeneracy is definitively broken when we take into account the evolution of abundance ratios (see next Section). For $\tau \geq 2$ Gyr, some star formation is predicted at detectable levels at the present time, contrarily to observations.

Therefore, we conclude that good agreement with the observed metallicity distribution is achieved only if the bulge formed on a short timescale, with a flat IMF and with a rather high star formation efficiency.

3.3.3 Evolution of the abundance ratios

Among the different α-elements we have considered, oxygen is the most sensitive to variations of the adopted parameters. Therefore, we are showing detailed plots for every parameter value only for oxygen, and we shall only discuss our best model with the other α-elements.

Oxygen

Figure 3.7 shows the evolutionary plots of the [O/Fe] abundance ratio with metallicity. The models are compared to the data of the IR spectroscopic database, Fulbright et al. (2007) and Zoccali et al. (2006). Each panel illustrates the effects of changing one of the model parameters as stated in §3.1. The last panel also shows the results obtained with models S3 and S4. We remind that when the bulk of Type Ia supernovae begins to explode, the [O/Fe] ratio has a downturn and a knee in the [O/Fe] vs. [Fe/H] curve is expected.

The reference model provides a satisfactory fit to the existing measurements and predicts the correct amount of oxygen enhancement, even though the slope of the predicted plot in the reference model is slightly flatter than the observations for supersolar [Fe/H]. However, as we shall see, the fit to this abundance plot cannot be improved without violating other constraints. The amount of α-enhancement depends first of all on the time-delay model, and therefore on the IMF index, more in particular on the

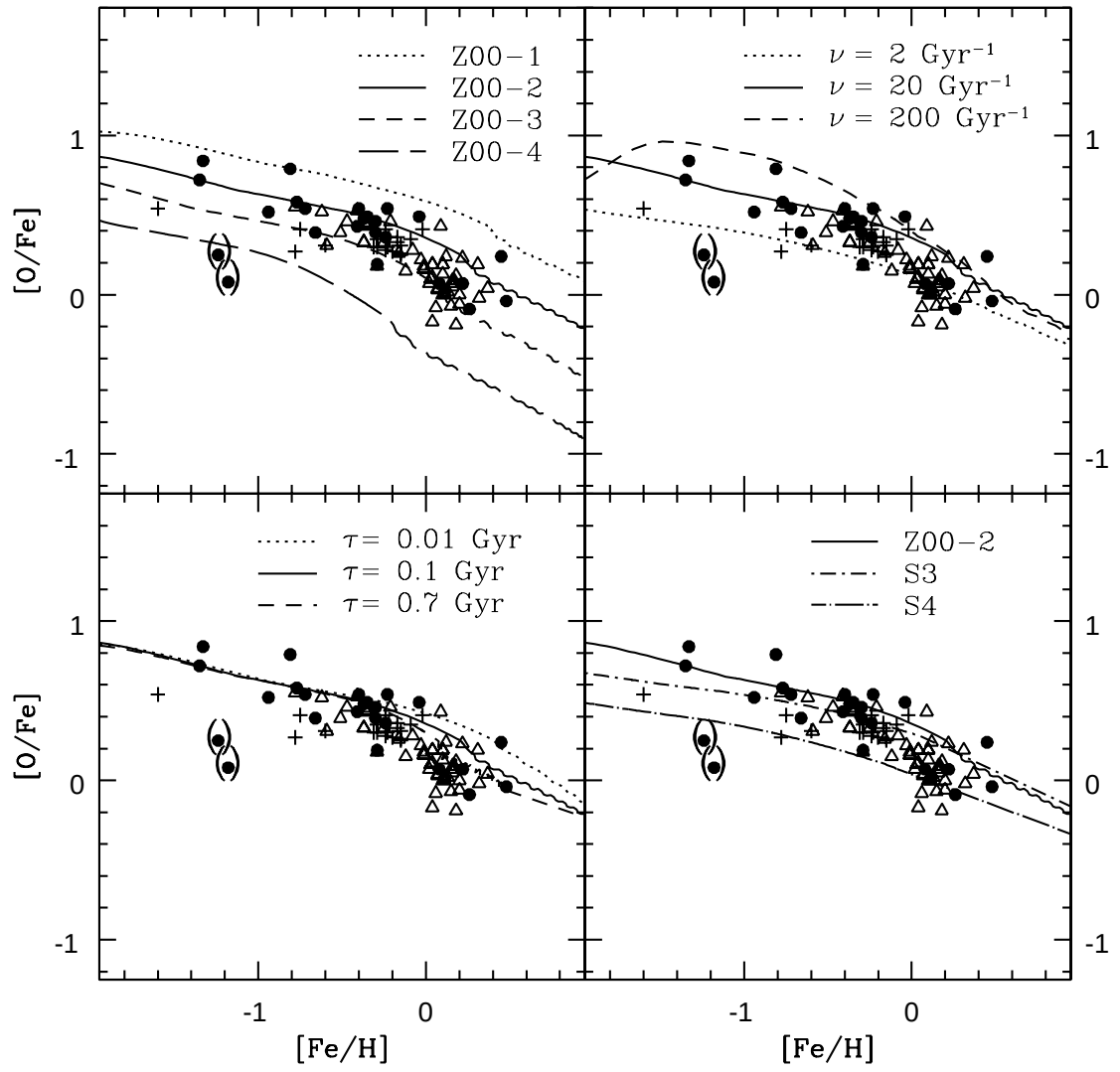

Figure 3.7: Evolution of [O/Fe] vs. [Fe/H] in the bulge for different values of the IMF index (upper left panel; see text for details), star formation efficiency (upper right panel), and infall timescale (lower left panel). The lower right panel shows the results obtained combining a longer infall timescales and milder star formation efficiencies for two different IMFs (see text for details). Data are the same as in Fig. 3.2 (first panel).

IMF of the Type II supernova progenitors. The larger the number of massive stars, the higher the plateau at low metallicities. Model Z00-1 overproduces oxygen, and is not consistent with data. Fig. 3.7 also allows us to exclude a Scalo (1986) exponent (model Z00-4) for massive stars in the bulge, since the corresponding evolution of [α/Fe] vs. [Fe/H] lies well below the observed data points. A Salpeter (1955) IMF (model Z00-3) cannot be excluded on the basis of these abundance ratios; however, it was ruled out by the metallicity distribution plot.

Concerning the star formation efficiency, a value of $\nu = 20$ Gyr^{-1} is consistent with the observed abundance ratios, whereas lower or higher values seem to be at variance with the (few) lowest-metallicity data. The model with $\nu = 200$ Gyr^{-1} predicts values of [O/Fe] which are larger than those of the reference model at low metallicities, but then the gas is consumed very rapidly and star formation cease; this gives rise to a sharper decrease in the [O/Fe] ratio at higher metallicities. The predicted slope is compatible with observations, however the absolute amount of oxygen enhancement is slightly overestimated, and in any case this model was already excluded on the basis of the metallicity distribution (Fig. 3.5). It is noteworthy that even though the star formation stops much earlier in time for higher ν's, the model trajectory before the wind still spans the same range in [Fe/H] for all values of the star formation efficiency ν. This is because at high values of the star formation efficiency, higher metallicities are attained in shorter times.

On the basis of the metallicity distribution, we already saw that models with $\nu = 2$ and 200 Gyr^{-1} must be excluded; considerations derived using the [O/Fe] abundance ratio provide a useful consistency check. We then suggest that a value of 20 Gyr^{-1} can fit both the metallicity distribution and the abundance ratios.

Instead, changing the infall timescale from 0.01 to 0.7 Gyr has almost no effect on the evolution of the [O/Fe] abundance ratio, and this holds also for other α-elements, if we exclude a small improvement of the agreement with data in the $\tau = 0.7$ Gyr case (which however, as well as the $\nu = 200$ Gyr^{-1} case, is excluded by the metallicity distribution plot). Therefore, there is no way of distinguishing between these models on the basis of considerations about abundance ratios, although we already excluded the cases of $\tau \ll 0.1$ Gyr and $\tau > 0.1$ Gyr which yielded metallicity distributions in contrast with the observed ones.

Finally, we discuss the results obtained with the "supplementary" models S3 and S4, whose metallicity distribution was consistent with observations. We can see that it

is necessary to assume a very flat IMF (model S3) to avoid underestimating the [O/Fe] ratio with the adoption of $\tau = 0.7$ Gyr and $\nu = 2$ Gyr^{-1}, and the predicted slope is much flatter than the observed one. For even longer timescales, flattening the IMF is no longer sufficient to fit the data. This is due to the fact that Type Ia supernovae have more time to pollute the interstellar medium with Fe causing the plot to turn down, falling below the observations. Therefore, formation timescales longer than ~ 1 Gyr must be excluded in any case. This is the consequence of the time-delay model for Type Ia supernovae in the case of different star formation histories, as already pointed out by Matteucci & Brocato (1990) and Matteucci (2000).

Other α-elements

In Figure 3.8 are shown the evolutionary plots of the abundance ratios of several α-elements (O, Mg, Si and Ca) to Fe versus Fe abundance, compared to the the data of the IR spectroscopic database and Fulbright et al. (2007). For O and for Mg also data from Zoccali et al. (2006) and Lecureur et al. (2007), respectively, were employed. We also show a solar neighbourhood reference line for comparison, calculated according to François et al. (2004). The plots are normalised to the Grevesse & Sauval (1998) solar abundances. A striking aspect of the predicted [α/Fe] vs. [Fe/H] relation is that the slope of the [α/Fe] ratios changes only at [Fe/H] $\simeq 0$ for the reference model, in agreement with the data and at variance with the solar vicinity where this occurs at [Fe/H] $= -1.0$. Indeed, it is evident that a star formation history and an IMF such as those suitable for the solar neighbourhood give results which do not agree with the bulge observations, the general trend being to severely underestimate the data especially at [Fe/H] $\gtrsim -1$, when Type I supernovae, whose formation is favoured by the steeper IMF, start polluting the interstellar medium considerably.

It is worth noting that our reference model predicts that the slopes of [O/Fe] and [Mg/Fe] vs. [Fe/H] are different, the latter being less steep. This is mainly due to the fact that whereas magnesium is mainly produced by a restricted range of stellar masses (around $20 - 25 M_{\odot}$) oxygen is produced by a broad interval of stellar masses, (from 10 to $100 M_{\odot}$) the O/Fe production ratio increasing with stellar mass. This different trend is present also in the solar vicinity data (see François et al. 2004) and is confirmed in the bulge by the observations of Fulbright et al. (2007), which cover a larger range of metallicities than the IR spectroscopic database (i.e. [Fe/H] $\gtrsim 0$ and [Fe/H] $\lesssim -1$).

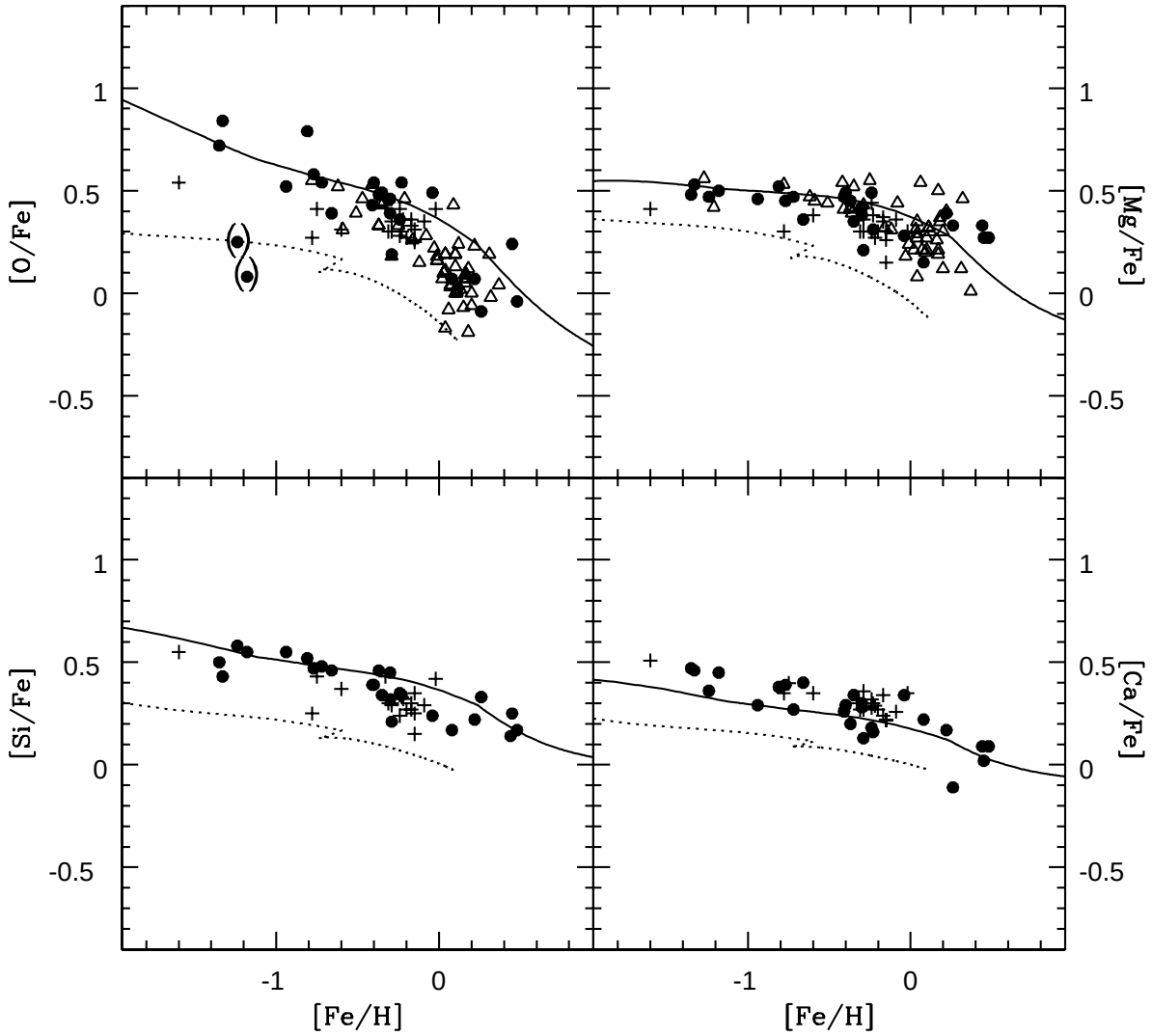

Figure 3.8: Evolution of [α/Fe] vs. [Fe/H] in the bulge for O, Mg, Si, Ca for the reference model (solid line). We also plotted a solar neighbourhood reference line (dotted line) for comparison. Data are the same as in Fig. 3.2. Both observations and predictions are normalised to the Grevesse & Sauval (1998) solar abundances.

This point will be treated more extensively in the next Chapter.

Carbon

Figures 3.9 and 3.10 show the evolutionary behaviours of C and N, which, in contrast to the α-elements, are mainly produced by low- and intermediate-mass stars (and therefore on long timescales). The available dataset for carbon is limited to the measurements of the giant stars, which however are known to undergo mixing processes along the red giant branch, severely affecting the carbon abundances (in fact, we can immediately see that none of the models lie beneath the observations, since carbon is likely to be depleted during the evolution along the red giant branch). Hence, the comparison between models and observations cannot allow to firmly constrain the models and to reach strong conclusions in general. The observations can only provide a lower limit to any plausible model.

The behaviour of [C/Fe] at low metallicities is largely affected by the assumed star formation efficiency, just as in the case of oxygen, whereas the curves show less discernible differences above the solar metallicity. A high value of the star formation efficiency ($\nu = 200$ Gyr^{-1}) enhances the number of stellar generations and therefore accelerates the formation of intermediate-mass stars which are the main C producers, but again [C/Fe] falls below the predictions of the reference model due to fast gas consumption. The steeply falling trend of [C/Fe] until ∼solar [Fe/H] is due to the fact that the C/Fe production factor is decreasing with decreasing mass for high-mass stars. In this case too, abundance data for metal-poor bulge stars can confirm or refute the conclusions reached on the basis of the metallicity distribution, even though large values of ν seem again excluded.

A change in the IMF has a major impact on the contribution from low-mass stars. The plots show a bump at [Fe/H] ranging from ~ -0.4 to 0.4, which corresponds to the time at which the first intermediate mass stars contribute to C enrichment, with the exception of the Z00-1 IMF, for which the star formation ceases before the bulk of intermediate-mass stars have time to die. This bump is not visible in the solar neighbourhood, and its occurrence in the bulge is related to the strong metallicity-dependence of the adopted C yields for low- and intermediate-mass stars (Van den Hoek & Groenewegen 1997), combined with the fact that in the bulge high metallicities

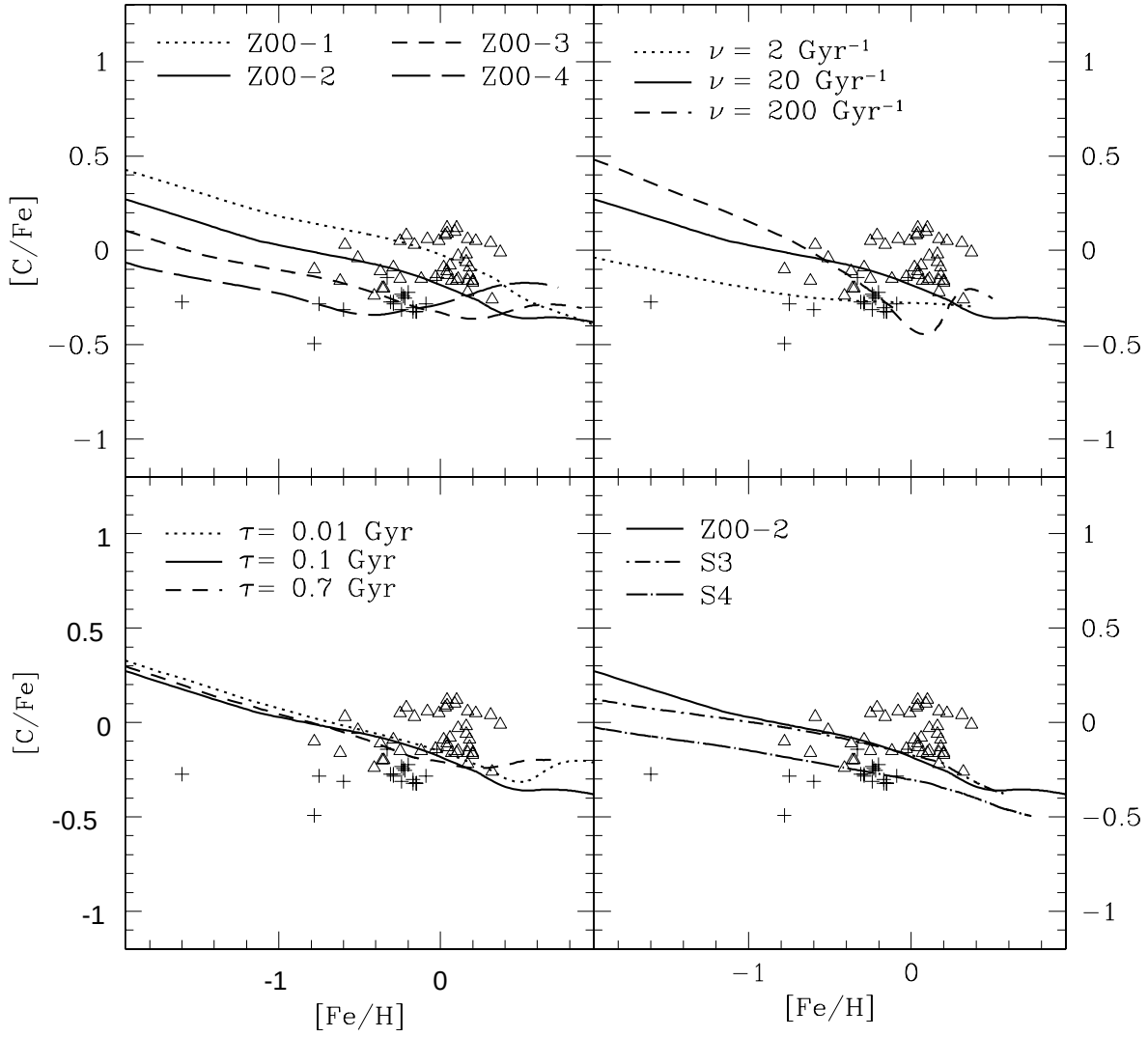

Figure 3.9: Evolution of [C/Fe] vs. [Fe/H] in the Galactic bulge for various choices of the IMF (upper left panel) star formation timescale (upper right panel), and infall timescale (lower left panel). The lower right panel shows the results obtained combining a longer infall timescale and a milder star formation efficiency for two different IMFs (see text for details). Data are from the IR spectroscopic database (plus signs; see text for detailed references) and Lecureur et al. (2007, triangles).

are reached very early. The feature is more pronounced for larger values of x because the formation of low- and intermediate-mass stars is favoured by these steeper IMFs. This is particularly evident from the difference between the plots adopting a Salpeter (1955) and a Scalo (1986) IMF, respectively. Before the onset of the intermediate-mass dominated regime, the amount of C enrichment increases for flatter IMFs due to the enhanced C production from massive stars; on the contrary, when the massive star dominated regime ends, C production is increased remarkably for steeper IMFs due to the enhanced contribution from low- and intermediate-mass stars. Again, the Scalo (1986) IMF looks rather implausible, since the predicted trend almost lies beneath all the data points, and this is likely to mean that C is underproduced for all metallicities in this model.

No appreciable change is seen when the adopted gas infall timescale is varied, with the exception of a slightly different position of the occurrence of the bump. The plots resulting from models S3 and S4 are also shown. Bearing in mind the paucity of data below [Fe/H] ~ -0.5, the model S4 predicts a trend which passes below the bulk of data points at [Fe/H] ~ 0.0, and since as we already stated C is likely to be affected by stellar evolution, this model probably strongly underpredicts the [C/Fe] ratio, again due to the Fe contribution from Type Ia supernovae. Instead, model S3 leads to a larger C production, the trend being only flatter than that of the reference model.

In any case, given the C depletion in giants, all models are likely to underestimate to some extent the pristine C abundance in the bulge giants especially at supersolar metallicity. Mass loss from massive stars (Maeder 1992; Meynet & Maeder 2002, 2003, 2005) can overcome this problem, since the C yield for stellar masses above $40M_{\odot}$ in the Maeder (1992) calculations reaches values which are more than one order of magnitude larger than the corresponding yields without mass loss. Preliminary results indicate that a strong increase of the [C/Fe] ratio indeed occurs around solar [Fe/H]. However, the effect of mass loss on the evolution of the C abundance in the solar neighbourhood must be discussed before drawing conclusions concerning the Galactic bulge.

The influence of the mass loss mechanism on the stellar yields and chemical evolution will be extensively discussed in the next Chapter, together with its detailed effects on the [O/Mg] ratio both in the Galactic bulge and in the solar neighbourhood.

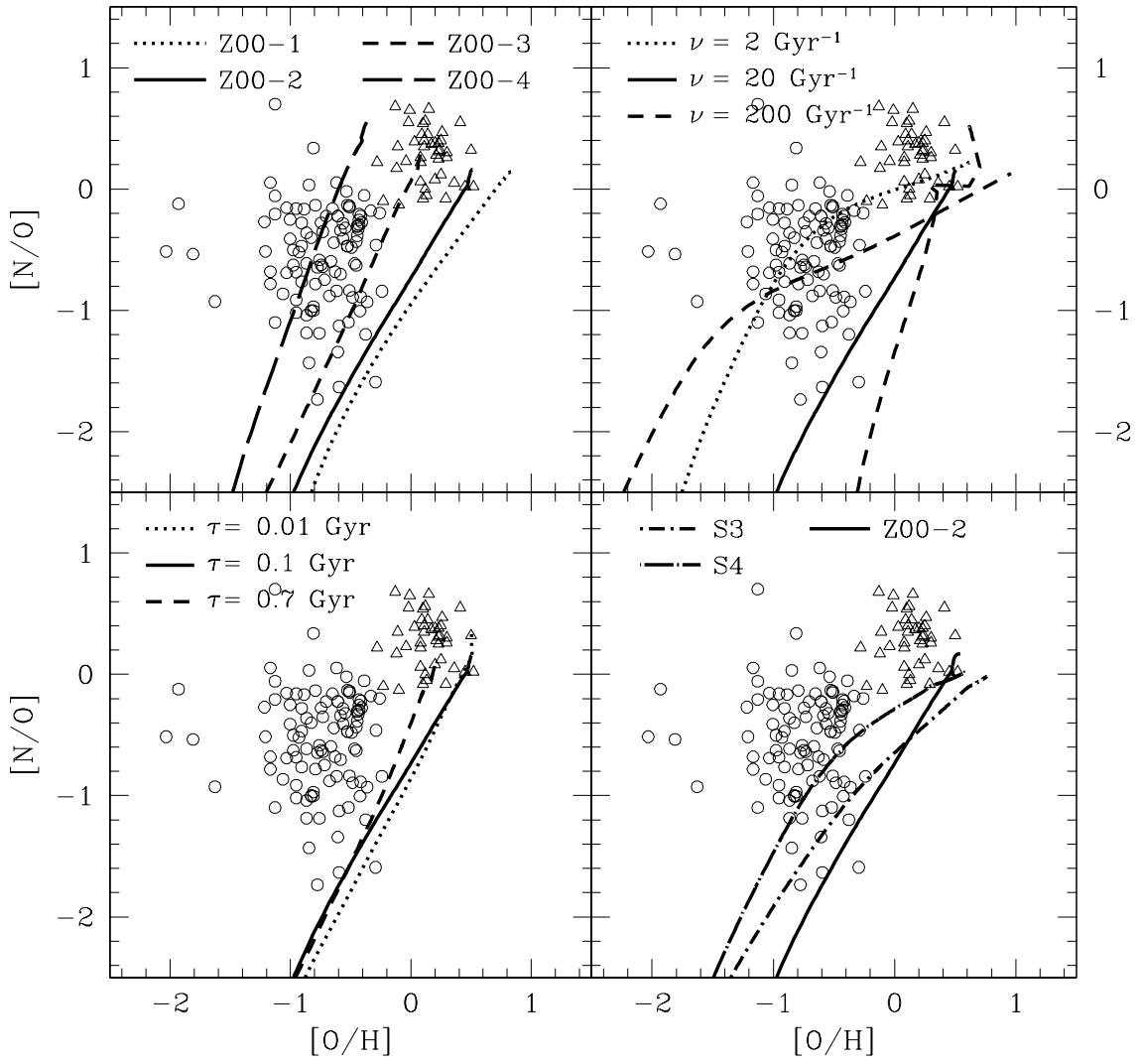

Figure 3.10: Evolution of [N/O] vs. [O/H] in the Galactic bulge for various choices of the IMF (upper left panel) star formation timescale (upper right panel), and infall timescale (lower left panel). The lower right panel shows the results obtained combining a longer infall timescale and a milder star formation efficiency for two different IMFs (see text for details). The abundances measured from bulge planetary nebulae, represented by the open circles, are taken from Górny et al. (2004), while abundances from giants (triangles) are taken from Lecureur et al. (2007).

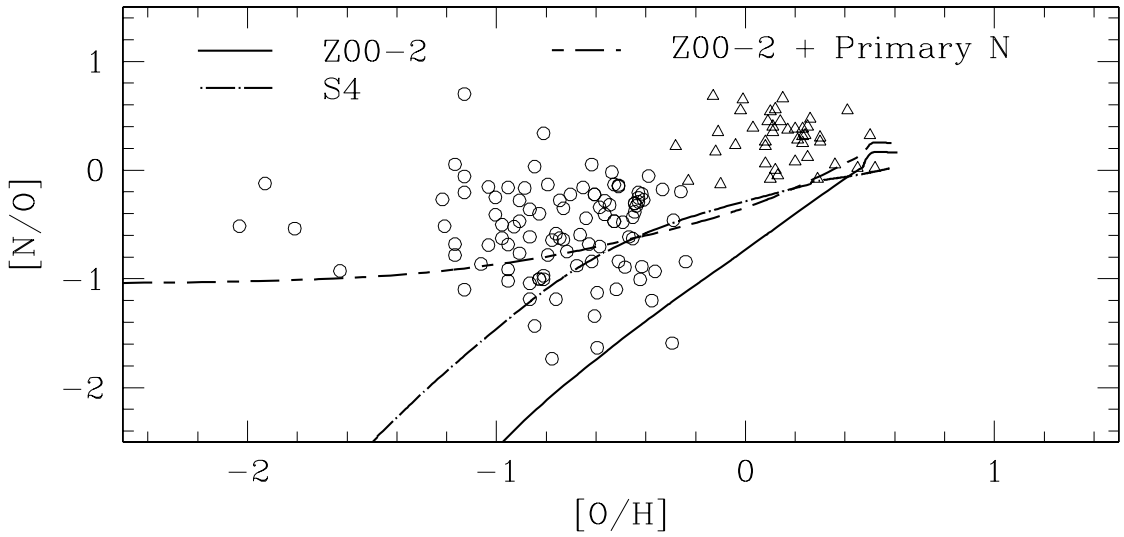

Figure 3.11: Evolution of [N/O] vs. [O/H] (right panels) in the Galactic bulge in our reference model compared to a model where primary production of N from massive stars is assumed (Matteucci 1986) and to model S4. Data are the same as in Fig. 3.10.

Nitrogen

Nitrogen is the element for which our reference model yields the less satisfactory agreement with data: in fact, it tends to lie much below the observational points, following their lower envelope. This is true also of the solar vicinity. As we can see from Fig. 3.10, there is no way of reproducing the average trend of the [N/O] abundance ratio with [O/H] for single-parameter variations unless we adopt parameters which have proved to lead to results at variance with other constraints: e.g. a very low star formation efficiency, which results into an underproduction of oxygen with respect to nitrogen and was dismissed on the basis of the resulting metallicity distribution (and also to some extent on the basis of the [O/Fe] plot); or a steep IMF, favouring the formation of low- and intermediate-mass stars (which are supposed to produce the bulk of N), which did not reproduce either the metallicity distribution or the evolution of [α/Fe] vs. [Fe/H].

A good agreement is instead achieved with the S4 case, since it achieves the same effect of a low efficiency of star formation (i.e. oxygen underproduction) while the longer formation timescale does not influence the evolution of abundance ratios. Models S3 still somewhat improves the match with data relative to the reference model, but the flatter IMF favours O enrichment with respect to model S4.

However, there is another way to obtain an acceptable fit to the observed abundances. In standard chemical evolution models nitrogen production from massive stars is supposed to be purely secondary, i.e. N is created starting from seed nuclei of C already present in the gas out of which the stars were born. Also low- and intermediate-mass stars are supposed to produce N in a secondary fashion but some primary N can be produced in intermediate mass stars during the third dredge-up episodes in conjunction with *hot-bottom burning*[3] (Renzini & Voli 1981; Van den Hoek & Groenewegen 1997). The consequence of the secondary production is that the abundance of nitrogen should increase with metallicity in the earliest evolutionary phases, and that is what most evolutionary models of the Galaxy predict, not only for the bulge, but also for the solar neighbourhood (Ballero et al. 2006; Chiappini et al. 2005).

Therefore, we investigate what happens to the reference model if we assume that massive stars of all masses produce a constant amount ($0.065 M_{\odot}$) of primary N at every metallicity. This hypothesis follows from the heuristic model of Matteucci (1986). The results are shown in Fig. 3.11 together with the plot of model S4. We see that this model seems to reproduce the average trend of the observations better than the standard model and, although it adopts an *ad hoc* assumption, it is useful to understand that some mechanism of primary production of nitrogen is likely to occur at any metallicity in massive stars. For example, Meynet & Maeder (2002) calculated that stellar rotation can produce primary nitrogen in massive stars, and although Chiappini et al. (2003b) demonstrated that their rotation yields are insufficient to produce the observed trend in the solar neighbourhood, this hypothesis is the most promising one, as shown by Chiappini et al. (2006). We thus suggest that a continuous primary N production from massive stars is necessary at any epoch, in analogy with what is required in the solar vicinity (see Chiappini et al. 2005, for an extensive discussion on this point).

From Fig. 3.10 one can also notice that model S4 differs from model Z00-2 with primary N for $[O/H] \lesssim -1$, since while in the latter the [N/O] ratio is almost independent of [O/H], in the S4 model the plot curves down sharply at low metallicities due to secondary production from massive stars, and at $[O/H] \sim -1$ primary production from low- and intermediate-mass stars becomes dominant.

A certain amount of self-pollution is required in any case to reproduce the [N/O] ratios measured in giants for $[O/H] \gtrsim 0$.

[3]The penetration of the convective envelope into the hydrogen burning shell, which leads to nucleosynthetic processes at the base of the envelope.

3.4 Summary and conclusions

We have tested our new chemical evolution models for the Galactic bulge against new observations, unavailable at the time of earlier chemical evolution models (e.g., Matteucci & Brocato 1990; Renzini 1993; Matteucci, Romano & Molaro 1999; Mollá et al. 2000). We have considered a scenario involving evolutionary timescales much faster than in the solar neighbourhood and in the halo as the most probable one. We have also adopted new chemical yields suggested by François et al. (2004) which provided the best fit to the solar neighbourhood abundance trends in the model of Chiappini et al. (2003b).

The agreement between the new observations and our predictions is quite good, especially for the Fe abundance distribution and the [α/Fe] trends.

Order-of-magnitude changes in the main parameters determining chemical evolution (star formation efficiency, stellar IMF, timescale of gas collapse) were applied in order to explore the consequences of such changes on the predicted stellar metallicity distribution and trend of chemical abundances as a function of metallicity.

Our main conclusions can be summarised as follows:

- A short formation timescale combined with a high star formation efficiency fits both the observed metallicity distribution and chemical abundance ratios. This is typical of a star formation history in a burst regime, i.e. strongly concentrated in the first stages of the lifetime of the system and vanishing very quickly, in analogy with elliptical galaxies. We suggest an efficiency of star formation of the order of 20 Gyr^{-1}. However the assumption of a closed box must be given up since it gives rise to an excessive amount of low-metallicity stars (even though not as seriously as in the case of the G-dwarf problem for the solar neighbourhood). A finite, though small, accretion time is instead required. We suggest that this timescale should be of the order of 0.1 Gyr.

- There exists a sort of degeneracy between the gas infall timescale and the efficiency of star formation, in the sense that values of τ longer than 0.1 Gyr can combine with values of ν lower than 20 Gyr^{-1} in order to match the observed metallicity distribution. However, such a degeneracy is broken when we consider also the evolution of [O/Fe] vs. [Fe/H] and in any case values of τ longer than 1 Gyr do not allow to fit the observed metallicity distribution as well.

- An IMF flatter than those suitable for the solar neighbourhood properties, such as that of Scalo (1986) or Weidner & Kroupa (2005), is necessary to reproduce the observational constraints. Namely, a value of $x = 0.95$ for massive stars (even smaller than that proposed by Matteucci et al. 1999, which was $x = 1.1$) gave the best overall fit. This can be theoretically understood if we note that the star formation in the bulge proceeds like in a burst and there are several suggestions in the literature about a top-heavy IMF in starbursts (e.g. Baugh et al. 2005, Nagashima et al. 2005). Figer (2005) also finds a flat IMF in the Arches cluster near the Galactic centre. The adopted flattening below $1M_{\odot}$ ($x = 0.33$), as suggested by luminosity function measurements (Zoccali et al. 2000) does not affect significantly the abundance distribution. However, extremely flat IMFs (e.g. that of Z00-1 model), if extrapolated to massive stars, will lead to some degree of oxygen overproduction.

- The adoption of the reference model explains the behaviour of the different [α/Fe] abundance ratios with metallicity very well, and predicts different slopes for different α-elements, according to their nucleosynthesis. There is no need to invoke a second infall episode, as suggested by other authors (Mollá et al. 2000; Costa et al. 2005) to explain the observed values of the abundance ratios. We do not exclude however a second infall episode on a much longer timescale such as that hypothesised by Mollá et al. (2000) as it may help explain the presence of a very young stellar population confined to the very centre of our Galaxy (e.g. Groenewegen & Blommaert 2005), but it must involve a minor fraction of the bulge gas mass.

- A certain amount of primary nitrogen from massive stars might be required in order to reproduce the average trend of [N/O] vs. [O/H] with the reference model. The same conclusion was reached for the solar neighbourhood by Chiappini et al. (2005) and Ballero et al. (2006). The phenomenon of primary N production from massive stars as a result of rotation was studied by Meynet & Maeder (2002, 2003, 2005) and Hirschi (2007) and although their yields are still not sufficient to explain the observed trend, this seems the most promising way (see Chiappini et al. 2006). These considerations followed from observations of N and O abundances in planetary nebulae; in order to firmly assess this point, abundance measurements in stars which have not experienced nitrogen self-enrichment are required, especially

at low metallicities. In alternative, carbon measurements in the same planetary nebulae we have considered might allow an estimate of the amount of N synthesised by the planetary nebula progenitor.

- In the near future new sets of empirical metallicity and abundance pattern distributions in different fields and based on high-resolution spectroscopy will also become available. This will dramatically improve the chance of a more robust and quantitative comparison between theory and observations, with the ultimate goal of drawing the formation and chemical evolution history of the Galactic bulge.

Chapter 4

O and Mg evolution in the Galactic bulge and solar neighbourhood

4.1 Mass loss and stellar yields

Mass loss in massive stars occurs due to the interaction of radiation flowing through the atmosphere of a star and the matter in the atmosphere. In massive stars, radiation pressure is important and their luminosity is a non-negligible fraction of the star's Eddington luminosity[1], i.e. the luminosity at which the radiation pressure overwhelms the gas pressure in the atmosphere, and which is given by:

$$L_{Edd,*} = \frac{4\pi c G M_{env}}{k_s} \tag{4.1}$$

where M_{env} is the envelope mass and k_s is the stellar surface opacity. The ionised atoms in the atmosphere absorb radiation and a net movement outwards is achieved; the absorbers are mainly metals. In the so-called Wolf-Rayet stars, with masses above $25-30M_{\odot}$, mass loss rates can reach $\dot{M}_{WR} \simeq 10^{-4}M_{\odot}$/yr. This way, they can lose their hydrogen envelope and explode as Type Ib supernovae (core-collapse supernovae with no H in their spectra), or even lose the helium envelope, in which case they explode as Type Ic supernovae (which miss He as well in their spectra).

Stellar yields can be affected by mass loss in massive stars. Maeder (1992) computed the wind contributions in He, C, N, O and Ne in stars in the mass range $1-120M_{\odot}$ and for metallicities $Z = 0.001$ and $Z = 0.02$. He found that, at solar metallicities and

[1]The reader must not confuse the stellar Eddington luminosity mentioned here with the Eddington luminosity defined for black holes in §6.5.2.

above, large amounts of He and C are ejected into the interstellar medium, reducing the synthesis of heavier elements; thus C and He are produced at the expense of O, while the same effect is not seen at low metallicities. Therefore, the nucleosynthesis production strongly depends on the initial stellar metallicity. The metallicity dependence of the stellar wind is due to the opacity of the material in the radiation-driven mass loss of massive stars, as originally proposed by Lucy & Solomon (1970). The effect of mass loss on stellar yields as a function of metallicity is particularly strong for Wolf-Rayet stars. By means of these stellar models Maeder (1992) was able to reproduce the number statistics of Wolf-Rayet and O-type stars in nearby galaxies with various metallicities. Later, Langer & Henkel (1995) also computed He and CNO isotope yields for mass-losing stars in the range $15 \leq M/M_{\odot} \leq 50$. They also found drastic differences relative to models without mass loss for the yields of oxygen in metal-rich stars more massive than $30M_{\odot}$.

More recently, Meynet & Maeder (2002, 2003, 2005) and Hirschi (2007) have computed a grid of models for stars with masses $> 20M_{\odot}$, including rotation and metallicity-dependent mass loss. The effect of metallicity-dependent mass loss in decreasing the O production in massive stars was confirmed, although they employed significantly lower mass loss rates, based on work by Vink et al. (2000) and Nugis & Lamers (2000). The new and improved mass-loss rates are factors of 2 to 3 lower than previously adopted by Maeder (1992); however, with these mass-loss rates and the inclusion of rotation the models are able to reproduce the frequency of Wolf-Rayet and O stars, the observed WN/WC ratio[2], and the observed ratio of Type Ib/Type Ic supernovae at different metallicities. It appears that the earlier high mass-loss rates made up for the omission of rotation in the stellar models. In galactic chemical evolution models, the effect of the Maeder (1992) yields was studied by Prantzos, Aubert & Audouze (1996), who concluded that the mass loss in massive stars has strong effects on the production of C and O.

In summary, the effect of metallicity-dependent mass loss on stellar yields appears relevant for stars with solar metallicities or larger, and therefore it should be taken into account in computing the bulge chemical evolution and the late stages of chemical evolution in the solar vicinity.

[2]Wolf-Rayet stars are subdivided into three subgroups according to their spectral features. Among these subgroups, WN are Wolf-Rayet stars where N dominates over C in their spectra, and WC are those where C dominates instead. The rare WO stars have C/O < 1.

4.2 Evidence for metallicity-dependent O yields

Oxygen and magnesium are among the most easily understood elements because their synthesis is restricted to well known processes in the cores of massive stars and they are thought to be unaffected by the complications of explosive nucleosynthesis (e.g. Woosley & Weaver 1995). They are particularly interesting as probes of massive stars and the SFR in chemically evolving stellar systems. Thus, one might expect that O and Mg abundances should vary in lock-step in all, or most situations, since O and Mg are both thought to be produced only by stars that end as core-collapse supernovae.

However, McWilliam & Rich (2004) found a steeply declining [O/Fe] ratio in the bulge stars with a slope almost consistent with no production of O above [Fe/H] $\gtrsim -0.5$. They suggested an O yield decline due to winds from massive stars, related to the Wolf-Rayet phenomenon. Later Fulbright et al. (2007) noted the apparent discord between nearly flat, enhanced, [Mg/Fe] and yet declining, although enhanced [O/Fe] in the bulge above [Fe/H] ~ -1.0; again, they suggested declining metallicity-dependent O yields related to the Wolf-Rayet phenomenon. Lecureur et al. (2007) also found a decreasing trend for [O/Mg] in the bulge stars, and suggested a difference in the stellar yields of O and Mg from massive stars.

This observed difference between Mg and O trends could potentially lead to a conflict in the estimated SFR and formation timescale of the bulge: if the steeper decline of [O/Fe], compared to [Mg/Fe], with increasing metallicity is due to the addition of Fe from Type Ia supernovae, then a lower SFR and longer bulge formation timescale would be indicated from O than for Mg. If the different decline rates for O and Mg are due to the supernova yields it is necessary to understand them in a consistent picture of nucleosynthesis and chemical evolution. Because O and Mg are produced only in the hydrostatic cores of massive stars, then if the O/Mg yield ratio declines as a function of metallicity, the same trend should be present in stellar systems, no matter what the SFR, provided that the formation timescale is long enough to permit all masses of Type II supernovae to occur. In fact, different slopes in the [Mg/Fe] and [O/Fe] ratios are visible in metal rich stars in the solar vicinity, where the [Mg/Fe] seems to reach a plateau for [Fe/H] > 0, but the [O/Fe] ratio continues to decrease (see Edvardsson et al. 1993; Castro et al. 1997; Feltzing & Gustafsson 1998; Bensby et al. 2005). This trend also suggests the effect of strongly metal dependent O yields in metal rich massive stars.

To test the metallicity dependence of the O/Mg ratio we compared (McWilliam et al. 2008) the abundance ratio of O/Mg seen in the Galactic bulge and in the Galactic

thin and thick disks. In particular we use [Mg/H] and [O/H] as metallicity indicators, rather than [Fe/H], in order to eliminate the effect of Fe from Type Ia supernovae. The observational evidence for a decrease in the oxygen yield, relative to magnesium, from Type II supernovae with increasing metallicity is summarised in Fig. 4.1. In the upper panel of Fig. 4.1 we show a plot of the [O/Mg] versus [Mg/H] for the bulge from the IR spectroscopic database (defined in Chapter 3), Zoccali et al. (2006), Fulbright et al. (2007), and Lecureur et al. (2007), compared with points for the solar neighbourhood thin and thick disks from Bensby et al. (2005). Contrary to what one might expect for two α-elements produced by the same stars the [O/Mg] ratio is not flat, but declines steeply for [Mg/H] values larger than -0.5 dex. The same effect is visible both in the bulge and disk stars. Note that in the lower panel of Fig. 4.1 we show the same observed [O/Mg] ratio, but with [O/H] as the metallicity indicator. For the bulge metallicity points we employ the mean [O/H], based on [Fe/H] and a fit to the trend of [O/H] versus [Fe/H]; it was motivated to reduce the scatter in the [O/H] metallicity axis resulting from the use of only the 6300 Å [O I] line for the oxygen abundances. Oxygen is useful as a metallicity indicator, despite the noise, because it contributes more than half of the total metallicity, Z. We avoided using the recent oxygen abundances for thick disk stars by Reddy et al. (2006), because these were based on the high excitation O I triplet lines near 7771 Å, and not on the robust [O I] 6300 Å indicator; the high excitation O I lines require uncertain corrections for non-LTE[3] effects.

In both figures there is a clear decline in the bulge [O/Mg] ratio of ~ 0.8 dex from low to high metallicity, including a markedly steeper descent above solar metallicity. It is notable, and very important, that the [O/Mg] trends for the Galactic disk closely overlap the bulge trends, and that both show the steeper decline above solar metallicity. A similarity in the evolution of the products of Type II supernovae in the disk and bulge is expected because O and Mg are produced on the same timescales. On the other hand, we expect to see the effect of the time delay model in the [α/Fe] ratios. We suggest that, to within the measurement uncertainties, the disk and bulge [O/Mg] versus [Mg/H] trends are the same. However, there is some leeway in this interpretation with a possibility that the bulge [O/Mg] ratios slightly exceed the disk ones for a given [Mg/H]. Some of the individual bulge studies may show offsets from the disk trend, but these are small; in this regard we note that in the Fulbright et al. (2007) study there was some evidence to support a systematic downward zero-point correction to the

[3]Local Thermodynamic Equilibrium.

oxygen abundances, by ~ 0.04 dex; if applied this would make a slight improvement to the already good agreement between disk and bulge O/Mg relations.

Fig. 4.1 also compares the composition of the bulge, formed within the initial $\sim$1 Gyr after the Big Bang, with the composition of disk stars formed up to the present epoch. The trend with [Mg/H] as metallicity indicator is particularly important because the [Mg/Fe] ratios in the bulge are significantly higher than in the disk due to Fe from Type Ia supernovae. Given these differences between the disk and bulge it is remarkable that the [O/Mg] trends with [Mg/H] and [O/H] follow each other so closely.

We begin to understand the O/Mg ratio trend by appreciating that both O and Mg are thought to be produced only by core-collapse supernovae. In particular it should be remembered that O production increases strongly with pre-supernova mass (e.g. Woosley & Weaver 1995), but more important for this investigation is the trend of O/Mg yield ratio with supernova progenitor mass. The François et al. (2004) yields show a strongly increasing O/Mg ratio with mass, with a range exceeding 1.5 dex. This high sensitivity to progenitor mass is similar to the predictions for hypernovae computed by Fryer et al. (2006); however, results from other calculations (Woosley & Weaver 1995, Tsujimoto et al. 1995, Nomoto et al. 1997, Limongi & Chieffi 2003, Kobayashi et al. 2006) show very shallow O/Mg trends with mass. A steeper O/Mg yield ratio with mass is due to Arnett (1991), with a range of ~ 0.5 dex.

If the O/Mg yield ratio is strongly sensitive to the mixture of supernova masses, the observed abundance ratios will be affected by the IMF. In particular, a flatter bulge IMF than the galactic disk would produce a higher [O/Mg] ratio in the bulge, if other parameters remain the same. However, the data seems to show a large overlapping of the [O/Mg] ratio in the bulge and disk stars, although some bulge stars show a higher ratio. In the previous Chapter, a flat IMF for the bulge was suggested in line with previous results (e.g. Matteucci & Brocato 1990, Matteucci et al. 1999), based on the observed bulge stellar metallicity distribution, which cannot be reproduced with the same IMF as the disk with the current set of parameters (this topic will be discussed more extensively in the next Chapter). Thus, the similarity of the O/Mg ratios in the bulge and disk suggests that either the O/Mg yield ratio is quite insensitive to stellar mass, in which case the yields of François et al. (2004) need to be modified, or that the IMF for the bulge is similar to that of the disk, with much less of a difference in slope than indicated in Chapter 3. More data will help to decide whether the abundance ratios in the bulge are higher or equal to those in the solar vicinity, while further theoretical and empirical

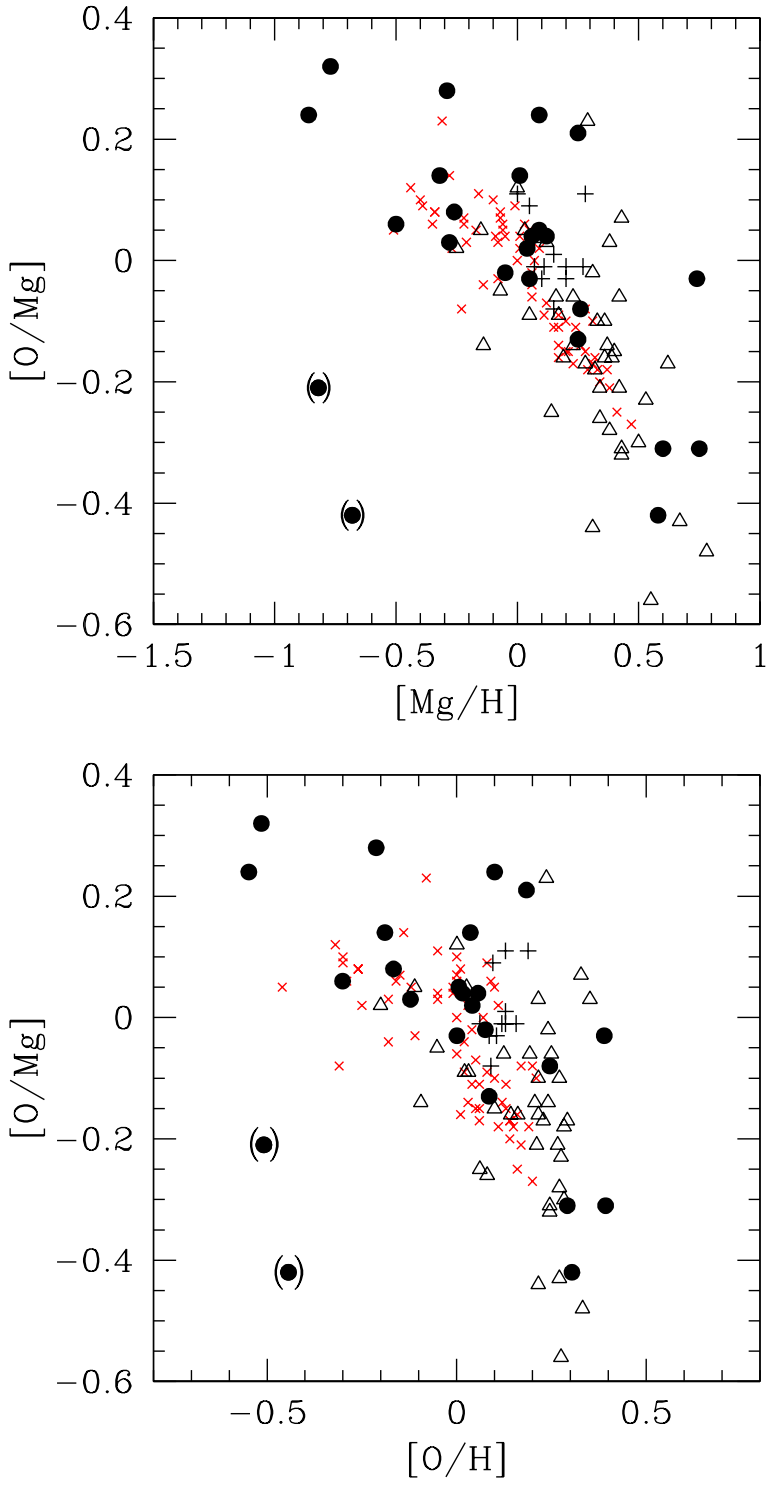

Figure 4.1: Data for the bulge (filled circles, plus signs and open triangles; see Fig 3.2 for references) compared with solar vicinity stars (crosses, Bensby et al. 2005) for [O/Mg] *vs.* [Mg/H] (upper panel) and [O/Mg] *vs.* [O/H] (lower panel).

studies may constrain the O and Mg yields from massive stars.

If O/Mg yields are a function of stellar mass the observed downward slope in [O/Mg] *vs.* [Mg/H] could be explained by a metallicity-dependent IMF, that increases the fraction of low-mass supernovae at higher metallicity; this would apply to both the disk and the bulge, but there is no evidence of a variable IMF in the disk. Therefore, we discard the notion of a metallicity-dependent IMF to explain the observed O/Mg trend.

Supposing that the O/Mg yields increase strongly with stellar mass, then during initial enrichment O/Mg ratios would be higher than at later times, because massive stars are the first to end as supernovae. Thus, over the period spanning the lifetime of massive stars there should be a decline in the average O/Mg ratio of a system. This low-metallicity effect might be seen at a higher metallicity in the bulge than other Galactic locations, due to the high SFR in the bulge. We adopt the simple notion that the observed similarity of the O/Mg slopes for both the Galactic disk and bulge reflects a metallicity modulation of the yields from core collapse supernovae; in principle this could be due to O or Mg yields, or both.

The bulge results are similar to those of Bensby et al. (2004), who identified the decline in [O/Mg] versus [Mg/H] in the Galactic thin and thick disk populations. They considered the possibility that metallicity-dependent O yields from massive stars could explain the observed trend, but dismissed this idea based on their interpretation of the O yields of massive stars from models, including rotation, by Meynet & Maeder (2002). Our understanding is that while rotation does increase the core mass, the effect of decreased O yields with increasing metallicity, due to mass loss, is clear in the works of Meynet & Maeder (2002, 2003, 2005) and Hirschi (2007); the effect on the yields is particularly noticeable for the most massive stars above solar metallicity (Meynet & Maeder 2005, Hirschi 2007). This result holds, despite the decrease in adopted mass-loss rates, compared to Maeder (1992).

4.3 The chemical evolution models

While for the Galactic bulge we made use of the model described in Chapters 2 and 3, for the chemical evolution of the Milky Way disk we adopted the model of Chiappini et al. (1997) with updated nucleosynthesis prescriptions as in François et al. (2004). This model is the so-called *two-infall model* where the halo and part of thick disk are formed during a first relatively short episode (< 2 Gyr) of accretion and star formation,

whereas the thin disk formed out of a second independent infall episode which lasted much longer ($\sim$ 8 Gyr in the solar vicinity) and formed the disk "inside-out". The adopted IMF is the one from Scalo (1986) and is considered constant in space and time; the star formation efficiency is $\nu = 1$ Gyr^{-1}.

In order to investigate the potential effect of mass loss on predicted O/Mg ratios we decided to update our current model with the Maeder (1992) yields that take into account the effect of mass loss for massive stars as a function of metallicity. We used the Maeder (1992) yields, rather than the latest results of Meynet & Maeder (2005), in order to maintain consistency with the pre-existing model employing the Woosley & Weaver (1995) yields; both Woosley & Weaver (1995) and Maeder (1992) models ignore the effects of rotation, but both provide similar yields near solar metallicity. In this way our calculation should show how the metallicity-dependent yields affect the current model.

In Fig. 4.2 we can see the differences between the yields of oxygen of Woosley & Weaver (1995) and Maeder (1992) for two different initial stellar metallicities. The effect of the metallicity-dependent mass loss is evident in the figure: especially for stars with masses larger than $25M_{\odot}$ and solar metallicity the O production is strongly depressed due to mass loss.

4.4 Results

4.4.1 [O/Mg] *vs.* [O,Mg/H]

In Fig. 4.3 we show the same data as in Fig. 4.1, but the theoretical predictions for the bulge and disk are superimposed. As one can see in both cases the slope of the [O/Mg] ratio is very well reproduced by the Maeder (1992) yields. In particular, both the observations and our predictions indicate a sudden steepening of the slope above solar metallicity, with good agreement between the predicted and observed slopes below and above the break-point.

In the present chapter, our model results have been normalised to the solar abundances predicted by the Milky Way model, which gives a very good fit to the Asplund et al (2005) solar abundances. The $\sim$0.2 dex zero-point offset between our predicted bulge [O/Mg] trend and the data suggests that either the yields of François et al. (2004) require adjustment, or that the adopted IMF of our reference model (Ballero et al. 2007a) is too flat, or a combination of these effects. Normalisation of the predictions to solar abundances is also an issue.

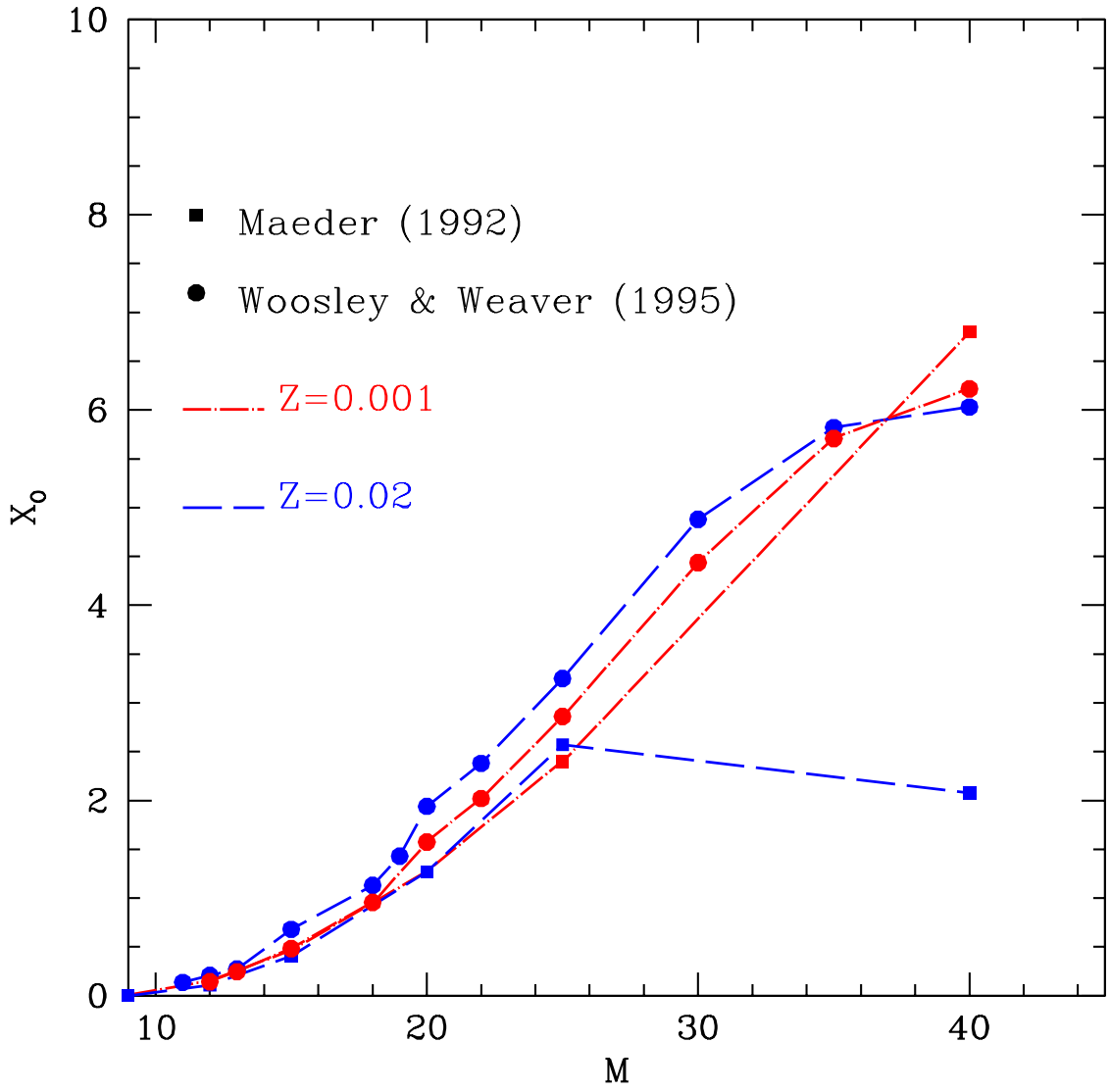

Figure 4.2: Comparison between the O yields of Maeder (1992) and Woosley & Weaver (1995) for massive stars as functions of initial stellar mass. The dramatic decline of O yields from high mass stars at solar metallicity for the Maeder (1992) models is due to mass loss of the outer layers, which prevents He and C from being synthesised into O.

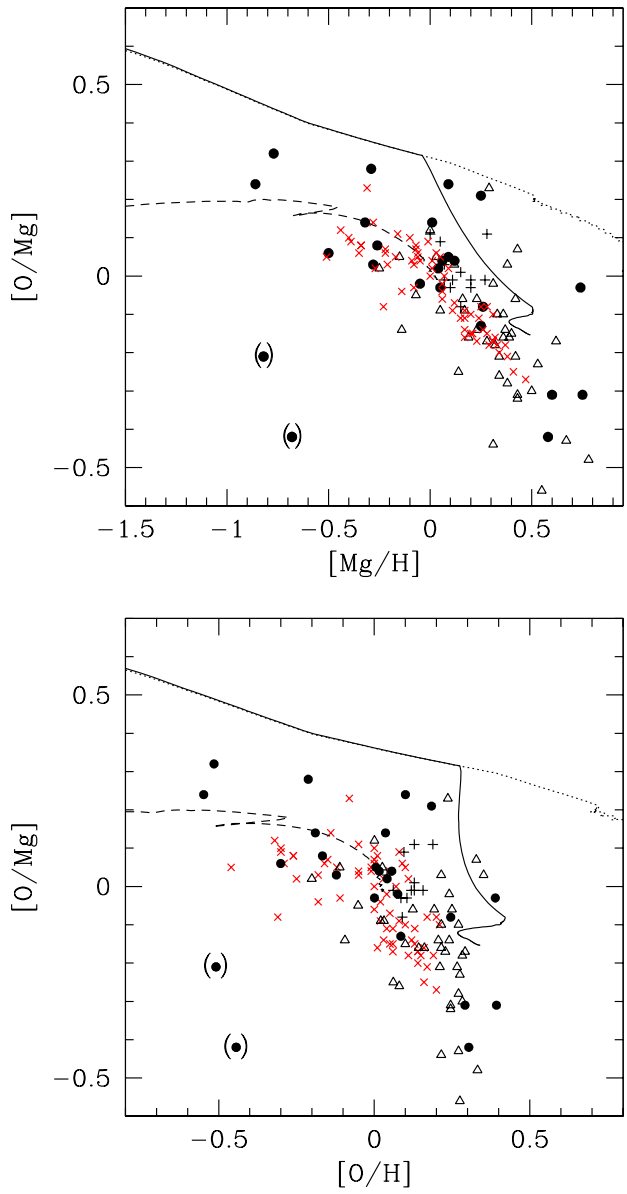

Figure 4.3: Comparison between the predicted [O/Mg] *vs.* [Mg/H] and [O/Mg] *vs.* [O/H] and the observations for the bulge and solar vicinity. The data are the same as in Fig. 4.1. The continuous line is the prediction for the bulge when the Maeder (1992) O yields are considered for metal rich massive stars. The dotted line is the predicted [O/Mg] by our reference model (Ballero et al. 2007a) by adopting the O yields as function of metallicity by Woosley & Weaver (1995). The dashed line represents the prediction for the solar neighbourhood when the O yields by Maeder (1992) are considered. In all models we have normalised the abundances to the solar abundances as predicted by the Milky Way model at $t_{\odot} = 9.2$ Gyr. These predicted abundances are in good agreement with recent solar abundance determination by Asplund et al. (2005).

Given that the bulge metallicity function suggests a flatter IMF than the disk (Ballero et al. 2007b; see next Chapter) and the difficulties involved with inverting chemical evolution models to obtain element yields, we suspect that the problem most likely arises in the adopted O/Mg yields of François et al. (2004). As we noted earlier the O/Mg yield trend with supernova progenitor mass, suggested by the results of François et al. (2004), is much steeper than most theoretical predictions; if this steep slope is in error we would expect to see an artificial zero-point offset in the predicted O/Mg ratio.

The zero-point problem does not concern the main conclusion that diminished oxygen yields, due to mass-loss from high metallicity Type II supernovae are responsible for the observed declining [O/Mg] trend with increasing [Mg/H] in the Galactic bulge and disk. This resolves the apparent discord between the bulge trends of [Mg/Fe] and [O/Fe] with [Fe/H]; now both are consistent with a high SFR in the bulge.

It is worth recalling that Asplund et al. (2005) found a lower O abundance in the sun than Grevesse & Sauval (1998), whereas there is little difference for the abundances of Mg and Fe. In Fig. 4.4 we show the same plot as in Fig. 4.3, but only for the bulge; the agreement between the slope predicted with Maeder (1992) yields and the data is again very good. Again, the predicted absolute values are higher than the data, but this depends on the normalisation to the solar abundances. In our reference model, where the solar abundances were those of Grevesse & Sauval (1998), the predicted [O/Mg] was lower, due to the higher O solar abundance suggested by Grevesse & Sauval (1998) relative to Asplund et al. (2005). In Fig. 4.4 we also show the same model predictions normalised to the Grevesse & Sauval (1998) solar abundances. We stress that the important points are that the slopes and break-points in the [O/Mg] trends with metallicity. It is also important to note that the predicted [O/Mg] in the bulge is higher than in the solar neighbourhood. In our models this mainly depends on the assumed IMF in the bulge which is flatter than in the solar vicinity. Such a flatter IMF seems to be unavoidable in order to reproduce the observed stellar metallicity distribution in the bulge, as extensively discussed in the next Chapter. The bulge parameters of our reference model concerning the IMF, SFR and infall timescale are not affected by the consideration of mass-loss dependent yields investigated here. For the IMF and SFR the work discussed in Chapter 3 was entirely constrained by [O/Fe] at metallicities below solar, for which mass-loss dependent yields are not a factor. While the [O/Fe] predictions of Chapter 3 provided a slightly better fit with in infall timescale near 0.7 Gyr, the metallicity distribution function excluded such value. In any case, the

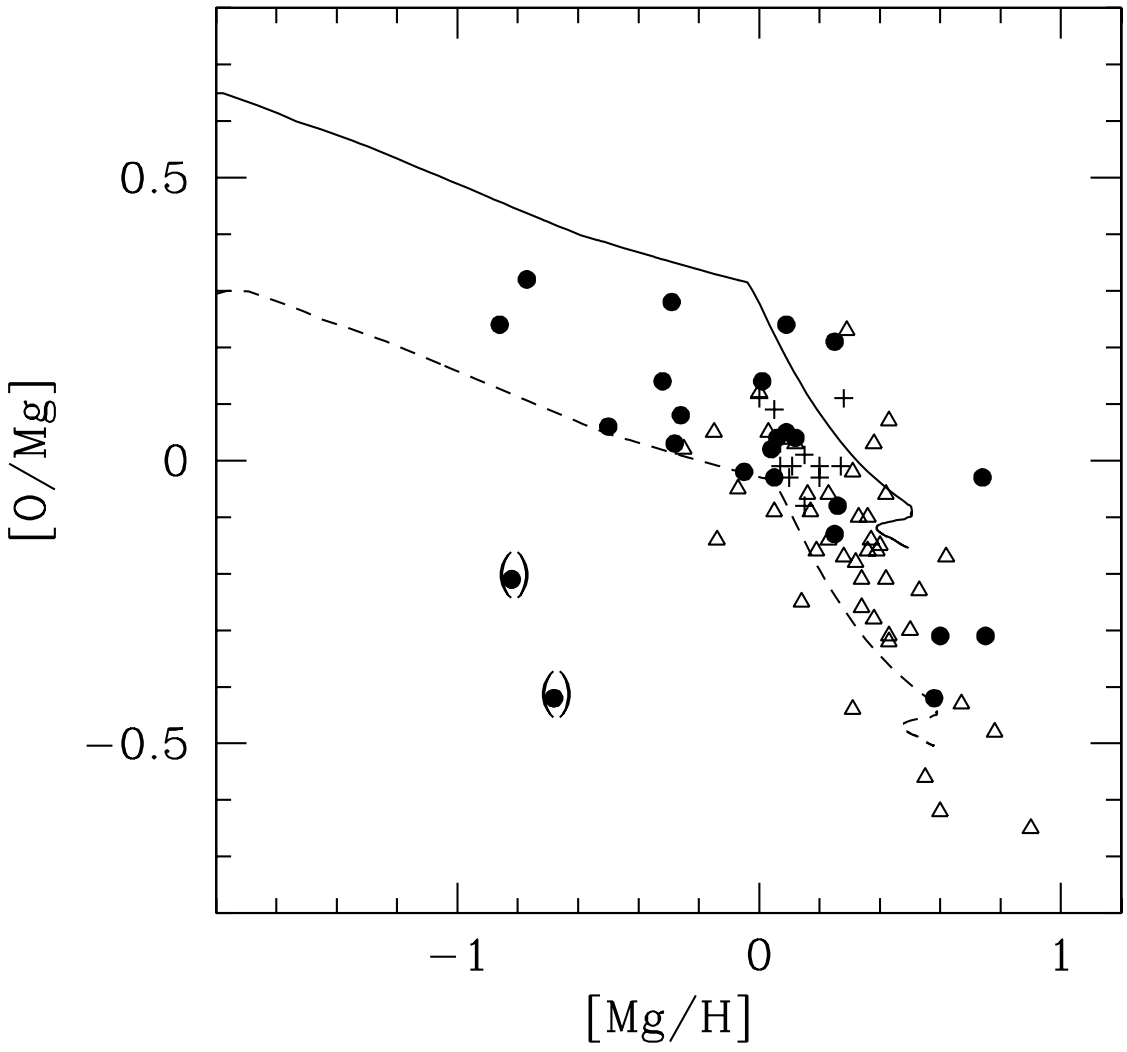

Figure 4.4: Predicted and observed [O/Mg] vs. [Mg/H] only for the bulge. The model (continuous line) is the one with Maeder's (1992) yields. The upper line refers to the predicted bulge abundances normalised to the solar predicted values by the Milky Way disk model, as in the curves of Fig. 4.3. The lower line instead refers to the predicted bulge abundances normalised to the Grevesse & Sauval (1998) solar abundances. The offset between the two curves mainly results from the solar abundances predicted by our model, which is in very good agreement with the one suggested by Asplund et al. (2005), but lower than previous estimates. Data sources: plus signs are the IR spectroscopic database (see §3.2 for specific references); open triangles are the data of Zoccali et al. (2006) and Lecureur et al. (2007); filled circles are the data from Fulbright et al. (2007).

metallicity-dependent oxygen yields considered here are consistent with $\tau = 0.1$ Gyr, which is the value adopted in our reference model.

4.4.2 [O/Fe] *vs.* [Fe/H]

The [O/Mg] *vs.* [Mg/H] or [O/Mg] *vs.* [O/H] plots do not contain the effects produced by the chemical enrichment of Type Ia supernovae, but only depend on the different yields for O and Mg because these two elements are produced on similar timescales. On the other hand, the effect of Type Ia supernova enrichment is clearly visible in the [α/Fe] *vs.* [Fe/H] plots, where the change in slope of the [O,Mg/Fe] ratios is mainly due to the time-delay with which the bulk of Fe is injected into the interstellar medium by Type Ia supernovae. The history of star formation plays an important role in the [α/Fe] versus [Fe/H] diagrams: in the bulge, which is assumed to have suffered an intense, burst-like star formation we expect a long plateau of enhanced α's and a turning point occurring at [Fe/H] ≥ 0, as opposed to the disk where the star formation proceeded much more smoothly and therefore we expect the turning point to occur at lower metallicities; and even more so in dwarf galaxies (Lanfranchi & Matteucci, 2004) where the star formation proceeded extremely slowly, thus giving rise to low [α/Fe] ratios at low [Fe/H]. The predictions for [O/Fe] versus [Fe/H] in the bulge compared with data can be seen in Fig. 4.5, and the fit is again excellent, also in the absolute value. The [O/Fe] predicted by our reference model (Ballero et al. 2007a) at high metallicities was flatter and in less good agreement with the observed points.

The metallicity-dependent decline in the oxygen yield brings understanding to the long-standing apparent discrepancy between the trend of [O/Fe] at high [Fe/H] and the [α/Fe] trends for Mg, Si, Ca and Ti in the Galactic disk. In the standard time-delay explanation for the decline of [α/Fe] with [Fe/H] all these elements should show similar declines. However, in the Galactic disk [O/Fe] continues a roughly linear decline above solar [Fe/H] to negative [O/Fe] values (Edvardsson et al. 1993, Castro et al. 1997, Feltzing & Gustafsson 1998, Bensby et al. 2004). The other α-elements reach a low plateau in [α/Fe], at the solar ratio, beginning near [Fe/H] ~ -0.4 to -0.2 dex; and this plateau continues to the most metal-rich disk stars. The unusual behaviour of oxygen is unexpected from the pure time-delay explanation for the decline in [α/Fe] with increasing [Fe/H] in the Galactic disk; however, the time-delay model well describes the plateau seen in the other α-elements, the α-enhancements seen in bulge stars (McWilliam & Rich 1994; Fulbright et al. 2007), subsolar [α/Fe] ratios seen in small subgroups of

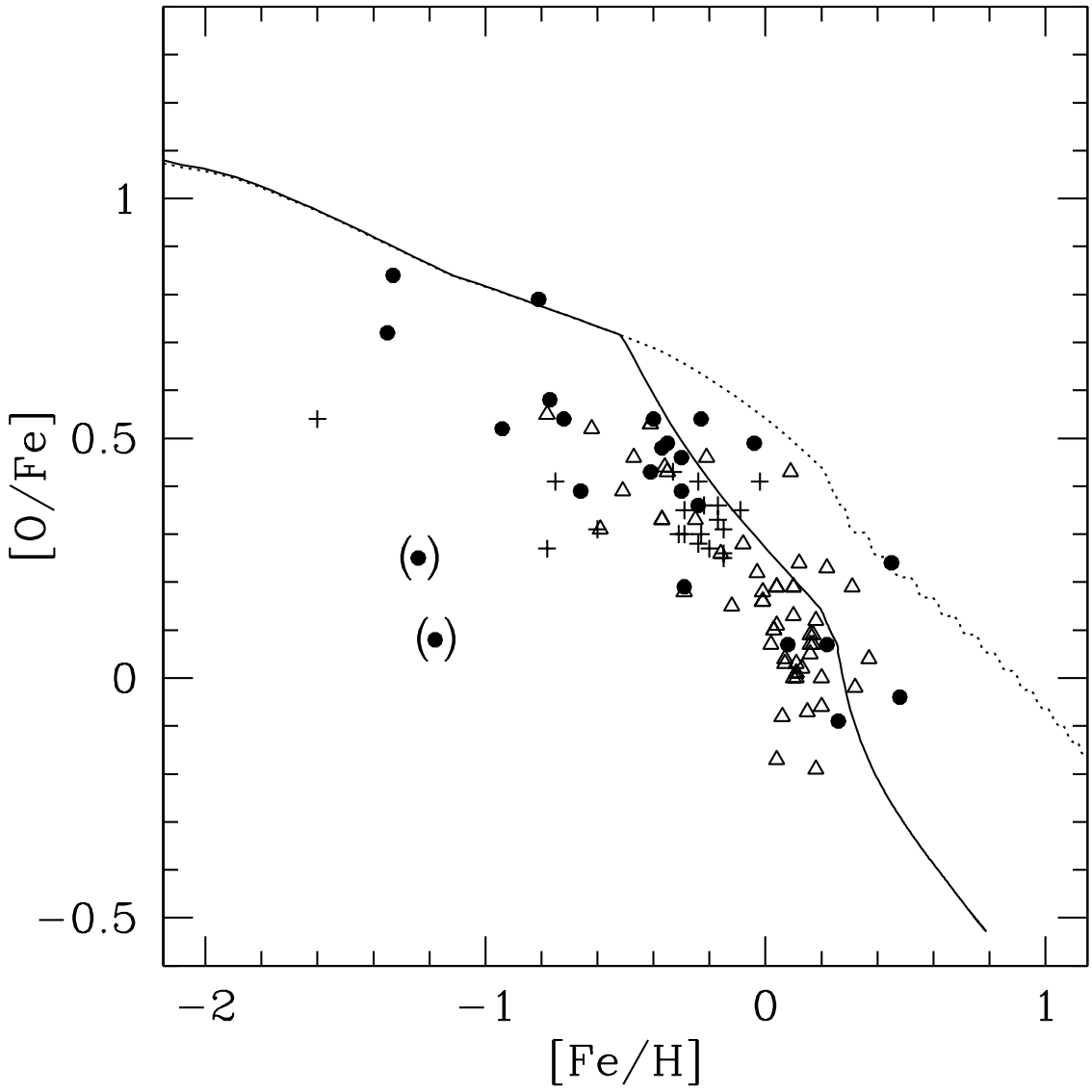

Figure 4.5: Predicted and observed [O/Fe] vs. [Fe/H]. The model with Maeder's yields is represented by the lower curve whereas the predictions without mass-loss from Ballero et al. (2007a) are represented by the red upper line. Both model predictions are normalised to the solar abundances as predicted by our Milky Way disk model. Data are from: the IR spectroscopic database (plus signs; see §3.2 for specific references), Zoccali et al. (2006), Lecureur et al. (2007, open triangles), Fulbright et al. (2007, filled circles).

halo stars (Brown et al. 1997; Nissen & Schuster 1997) and the decline in [α/Fe] ratios at lower [Fe/H] in dwarf galaxies (Geisler et al. 2005).

The solution is that in the disk both the time delay reduction in [α/Fe] and metallicity-dependent decline in oxygen yields operate; this is why the [O/Fe] ratios show a different behaviour than other α-elements in super-metal-rich stars.

4.5 Summary and conclusions

A summary of recent observational measurements of [O/Mg] versus [Mg/H] and [O/H] indicate that the [O/Mg] ratio have similar trends in the Galactic bulge and solar neighbourhood.

We reject the possibility that a metallicity-dependent IMF in the disk and bulge is responsible for the observed slopes. The similarity of abundance trends for the two systems suggests a metallicity-dependent modulation of the supernova O/Mg yield ratio. The O/Mg slope is qualitatively consistent with a metallicity-dependent decline in oxygen yields due to winds from massive stars, and related to the Wolf-Rayet phenomenon, as suggested by McWilliam & Rich (2004) and Fulbright et al. (2007).

To quantitatively test the significance of metallicity-dependent mass loss from massive stars on the O/Mg trend in the bulge and disk we have extended the bulge chemical evolution model of Ballero et al. (2007a) discussed in the previous Chapters by including the metallicity-dependent oxygen yields of Maeder (1992) resulting from stellar winds in massive stars. We find that the predicted slopes and break-points of the [O/Mg] trend with [O/H] and [Mg/H], and [O/Fe] versus [Fe/H], are very well reproduced with the inclusion of mass loss, although zero-point differences of up to $\sim$0.2 dex exist with observations. The inclusion of the metal-dependent O yields into the Ballero et al. (2007a) model substantially improves the comparison between observed and predicted abundance trends. Thus, the simple inclusion of the known effects of mass-loss on the oxygen yields of massive stars is enough to explain much of the O/Mg trend in the bulge and disk.

The $\sim$0.2 dex zero-point difference between our calculations and the observations indicates that either the semi-empirical yields of François et al. (2004) have too high a sensitivity on supernova progenitor mass, or that the IMF of our reference model is too flat; the observations might also be explained with a combined change of yields and IMF. Future observations and theoretical investigations into yields from massive stars

are required to resolve this issue. However, preliminary calculations indicate that by adopting Salpeter (1955) IMF, although it reduces the offset in the [O/Mg] plots, the correct slope and break point for supersolar metallicities are poorly reproduced. On the other hand, a plot obtained with a model where a Scalo (1986) IMF is adopted does not cover the whole range of [Mg/H] values but only extends up to ∼solar [Mg/H].

By including the Maeder (1992) metal-dependent yields we remove the previous disagreement between the IMF slope obtained by the fit of the model illustrated in the previous Chapter to the trend of [O/Fe] with [Fe/H] compared to the slope we found by fitting the metallicity distribution function. Now the methods give consistent results for the IMF slope.

Our improvement to the chemical evolution predictions concerning the O/Mg slope greatly reduces the apparent inconsistency between [O/Fe] and [Mg/Fe] trends in the high metallicity bulge stars: both elements are more consistent with a rapid bulge formation timescale, as suggested by Matteucci et al. (1999) and Ballero et al. (2007a).

Chapter 5

Universal or environment-dependent IMF?

5.1 The issue of the IMF

The question of which is the most suitable initial mass distribution for bulges of galaxies is not addressed very often. In fact, bulge evolution models (e.g. Samland et al. 1997; Ferreras et al. 2003; Immeli et al. 2004; Costa et al. 2005) usually assume *a priori* that the zero age main sequence masses of stars are distributed following a power-law distribution:

$$\phi(m) \propto m^{-(1+x)} \tag{5.1}$$

with a Salpeter (1955) index ($x = 1.35$). Basic physical arguments support the idea of an IMF varying among different environments (see e.g. Padoan et al. 1997; Larson 1998; or Nakamura & Umemura 2001; Schaerer 2002; Bromm & Larson 2004 for Population III stars).

On the other hand, so far there has not been a convincing observational evidence of such a variation in the stellar IMF based on direct stellar counts (see e.g. Chabrier 2003 for an extensive review). Massey (1998) find that the IMF is well represented by a Salpeter slope over an order of magnitude in metallicity, in the clusters and associations of the Milky Way and Magellanic Clouds, as well as in OB associations, while the slope appears to be much steeper in the field ($x \sim -3$). The invariance of the stellar IMF was confirmed by subsequent works. Kroupa (2001) summarised the available constraints by means of the multi-part power-law shape

$$\phi(m) \propto m^{-(1+x_i)} \tag{5.2}$$

where

$$\begin{aligned} x_1 &= 0.3 \text{ for } 0.08 \leq m/M_\odot \leq 0.5 \\ x_2 &= 1.3 \text{ for } 0.5 \ \ \leq m/M_\odot \end{aligned} \tag{5.3}$$

which we call the Universal IMF (UIMF).[1]

However, the IMF integrated over galaxies, which controls the distribution of stellar remnants, number of supernovae, and the chemical enrichment of a galaxy, is generally different from the stellar IMF and is given by the integral of the latter over the embedded star-cluster mass function, which varies from galaxy to galaxy. Weidner & Kroupa (2005) find such integrated galaxial IMF (IGIMF) to be steeper than the UIMF for a range of plausible scenarios, and they suggest a "maximum scenario", based on the Scalo (1986) star-count analysis of the local Galactic field, with an IGIMF which has the following indexes:

$$\begin{aligned} x_1 &= 0.3 \text{ for } 0.08 \leq m/M_\odot \leq 0.5 \\ x_2 &= 1.3 \text{ for } 0.5 \ \ \leq m/M_\odot \leq 1 \\ x_3 &= 1.7 \text{ for } 1 \ \ \ \ \leq m/M_\odot \end{aligned} \tag{5.4}$$

In the following, we will refer to this IMF as to the IGIMF.

Conversely, Piotto & Zoccali (1999) and Paresce & De Marchi (2000) measured the present-day mass function in Galactic globular clusters below $\sim 0.7 M_\odot$. They found evidence of variation in the slope of the mass function among different environments, with a tendency toward flatter slopes in globular clusters compared to the Galactic field IMF; Paresce & De Marchi (2000) also state that, in the considered mass range, the observed mass function represents the true stellar IMF for these environments. Zoccali et al. (2000) derived the IMF below $1 M_\odot$ in the Galactic bulge and concluded that it is shallower than the Salpeter slope; it also shows similarity with the IMF of globular clusters. However, the somewhat smaller x_1 is probably the result of the evaporation of low-mass stars from the cluster (Baumgardt & Makino 2003), while the Galactic bulge result is still consistent with the UIMF, within the uncertainties. On the other hand, Paumard et al. (2006) performed observations of 40 OB supergiants, giants and main sequence stars in the central parsec of the Galaxy, and concluded that the K-band luminosity function of massive stars suggests a top-heavy stellar IMF.

Concerning the range of masses over which star formation is possible, although stellar instabilities that potentially lead to disruption already occur above $60 - 120 M_\odot$ (Schwarzschild & Härm 1959), stars of $\sim 140 - 155 M_\odot$ were observed in the core of the

[1] This IMF is the form corrected for unresolved binaries.

R136 cluster (Massey & Hunter 1998) and in the Arches cluster (Figer 2005). Although Massey (2003) sustains that this upper limit may indeed be statistical rather than physical (i.e. there may not be regions that are rich enough to allow the detection of stars more massive than that), Oey & Clarke (2005) studied the content of massive stars in 9 clusters and OB associations in the Milky Way and Magellanic Clouds and find that the expectation value for the maximum stellar mass lies, with high significance, in the range $120 - 200 M_{\odot}$. This agrees with the conclusion of Weidner & Kroupa (2004) that a fundamental maximum limit for stellar masses can be constrained at about $150 M_{\odot}$, unless the true stellar IMF has $x > 1.8$.

Attempts to constrain the IMF in the bulge of our Galaxy based on observations of chemical abundances were carried out by Matteucci & Brocato (1990) and Matteucci et al. (1999), who fixed the index by the requirement of reproducing the observed metallicity distributions of Rich (1988) and McWilliam & Rich (1994), respectively. They both concluded that the bulge IMF must be flatter than the Salpeter one, in general, and lie in the range $x = 1.1 - 1.35$, thus favouring the production of massive stars with respect to the solar vicinity. An even flatter IMF index was chosen in our investigation (Ballero et al. 2007a), since we showed that it is necessary to assume $x_2 \simeq 1$ (where x_2 is essentially the one defined in Eq. 5.3) to fit the metallicity distributions of Zoccali et al. (2003) and Fulbright et al. (2006) for the Galactic bulge and of Sarajedini & Jablonka (2005) for the bulge of M31. Even shallower IMFs ($x = 0.33$) are compatible with these observed distributions, but give rise to a certain amount of oxygen overproduction.

We tested (Ballero et al. 2007b) the effect of adopting both the UIMF and the IGIMF on the predicted bulge metallicity distribution and to compare the results with the metallicity distributions employed in Ballero et al. (2007a). These IMFs will be extended to a much higher upper mass limit than in previous models, so we will try to find the combination of metal yields and evolutionary parameters that best fit the observations with these two IMFs.

5.2 Model results

In Chapter 3 we showed that an IMF with the Salpeter (1955) index ($x = 1.35$) for $1 \leq m/M_{\odot} \leq 80$ or with the Scalo (1986) index ($x = 1.7$) for $2 \leq m/M_{\odot} \leq 80$ could not fit the observed metallicity distributions in any way, causing the resulting distribution

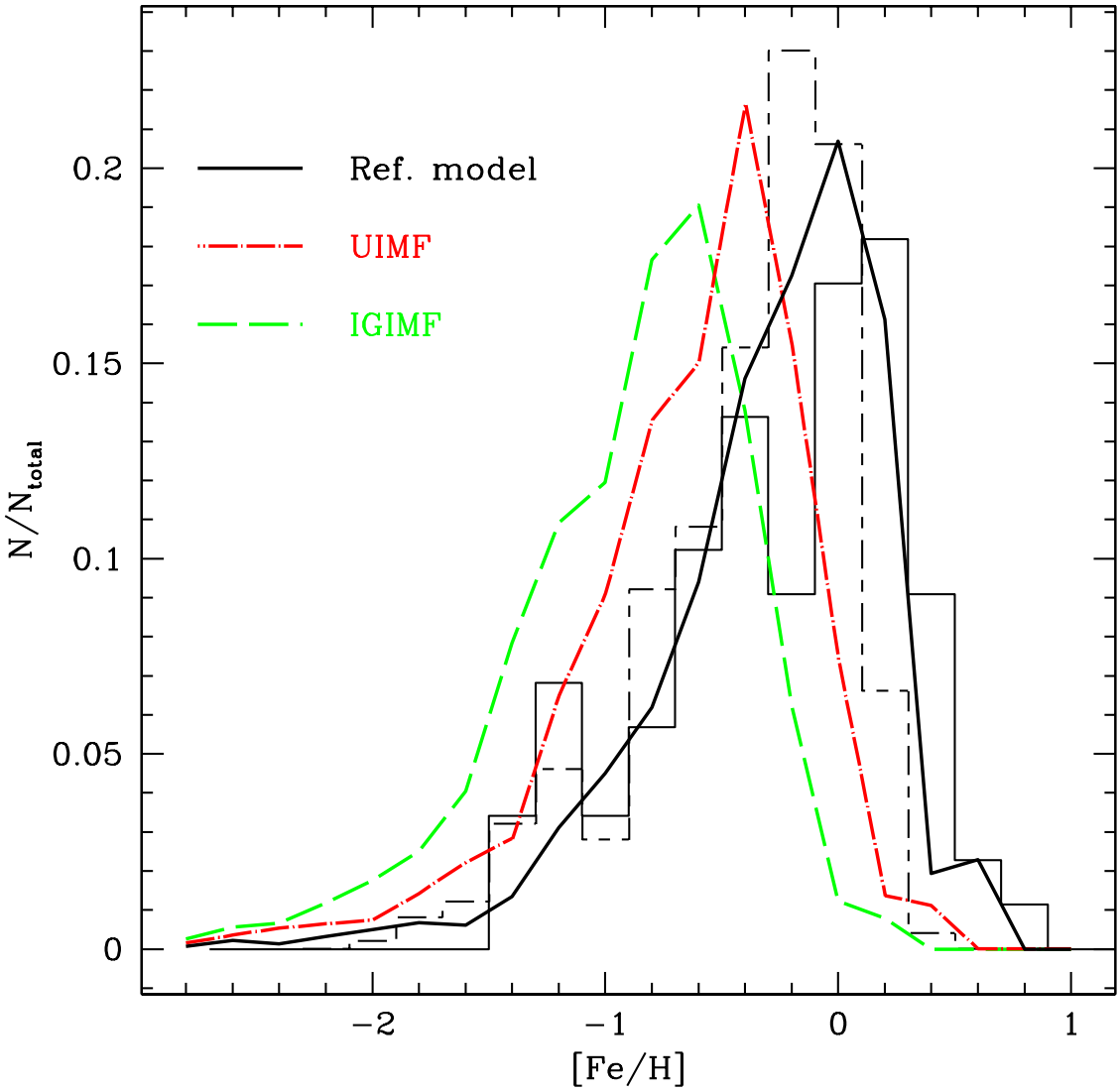

Figure 5.1: [Fe/H] distributions calculated with the adoption of different IMFs. The solid line represents our reference model (Ballero et al. 2007a). The data are compared with the observed distributions of Zoccali et al. (2003, dashed histogram) and Fulbright et al. (2006, solid histogram).

to be shifted towards low metallicities. Figure 5.1 compares the metallicity distribution obtained with the reference model and with the adoption of the UIMF and IGIMF, as described by Eqs. 5.3 and 5.4, extended to an upper mass limit of $150M_{\odot}$, and with all the other parameters kept constant with respect to the reference model. The yields of François et al. (2004) have been extrapolated in the range $80 - 150M_{\odot}$ by freezing them above $80M_{\odot}$. It is quite evident that the UIMF reproduces neither of the observed metallicity distributions, being shifted to metallicities that are too low. Even worse results are obtained with the IGIMF, which has $<$[Fe/H]$>\simeq -0.9$, i.e $\simeq 0.5 - 0.7$ dex lower than the observed ones. Most evidently, the metallicity distributions calculated with the UIMF and the IGIMF are almost indistinguishable from those obtained with models Z00-3 and Z00-4 of §3.1 (see Fig. 3.5, upper panel). This means that with the current yields, the contribution from stars in the mass range $80 - 150M_{\odot}$ to the Fe enrichment is negligible.

Now we test whether increasing the production of Fe in this range of masses can provide an Fe enrichment sufficient to shift the calculated metallicity distribution to the suitable position. Then, we shall review the effect of other evolutionary parameters other than the IMF such as the star formation efficiency and the infall timescale.

5.2.1 Constraining yields for very massive stars

We tried to force the UIMF by changing the yields above $80M_{\odot}$, which have not been constrained so far. We found out (see Fig. 5.2) that, even if we adopt stellar yields as large as ten times the extrapolated ones (Model UIMF10), which is rather unrealistic, the predicted metallicity distribution is only negligibly affected. Only if we double all the Fe yields from massive stars ($M > 8M_{\odot}$, Model UIMF2) does the calculated metallicity distribution become consistent with the observations, but this would require also doubling the yields of other elements in order to preserve the agreement with e.g. the [α/Fe] vs. [Fe/H] plots (see Ballero et al. 2007a), and this is theoretically implausible. Also, the adoption of these Fe yields for the solar neighbourhood would destroy the agreement of the two-infall model with the observed solar vicinity metallicity distribution (e.g. Chiappini et al. 2003b; Hou et al. 2000).

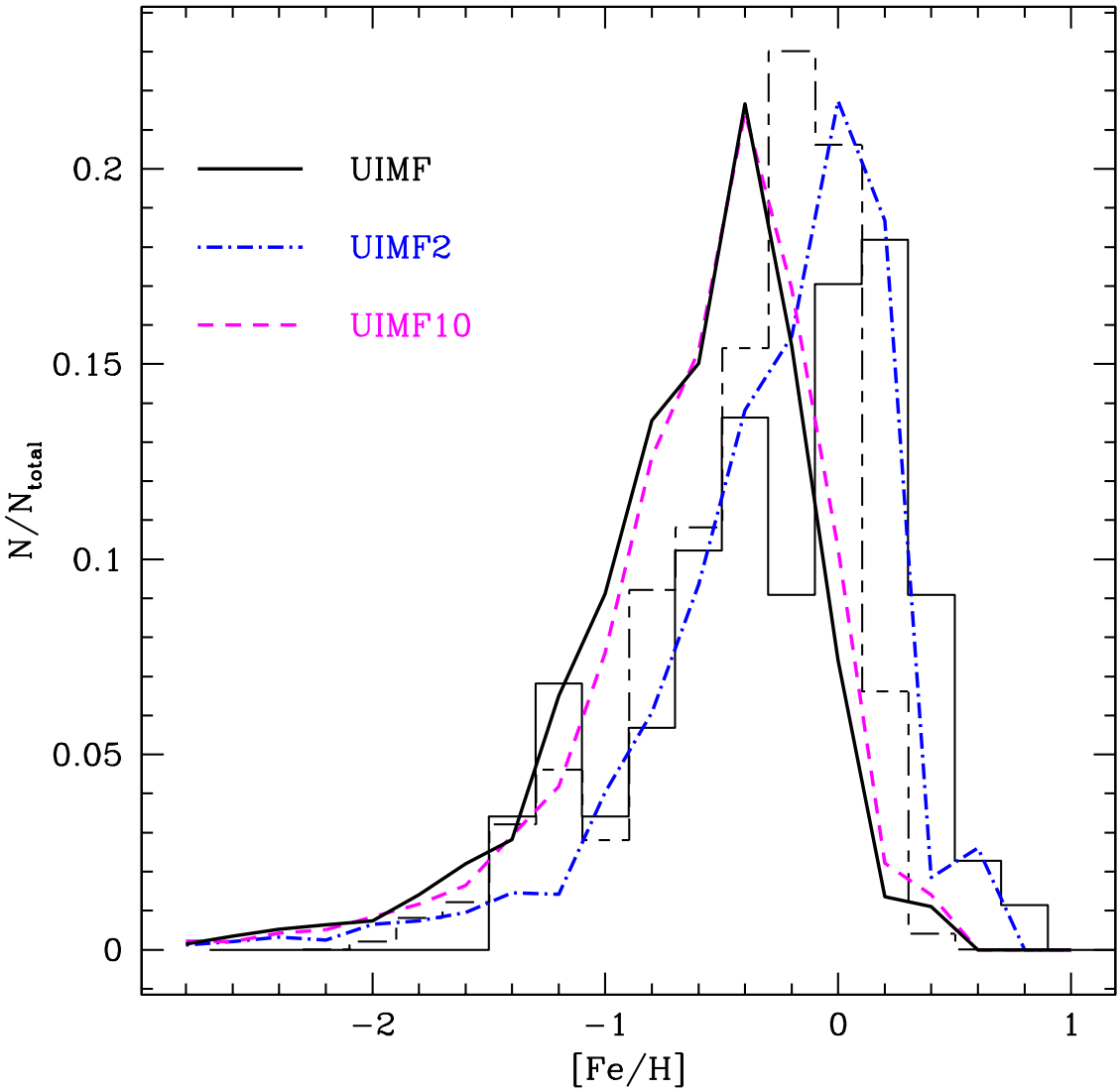

Figure 5.2: [Fe/H] distributions obtained with the UIMF and the adoption of different yields for massive stars (see text for details), compared to the same observed distributions of Fig. 5.1. A huge variation in the Fe yields above $80M_{\odot}$ leads to a negligible shift in the metallicity distribution.

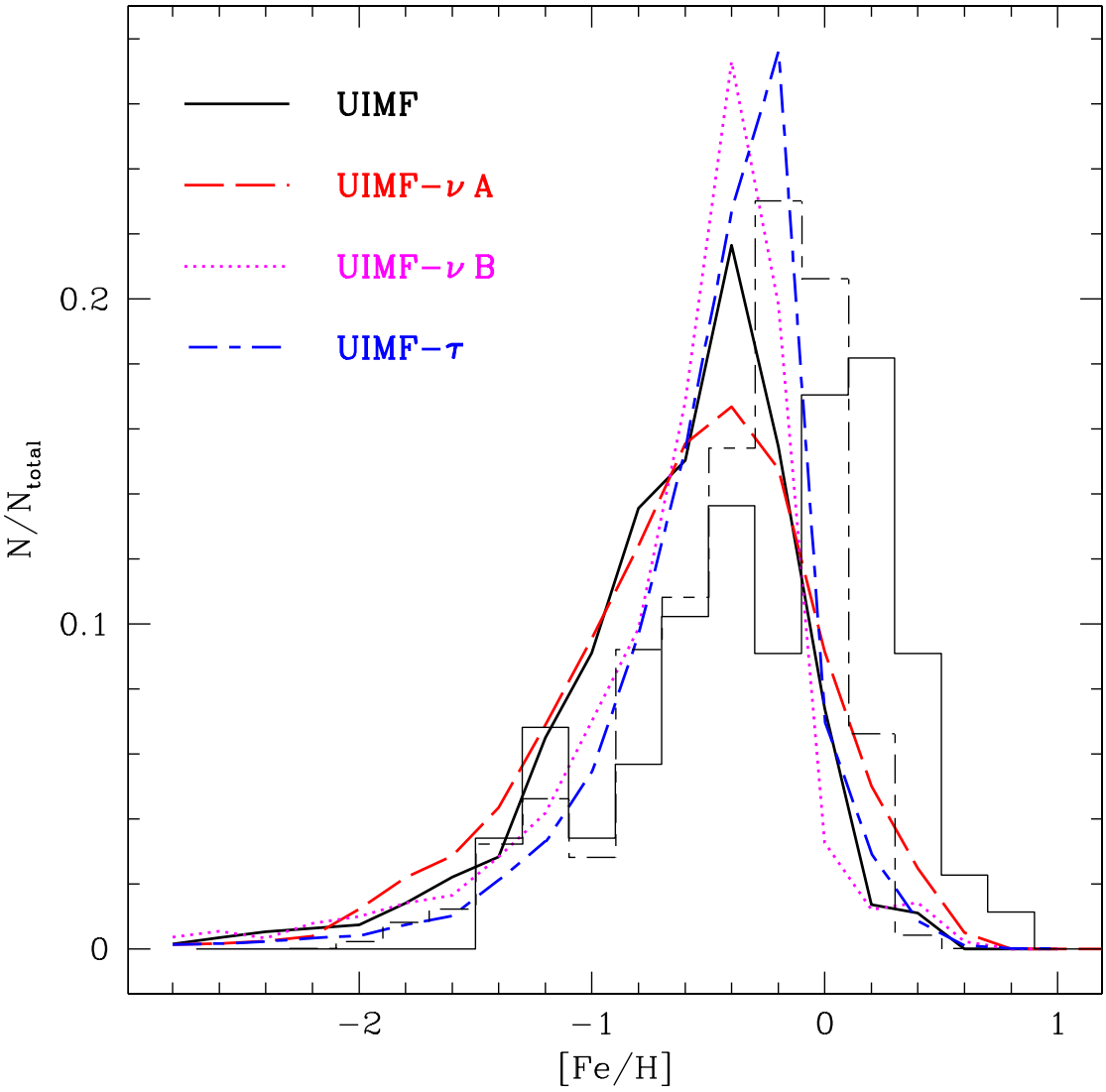

Figure 5.3: Comparison of the observed metallicity distributions with those calculated with the UIMF and with models that adopt different values for the star formation efficiency (UIMF-νA and B) and the gas infall timescale (UIMF-τ). Namely, higher values were chosen for τ and both higher and lower values for ν. Observations are the same as in Fig. 5.1.

5.2.2 The effect of other evolutionary parameters

The main contributors to the chemical enrichment in the bulge are Type II supernovae, which have massive progenitors, since the timescales of enrichment are so short. As a consequence of that, Ballero et al. (2007a) predict overabundance of α-elements relative to Fe for a wide range of [Fe/H]. It should be possible to obtain a larger enrichment from Type Ia supernovae, which originate from low- and intermediate-mass stars, by adjusting other parameters that have an effect on chemical evolution, such as the star formation efficiency ν or the infall timescale τ. Therefore, we also investigated two more models: Model UIMF-νA, where we set $\nu = 5$ Gyr^{-1}, and Model UIMF-τ, where $\tau = 0.25$ Gyr. The star formation and gas consumption in this case should be slower, giving Type Ia supernovae more time to enrich the interstellar medium with Fe. However, it should be possible to enhance the Fe production by increasing the contribution of Type II supernovae with a faster enrichment, i.e. increasing the star formation efficiency; therefore, we also considered Model UIMF-νB, where $\nu = 50$ Gyr^{-1}.

We see in Fig. 5.3, however, that the attempt to shift the position of the metallicity distribution by means of a change in these parameters is not successful, as already shown in Ballero et al. (2007a) since they mainly act on the broadness of the distribution.

In the case of a very high star formation efficiency, the effect can be explained if we consider that gas consumption occurs very rapidly and that stars are no longer formed after a very short time. On the other hand, since the enrichment is very fast, there is a lack of metal-poor stars. The opposite occurs in the case of a lower star formation efficiency. In the case of different timescales of infall, the peak is actually shifted, as can be seen from the figure, but the correct shape of the metallicity distribution is not preserved. This is because, if the gas is accreted more slowly, the number of stars produced at low metallicities is lower, so the calculated metallicity distribution gets sharper.

5.2.3 Results for M31

Fig. 5.4 shows the metallicity distributions resulting from our reference model and the model with the UIMF compared to the metallicity distribution of M31 as measured by Sarajedini & Jablonka (2005) translating the observed colour-magnitude diagram at ~ 1.6 kpc (G170 bulge field) from the centre into a metallicity distribution function by means of red giant branches with various metallicities. This metallicity distribution,

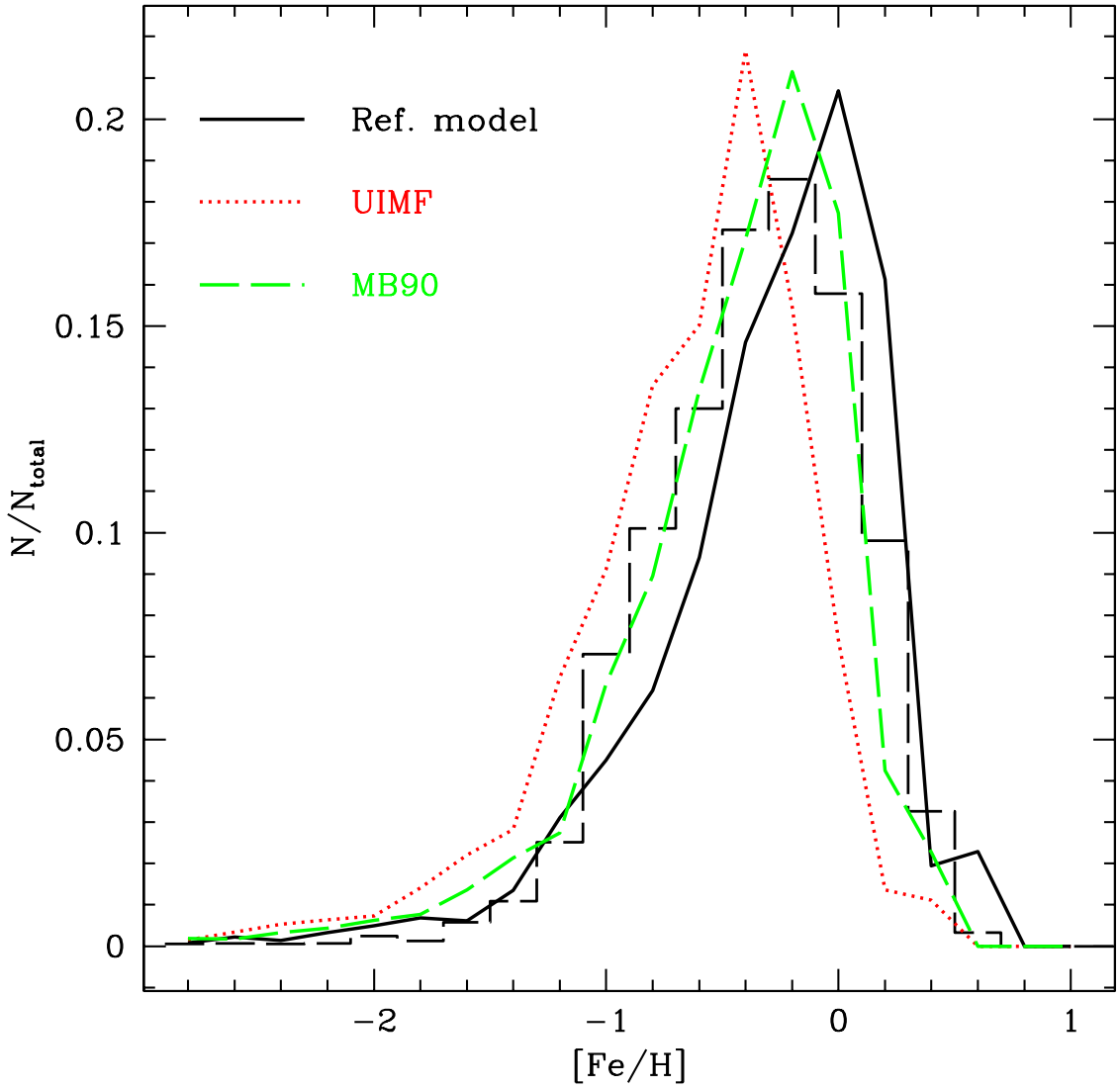

Figure 5.4: [Fe/H] distribution function for the G170 field of the M31 bulge (histogram) measured by Sarajedini & Jablonka (2005) compared with the results of our reference model (Ballero et al. 2007a) and of the UIMF model. We also show the results of model MB90, which is intermediate between the two and provides the best fit to the observed metallicity distribution.

though still consistent with the ones of the Galactic bulge and therefore indicating a similar enrichment history of the two bulges, is slightly more metal-poor on average and is compatible with both the reference model and the model with the UIMF; however, we also plotted the metallicity distribution calculated with $x_2 = 1.1$, like in Matteucci & Brocato (1990, model MB90), which gives the best fit. In any case, we can safely conclude that an IMF with $x \sim 1$ is more suitable for galactic bulges than the UIMF.

5.2.4 Discussion

Other possibilities that could affect the chemical evolution have not been investigated. The lower mass cutoff M_{inf} of the IMF is constrained by measurements in the bulge field and cluster giant stars (Kuijken & Rich 2002; Zoccali et al. 2003; Rich & Origlia 2005) that indicate that the bulk of them is roughly 10 Gyr old; therefore, the value of the lowest mass cutoff cannot be higher than $\sim 1M_{\odot}$. No difference is expected to arise if we increase M_{inf} to that value, since stars below $1M_{\odot}$ have not yet contributed to the bulge enrichment. Furthermore, it has already been shown by Ballero et al. (2006) that the adoption of a mass cutoff of $10M_{\odot}$ for the so-called Population III stars up to a metallicity suitable for the formation of these stars (i.e. $Z \simeq 10^{-8} - 10^{-4}$; Bromm & Larson 2004) has almost no effect on the predicted metallicity distribution, and even less in the bulge since such metallicities are reached in a very short time.

Lowering the SFR with the UIMF/IGIMF models in the bulge and accreting populations with supersolar metallicity, such as are evident in the ancient super-metal-rich open cluster NGC6791 (Salaris et al. 2004), or accreting supersolar gas may be able to match the observed metallicity distribution in the bulges of the Milky Way and M31. This scenario would avoid changing the IMF, but would also imply substantial accretion events in the build-up of bulges. Such accretion episodes are likely to modify the [α/Fe] *vs.* [Fe/H] plots at variance with observations. Due to the stochastic nature of mergers, each of them would introduce a wide spread in the plots, which is not observed. Continuous outflows have the effect of lowering the effective yields (see Tosi et al., 1998) and thus cannot be invoked to reproduce the observed metallicity distribution with the adoption of the UIMF.

Observed distribution	$\mathcal{M}$	μ	σ
Zoccali et al. (2003, MW)	-0.2	-0.397	0.444
Fulbright et al. (2006, MW)	$+0.2$	-0.248	0.523
Sarajedini & Jablonka (2005, M31)	-0.2	-0.369	0.438
Models			
Ref. Model	$+0.0$	-0.297	0.502
UIMF	-0.4	-0.632	0.501
IGIMF	-0.6	-0.896	0.494
UIMF2	$+0.0$	-0.272	0.514
UIMF10	-0.4	-0.580	0.493
MB90	-0.2	-0.447	0.493
UIMF-νA	-0.4	-0.481	0.587
UIMF-νB	-0.4	-0.599	0.503
UIMF-τ	-0.2	-0.550	0.417

Table 5.1: Statistical properties of the measured (upper part) and calculated (lower part) metallicity distributions of galactic bulges.

5.3 Summary and conclusions

We have tested the possibility of the UIMF of Kroupa (2001) or the "maximal" IGIMF of Weidner & Kroupa (2005) as plausible ones in the bulge of our galaxy and of M31. To this purpose, we included those IMFs in the chemical evolution model discussed in Chapter 3 (Ballero et a. 2007a), which well reproduces the properties of the Galactic bulge. The upper mass limit was extended to $150M_{\odot}$ in agreement with late findings (Weidner & Kroupa 2004; Oey & Clarke 2005; Figer 2005; Koen 2006), and the stellar yields of François et al. (2004) were extrapolated up to that mass. An attempt to constrain the yields above $80M_{\odot}$ by assuming *a priori* the validity of the UIMF was also made, and other parameters such as the star formation efficiency or infall timescale were varied in order to achieve a better fit.

Table 5.1 summarises the statistical properties of the observed and calculated distributions. The first column shows the reference or the model name; the second column reports the position of the peak on the [Fe/H] axis, i.e. the mode $\mathcal{M}$; and in the third and fourth columns the average μ and the standard deviation σ of the considered distribution are shown, respectively. Together with the reference, it is indicated whether it applies to the Milky Way or M31 bulge. It was found that it is not possible to reproduce

in a satisfactory way the observed metallicity distributions of the Galactic bulge and of M31 with the UIMF, which has a Salpeter (1955) index above $0.5M_{\odot}$, because the predicted metallicity distribution is too metal-poor. The adoption of the IGIMF, which has a Scalo (1986) index above $1M_{\odot}$, worsens the agreement further. This highlights the fact that the main Fe contributors in galactic bulges are Type II supernovae, since the timescales of enrichment are so short. Changing the nucleosynthesis prescriptions does not have remarkable effects, unless very unrealistic assumptions about the stellar yields of all massive stars are made. Even dramatic changes of yields above $80M_{\odot}$ do not basically affect the calculated distribution. We thus do not exclude the possibility of a higher mass-cutoff, but show that it is impossible to put constraints on it based on chemical abundances, since the weight in the IMF of stars in the mass range $80 < m/M_{\odot} < 150$ is negligible.

Changes in ν and τ do not lead to any improvement because they mainly have an effect on the breadth of the distribution and not on the position, which is governed by the adopted IMF. This clearly indicates that, if the bulges of the Galaxy and M31 formed inside-out through the accretion of very metal-poor gas, a variation in the stellar IMF is necessary among different environments and that an IMF index around $x \sim 1$, flatter than that of the UIMF, is preferable for galactic bulges. Theoretically speaking, as already discussed in §3.4, this can be explained if we note that the star formation in bulges proceeds like in a burst (see Elmegreen 1999); there are suggestions in the literature (e.g. Baugh et al. 2005; Nagashima et al. 2005; Okamoto et al. 2005) about a top-heavy IMF in starbursts. Figer (2005) also finds a flat IMF in the Arches cluster near the Galactic centre (however, see also Kim et al. 2006).

Chapter 6

Chemical evolution of Seyfert galaxies and bulge photometry

6.1 The co-evolution of AGNs and spheroids

The outstanding question of the co-evolution of active galactic nuclei (AGNs) and their host galaxies has received considerable attention in the past decades, since various pieces of evidence have pointed to a link between the formation of supermassive black holes and the formation and evolution of their host spheroids: for example, the usual presence of massive dark objects at the centre of nearby spheroids (Ford et al. 1997; Ho 1999; Wandel 1999); the correlation between the black hole mass and the stellar velocity dispersion of the host (for quiescent galaxies, Ferrarese & Merritt 2000; Gebhardt et al. 2000a; Tremaine et al. 2002; for active galaxies, Gebhardt et al. 2000b; Ferrarese et al. 2001; Shields et al. 2003; Onken et al. 2004; Nelson et al. 2004) or its mass (Kormendy & Richstone 1995; Magorrian et al. 1998; McLure & Dunlop 2002; Marconi & Hunt 2003; Dunlop et al. 2003; Häring & Rix 2004); the similarity between the light evolution of QSO population and the star formation history of galaxies (Cavaliere & Vittorini 1998; Haiman et al. 2004); the establishment of a good match among the optical QSO luminosity function, the luminosity function of star-forming galaxies and the mass function of dark matter halos at $z \sim 3$ (Haenhelt et al. 1998).

As we said in §1.3, the most widely accepted explanation for the luminosity emitted by an AGNs is radiatively efficient gas accretion onto a central supermassive black hole. The outflows from AGNs can profoundly affect the evolution of the host galaxy, e.g. by quenching or inducing the star formation (e.g., see Ciotti & Ostriker 2007, and

references therein). The mutual feedback between galaxies and QSOs was used as a key to solving the shortcomings of the semianalytic models in galaxy evolution, e.g. the failure to account for the surface density of high-redshift massive galaxies (Blain et al. 2002; Cimatti et al. 2002) and for the α-enhancement as a function of mass (Thomas et al. 2002), since it could provide a way to invert the hierarchical scenario for the assembly of galaxies and star formation (see e.g. Monaco et al. 2000; Granato et al. 2004; Scannapieco et al. 2005).

The chemical abundances of the QSOs were first studied by Hamann & Ferland (1993), who combined chemical evolution and spectral synthesis models to interpret the N V/C IV and N V/He II broad emission line ratios and found out that the high metallicities and the abundance ratios of the broad-line region are consistent with the outcomes of the models for giant elliptical galaxies (Arimoto & Yoshii 1987; Matteucci & Tornambè 1987; Angeletti & Giannone 1990), where the timescales of star formation and enrichment are very short, and the IMF is top-heavy. In the same year, Padovani & Matteucci (1993) and Matteucci & Padovani (1993) employed the chemical evolution model of Matteucci (1992) to model the evolution of radio-loud QSOs, which are hosted by massive ellipticals, following in detail the evolution of several chemical species in the gas. They supposed that the mass loss from dying stars after the galactic wind provides the fuel for the central black hole and modeled the bolometric luminosity as $L_{bol} = \eta \dot{M} c^2$, with a typical value for the efficiency of $\eta = 0.1$, and were successful in obtaining the estimated QSO bolometric luminosities and the observed ratio of AGN to host galaxy luminosity. Then, they studied the evolution of the chemical composition of the gas lost by stars in elliptical galaxies and spiral bulges for various elements (C, N, O, Ne, Mg, Si and Fe) and found out that the standard QSO emission lines were naturally explained by the high SFR of spheroids at early times.

The relatively weak observed time dependence of the QSO abundances for $t \gtrsim 1$ Gyr was also predicted. The model of Matteucci & Padovani (1993) still followed the classic wind scenario, where the efficiency of star formation decreases with increasing galactic mass and which was found to be inconsistent with the correlation between spheroid mass and α-enhancement (Matteucci 1994). Moreover, Padovani & Matteucci (1993) had to assume that the accretion onto the black hole would not last longer than $\sim 10^8$ years in order to avoid excessively large final black hole masses.

Other works (Friaça & Terlevich 1998; Romano et al. 2002; Granato et al. 2004), which had a more refined treatment of gas dynamics, limited their analysis of chemical

abundances to the metallicity Z and the [Mg/Fe] ratio and their correlation with the galactic mass.

All these studies were mainly devoted to studying the co-evolution of radio-loud QSOs and their host spheroids, which are elliptical galaxies. We extended (Ballero et al. 2008) the approach of Padovani & Matteucci (1993) to AGNs hosted by spiral bulges, using our chemical evolution model for the bulge as a baseline model with the introduction of the treatment of feedback from the central black hole and a more sophisticated way of dealing with the accretion rate. Since Seyfert nuclei tend to be hosted by disk-dominated galaxies, our study was applied to this class of objects.

6.2 Observations of abundances in QSOs and Seyfert galaxies

Estimates of chemical abundance ratios in AGNs are not an easy task. The use of emission lines is subject to large uncertainties due to the dependence of the lines on several parameters that are difficult to quantify (e.g. column density, microturbulence, collisional excitation, etc.). This is a problem since most measurements of the [Fe/Mg] abundance ratio, which provides a clock for constraining the ages of QSOs and their timescales of enrichment, rely on the flux ratio of the Fe II (UV bump) and Mg II (λ2800) emission lines. The true physical origin of the Fe II UV complex was questioned by Verner et al. (2003), Baldwin et al. (2004) and Korista et al. (2004), who show that the flux ratio does not scale directly with the abundance ratio due to the thermostatic effect of coolants. Absorption lines could be a better probe of QSO environments, especially narrow absorption lines that avoid saturation and blending of important abundance diagnostics. However, these data require large signal-to-noise ratios and are therefore harder to obtain. Moreover, they are not free from uncertainties concerning the shape of ionising spectrum, the lack of ionisation constraints, the unknown coverage fraction and the exact location of the absorbers (see Hamann & Ferland, 1999 for an extensive review about QSO abundance diagnostics).

Given these caveats, it is evident, in any case, that the emission spectrum of AGNs is particularly alike for a very wide range of redshifts and luminosities (Osmer & Shields 1999). The most probable explanation is a similarity of chemical abundances. In particular, the analysis of the Fe II(UV bump)/Mg II(λ2800) flux ratio in various redshift ranges (Thompson et al. 1999; Iwamuro et al. 2002; Freudling et al. 2003; Dietrich et

al. 2003a; Barth et al. 2003; Maiolino et al. 2003; Iwamoto et al. 2004) is consistent with an [Fe/Mg] abundance ratio that is slightly supersolar and almost constant out to $z \sim 6.4$. This result was also confirmed for $z \sim 6$ QSOs by very recent works (Kurk et al. 2007; Jiang et al. 2007). A weak trend with luminosity has been detected (Dietrich et al. 2003a). Due to the time delay necessary for Fe enrichment from Type II supernovae in a star formation history typical of elliptical galaxies (see Matteucci & Recchi 2001), this means that the surrounding stellar population must already be in place by the time the AGN shines and that, in a well-mixed interstellar medium, star formation must have begun $\gtrsim 10^8$ years before the observed activity, i.e. at redshifts $z_f \gtrsim 10$ (Hamann et al. 2002; Hamann et al. 2004).

Many efforts have been devoted to the measurement of nitrogen lines, since due to its secondary nature, the N abundance relative to its seed nuclei (e.g. oxygen) is a good proxy for metallicity. As abundance indicators, broad emission line ratios of N V/C IV and N V/He II were analysed by Hamann & Ferland (1993). Hamann & Ferland (1999) also indicated N V/C IV and N V/O VI in narrow absorption line systems as possible abundance indicators. More recently, Hamann et al. (2002) favour N III]/O III] and N V/(C IV + O VI) as the most robust abundance indicators. The general conclusions drawn from these diagnostics are that the AGNs appear to be metal rich at all observed redshifts, with metallicities ranging from solar up to $\sim$ 10 times solar. Dietrich et al. (2003b) studied a sample of 70 high-redshift QSOs ($3.5 \lesssim z \lesssim 5.0$) and, based on emission-line flux ratios involving C, N, O and He, estimated an average overall metallicity of $\sim 4 - 5 Z_\odot$ for the emitting gas. A similar estimate ($\sim Z_\odot$) was drawn more recently by Nagao et al. (2006), who examined 5344 spectra of high-redshift ($z \geq 2$) QSOs taken from the SDSS DR2; they also confirm the detected trend in the N/He and N/C emission line ratios, which suggests that there might be a correlation with luminosity, i.e. more luminous QSOs, residing in more massive galaxies, are more metal rich. Bentz et al. (2004) suggested that some very nitrogen-enriched QSOs may be caught at the peak of metal enrichment, e.g. near the end of their accretion phases, although their conclusions are not definite. Work carried out on intrinsic narrow absorption line systems (Petitjean & Srianand 1999; Hamann et al. 2003; D'Odorico et al. 2004) confirms that the observed N, C and Si abundance ratios are consistent with at least solar metallicities. In particular, D'Odorico et al. (2004) interpreted their observations as suggestive of a scenario of rapid enrichment due to a short ($\sim$ 1 Gyr) star formation burst. The amount of emission from dust and CO in high-redshift QSOs

(Cox et al. 2002) corroborate the idea of massive amounts of star formation preceding the shining of the AGN. However, there is no need for exotic scenarios to explain the production of heavy elements near QSOs (e.g. central star clusters, star formation inside accretion disks), since normal chemical evolution of ellipticals is sufficient to this purpose (Hamann & Ferland 1993; Matteucci & Padovani 1993).

The majority of conclusions concerning QSOs has been found to hold also for Seyfert galaxies, i.e. observations seem to confirm that most Seyfert galaxies are metal rich. An overabundance of nitrogen by a factor ranging from about 2 to 5 was first detected in the narrow line region of Seyferts by Storchi-Bergmann & Pastoriza (1989, 1990), Storchi-Bergmann et al. (1990) and Storchi-Bergmann (1991), and was later confirmed by Schmitt et al. (1994). Further work by Storchi-Bergmann et al. (1996) allowed them to derive the chemical composition of the circumnuclear gas in 11 AGNs, and high metallicities were found (O ranging from solar to $2-3$ times solar and N up to $4-5$ times solar). This trend was also measured in more recent works (Wills et al. 2000; Mathur 2000). Fraquelli & Storchi-Bergmann (2003) examined the extended emission line region of 18 Seyferts and claimed that the range in the observed [N II]/[O II] line ratios can only be reproduced by a range of oxygen abundances going from 0.5 to 3 times solar. By a means of a multi-cloud model, Rodríguez-Ardila et al. (2005) deduce that a nitrogen abundance higher than solar by a factor of at least two would be in agreement with the [N II]+/[O III]+ line ratio observed in the narrow line Seyfert 1 galaxy Mrk 766. Finally, Fields et al. (2005a) use a simple photoionization model of the absorbing gas to find that the strongest absorption system of the narrow line Seyfert 1 galaxy Mrk 1044 has $\mathrm{N/C} \gtrsim 4(\mathrm{N/C})_{\odot}$.

In the circumnuclear gas of the same galaxy, using column density measurements of O VI, C IV, N V and H I, Fields et al. (2005b) claimed that the metallicity is about 5 times solar. This is consistent with expectations from previous studies. Komossa & Mathur (2001), after studying the influence of metallicity on the multi-phase equilibrium in photoionized gas, stated that in objects with steep X-ray spectra, such as narrow line Seyfert 1 galaxies, such an equilibrium is not possible if Z is not supersolar. Studying forbidden emission lines, Nagao et al. (2002) derived $Z \gtrsim 2.5 Z_{\odot}$ in narrow line Seyfert 1 galaxies, whereas the gas of broad line Seyferts tends to be slightly less metal rich.

An overabundance of iron was suggested to explain the strong optical Fe II emission in narrow line Seyferts (Collin & Joly 2000) and could provide an explanation for the absorption features around ~ 1 keV seen in some of these galaxies (Ulrich et al. 1999;

M_b ($M_\odot$)	ν (Gyr^{-1})	R_e (kpc)	t_{GW} (Gyr)
2×10^9	11	1	0.31
2×10^{10}	20	2	0.27
10^{11}	50	4	0.22

Table 6.1: Features of the examined models, in order: bulge mass, star formation efficiency, bulge effective radius. The table also reports the time of occurrence of the galactic wind.

Turner et al. 1999) or for the strength of the FeKα lines (Fabian & Iwasawa 2000). By constraining the relationship between iron abundance and reflection fraction, Lee et al. (1999) show that the observed strong iron line intensity in the Seyfert galaxy MCG−6-30-15 is explained by an iron overabundance by a factor of ~ 2 in the accretion disk. Ivanov et al. (2003) find values for [Fe/H] derived from the Mg I 1.50μm line ranging from −0.32 to +0.49, but these values were not corrected for dilution effects from the dusty torus continuum, so are probably underestimated.

6.3 Building models for other bulges

We recall that, in our reference model (Ballero et al. 2007a), the parameters that allow a best fit of the metallicity distributions and the [α/Fe] *vs.* [Fe/H] ratios measured in the bulge giants are the following: $\nu = 20$ Gyr^{-1}, $\tau = 0.1$ Gyr, and two slopes for the IMF, namely $x_1 = 0.33$ for $0.1 \leq m/M_\odot \leq 1$ (in agreement with the photometric measurements of Zoccali et al. 2000) and $x_2 = 0.95$ for $1 \leq m/M_\odot \leq 80$. We also consider the case $x_2 = 1.35$ (Salpeter 1955) for comparison.

This model holds for a galaxy like ours with a bulge of $M_b = 2 \times 10^{10} M_\odot$. We are going to predict the properties of Seyfert nuclei hosted by bulges of different masses, therefore some model parameters will have to be re-scaled. We choose to keep the IMF constant and to scale the effective radius and the star formation efficiency following the inverse-wind scenario (Matteucci 1994). The possibility of changing the infall timescale with mass is not explored for the moment. Table 6.1 reports the adopted parameters for each bulge mass.

6.4 Photometry of bulges

By matching chemical evolution models with a spectro-photometric code, it has been possible to reproduce the present-day photometric features of galaxies of various morphological types (Calura & Matteucci 2006; Calura et al. 2007b) and to perform detailed studies of the evolution of the luminous matter in the Universe (Calura & Matteucci 2003; Calura et al. 2004). By means of the chemical evolution model plus a spectro-photometric code, we are now attempting to model the photometric features of galactic bulges. All the spectro-photometric calculations are performed by means of the code developed by Jimenez et al. (2004) and based on the stellar isochrones computed by Jimenez et al. (1998) and on the stellar atmospheric models by Kurucz (1992). The main advantage of this photometric code is that it allows to follow in detail the metallicity evolution of the gas, thanks to the large number of simple stellar populations calculated by Jimenez et al. (2004) by means of new stellar tracks, with ages between 10^6 and 1.4×10^{10} yr and metallicities ranging from $Z = 0.0002$ to $Z = 0.1$.

Starting from the stellar spectra, we first build simple stellar population models consistent with the chemical evolution at any given time and weighted according to the assumed IMF. Then, a composite stellar population consists of the sum of different simple stellar populations formed at different times, with a luminosity at an age t_0 and at a particular wavelength λ given by

$$L_\lambda(t_0) = \int_0^{t_0} \int_{Z_i}^{Z_f} \psi(t_0 - t) L_{SSP,\lambda}(Z, t_0 - t) dZ dt, \tag{6.1}$$

where the luminosity of the simple stellar population can be written as

$$L_{SSP,\lambda}(Z, t_0 - t) = \int_{M_{min}}^{M_{max}} \phi(m) l_\lambda(Z, m, t_0 - t) dm \tag{6.2}$$

and where $l_\lambda(Z, m, t_0 - t)$ is the luminosity of a star of mass m, metallicity Z and age $t_0 - t$; Z_i and Z_f are the initial and final metallicities, M_{min} and M_{max} are the lowest and highest stellar masses in the population, $\phi(m)$ is the IMF and $\psi(t)$ is the SFR at the time t. Peletier et al. (1999) have shown that dust in local bulges is very patchy and concentrated in the innermost regions, i.e. within distances of ~ 100 pc. They also showed that dust extinction effects are negligible at distances of $\sim 1 R_{eff}$. In addition, we compared our photometric predictions to observational results largely unaffected by dust, such as the ones by Balcells & Peletier (1994). For these reasons, in all our spectro-photometric calculations, we do not take dust extinction into account.

The photometrical evolution of actual Seyfert galaxies, which requires modelling of the AGN continuum and, for Type 2 Seyferts, of the dusty torus, is not treated at present and may be the subject of a future investigation.

6.5 Energetics of the interstellar medium

In Chapter 2, we calculated the binding energy ΔE_g of the bulge gas following Bertin et al. (1992), i.e. by treating the bulge as a scaled-down two-component elliptical (thus ignoring the disk contribution). We also assumed that the thermal energy of the bulge interstellar medium was mainly contributed by the explosion of Type Ia and Type II supernovae. In the present exploration, not only do we adopt a more realistic disk galaxy model to better estimate the binding energy of the gas in the bulge, but we also consider the additional contribution to the gas thermal energy given by the black hole feedback, so that

$$E_{th}(t) = E_{th,SN}(t) + E_{th,AGN}(t) \tag{6.3}$$

The various simplifying assumptions adopted in the evaluation of the gas binding energy and of the black hole feedback will be discussed in some detail in the following sections. The gas binding energy and thermal energy which are calculated in the next subsections will then be compared as in Eq. 2.9 in order to estimate the time of occurrence of the galactic wind.

6.5.1 The binding energy

If we define

$$\Psi(r,t) = \pi R_e^2 \psi(r,t) \tag{6.4}$$

(i.e. the volume SFR) and

$$\dot{M}_* = \int_{0.1}^{80} \phi(m)\Psi(r, t-\tau_m)R_m(t-\tau_m)dm \tag{6.5}$$

where R_m is the return mass fraction (i.e. the fraction of mass in a stellar generation that is ejected into the interstellar medium by stars of mass m; see Tinsley 1980) and τ_m is the lifetime of a star of mass m, then, before the galactic wind, the mass of gas in the bulge evolves at a rate

$$\dot{M}_g(t < t_{GW}) = \dot{M}_{inf} + \dot{M}_* - \Psi(r,t) - \dot{M}_{BH}; \tag{6.6}$$

i.e. gas is accreted from the halo, is returned by stellar mass loss, and is subtracted by star formation and black hole accretion. After the wind, star formation vanishes and we suppose that the infall is arrested due to the development of a global outflow. Therefore, this equation reduces to

$$\dot{M}_g(t > t_{GW}) = \dot{M}_* - \dot{M}_{BH} - \dot{M}_W \tag{6.7}$$

where $\dot{M}_W$ is the rate of mass loss due to the galactic wind. We assume that all the gas present at a given time is lost, so that $\dot{M}_W = \dot{M}_* - \dot{M}_{BH}$. In the present treatment the galaxy mass model is required in order to estimate the binding energy of the gas in the bulge, a key ingredient in establishing of the wind phase. In particular, the current galaxy model is made by three different components, namely:

- A spherical Hernquist (1990) distribution representing the stellar component of the bulge:

$$\begin{cases} \rho_b(r) &= \dfrac{M_b}{2\pi}\dfrac{r_b}{r(r+r_b)^3}, \\ \Phi_b(r) &= -\dfrac{GM_b}{r+r_b} \end{cases} \tag{6.8}$$

  where M_b is the bulge mass, Φ_b the bulge potential and r_b the scale radius of the bulge, related to its effective radius by the relation $R_e \simeq 1.8 r_b$.

- A spherical isothermal dark matter halo with circular velocity v_c:

$$\begin{cases} \rho_{DM}(r) &= \dfrac{v_c^2}{4\pi G r^2} \\ \Phi_{DM}(r) &= v_c^2 \ln \dfrac{r}{r_0} \end{cases} \tag{6.9}$$

  where r_0 is an arbitrary scale-length.

- A razor-thin exponential disk with surface density

$$\Sigma_d(R) = \frac{M_d}{2\pi R_d^2} e^{-R/R_d} \tag{6.10}$$

  where M_d is the total disk mass, R the cylindrical radius, and R_d the disk scale radius. As is well known, the gravitational potential of a disk can in general be expressed by using the Hankel-Fourier transforms (e.g. Binney & Tremaine 1987): however, as shown in Appendix, under the assumption of a spherical gas distribution, the contribution to the gas binding energy can be easily calculated without using the explicit disk potential.

In fact, we assume that the gas distribution before the establishment of the galactic wind is spherically symmetric and parallel to the stellar one; i.e.

$$\rho_g(r) = \frac{M_g}{2\pi} \frac{r_b}{r(r+r_b)^3}. \tag{6.11}$$

In order to estimate the energy required to induce a bulge wind, we define a *displacement radius* r_t, and we calculate the energy required to displace at r_t the gas contained at $r < r_t$ (while maintaining spherical symmetry). We adopt a reference value of $r_t = 3R_e$; the calculated values of the binding energy do not change significantly for r_t ranging from $2R_e$ to $10R_e$. A spherically symmetric displacement (while not fully justified theoretically) allows a simple evaluation of the gas binding energy, and it is acceptable in the present approach. Consistent with the assumption above,

$$\Delta E_g = \Delta E_{gb} + \Delta E_{gDM} + \Delta E_{gd} \tag{6.12}$$

where the various terms at the right hand side describe the gas-to-bulge, gas-to-dark matter and gas-to-disk contributions. Elementary integrations show that

$$\Delta E_{gb} = 4\pi \int_0^{r_t} \rho_g(r)[\Phi_b(r_t) - \Phi_b(r)]r^2 dr = \frac{GM_gM_b}{r_b} \frac{\delta^3}{3(1+\delta)^3} \tag{6.13}$$

and

$$\Delta E_{gDM} = 4\pi \int_0^{r_t} \rho_g(r)[\Phi_{DM}(r_t) - \Phi_{DM}(r)]r^2 dr = M_g v_c^2 \left[\ln(1+\delta) - \frac{\delta}{1+\delta}\right] \tag{6.14}$$

where $\delta \equiv r_t/r_b$, while

$$\Delta E_{gd} = \frac{GM_gM_d}{R_d} \times \widetilde{\Delta E_{gd}} \tag{6.15}$$

and the function $\widetilde{\Delta E_{gd}}$ is given in Appendix. Of course, ΔE_g is linearly proportional to the gas mass in the bulge.

In Fig. 6.1 we see that, for a $10^{10} M_\odot$ bulge like ours, the dominant contribution arises from the dark matter halo, whereas the bulge and disk contributions are comparable, both about one order of magnitude smaller than the dark matter halo one. This differs from previous calculations (Ballero et al. 2007a) in the way that the bulge contribution is reduced by almost one order of magnitude. The same is true of the bulges of other masses. We must consider, moreover, that in the inside-out scenario for the Galaxy formation (Chiappini et al. 1997) the disk will probably form much later than the bulge, so its contribution to the potential well during the bulge formation could be negligible. Thus, what we explore is the extreme hypothesis that the disk has been in place since the beginning of the bulge evolution.

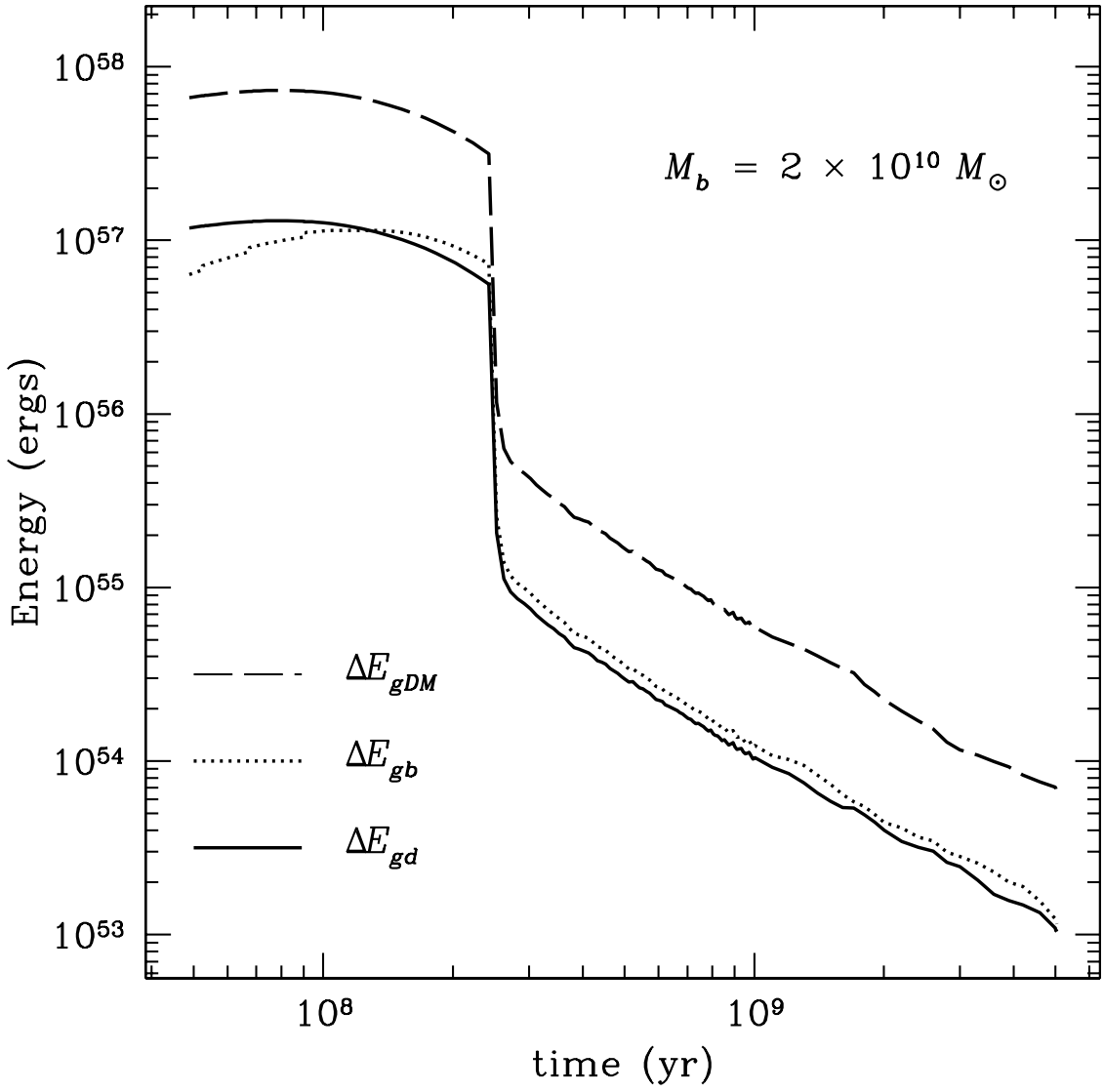

Figure 6.1: Time evolution of the different contributions to the gas binding energy in the bulge of a Milky Way-like galaxy: dark matter halo (dashed line), bulge (dotted line), and exponential disk (solid line). In particular, $M_b = 2 \times 10^{10} M_\odot$, $R_e = 2$ kpc, $v_c = 200$ km/s, $M_d = 10^{11} M_\odot$ and $R_d = 4.3$ kpc.

6.5.2 Black hole accretion and feedback

In our phenomenological treatment of black hole feedback, we only considered radiative feedback, thus neglecting other feedback mechanisms such as radiation pressure and relativistic particles, as well as mechanical phenomena associated with jets. From this point of view we are following the approach described in Sazonov et al. (2005), even though several aspects of the physics considered there (in the context of elliptical galaxy formation) are not taken into account. In fact, we note that these phenomena can only be treated in the proper way by using hydrodynamical simulations.

We suppose that the bulge gas is fed into the spherically accreting black hole at the Bondi rate $\dot{M}_B$. However, the amount of accreting material cannot exceed the Eddington limit, i.e.:

$$\dot{M}_{BH} = \min(\dot{M}_{Edd}, \dot{M}_B). \tag{6.16}$$

The Eddington accretion rate, i.e. the accretion rate beyond which radiation pressure overwhelms gravity, is given by

$$\dot{M}_{Edd} = \frac{L_{Edd}}{\eta c^2} \tag{6.17}$$

where η is the efficiency of mass-to-energy conversion. In general, $0.001 \leq \eta \leq 0.1$, and we adopt the maximum value $\eta = 0.1$ (Yu & Tremaine 2002). The Eddington luminosity is given by

$$L_{Edd} = 1.3 \times 10^{46} \frac{M_{BH}}{10^8 M_\odot} \text{ erg s}^{-1}. \tag{6.18}$$

The Bondi accretion rate describes the stationary flow of gas from large distances onto the black hole, for a given gas temperature and density (see Bondi 1952), and is given by

$$\dot{M}_B = 4\pi R_B^2 \rho_B c_S, \tag{6.19}$$

where

$$R_B = \frac{G M_{BH} \mu m_p}{2\gamma k T} = 16 \text{ pc } \frac{1}{\gamma} \frac{M_{BH}}{10^8 M_\odot} \left(\frac{T}{10^6 \text{K}} \right)^{-1} \tag{6.20}$$

with

$$c_s^2 = \left(\frac{\partial p}{\partial \rho} \right)_{isot} = \frac{kT}{\mu m_p}, \tag{6.21}$$

and ρ_B (the gas density at R_B) can be estimated as

$$\rho_B = \frac{\bar{\rho}_e}{3} \left(\frac{R_e}{R_B} \right)^2. \tag{6.22}$$

In the code we adopt $\gamma = 1$ (isothermal flow). If we assume that all the gas mass is contained within $2R_e$, the mean gas density within R_e is given by

$$\bar{\rho}_e = \frac{3M_g}{8\pi R_e^3}. \tag{6.23}$$

The equilibrium gas temperature can be estimated as the bulge virial temperature.

$$T_{vir} \simeq \frac{\mu m_p \sigma^2}{k} = 3.0 \times 10^6 \text{ K } \left(\frac{\sigma}{200 \text{ km s}^{-1}}\right)^2, \tag{6.24}$$

where σ is the one-dimensional stellar velocity dispersion in the bulge, which is given by

$$\sigma^2 \equiv -\frac{W_b}{3M_b}. \tag{6.25}$$

The virial potential trace W_b for the bulge is obtained by summing the contribution of the three galaxy components, i.e.

$$W_b = W_{bb} + W_{bDM} + W_{bd} = -\frac{GM_b^2}{6r_b} - M_b v_c^2 - \frac{GM_d M_b \widetilde{W_{bd}}}{R_d} \tag{6.26}$$

where the term $\widetilde{W_{bd}}$ is given in Appendix.

The bolometric luminosity emitted by the accreting black hole is then calculated as

$$L_{bol} = \eta c^2 \dot{M}_{BH}. \tag{6.27}$$

Finally, we assume that the energy released by the black hole is the integral of a fraction f of this luminosity over the time-step:

$$E_{th,BH} = f \int_t^{t+\Delta t} L_{bol} dt \simeq f L_{bol} \Delta t. \tag{6.28}$$

The value of f can vary between 0 and 1; we assume $f = 0.05$ (Di Matteo et al. 2005). The seed black hole mass was modified in a range $5 \times 10^2 - 5 \times 10^4 M_\odot$ without any appreciable change in the results. Therefore, we adopt a universal seed black hole mass of $10^3 M_\odot$.

6.6 Results

6.6.1 Mass loss and energetics

Fig. 6.2 shows the evolution of the Eddington and Bondi accretion rates. We can see that the history of accretion onto the central black hole can be divided into two phases:

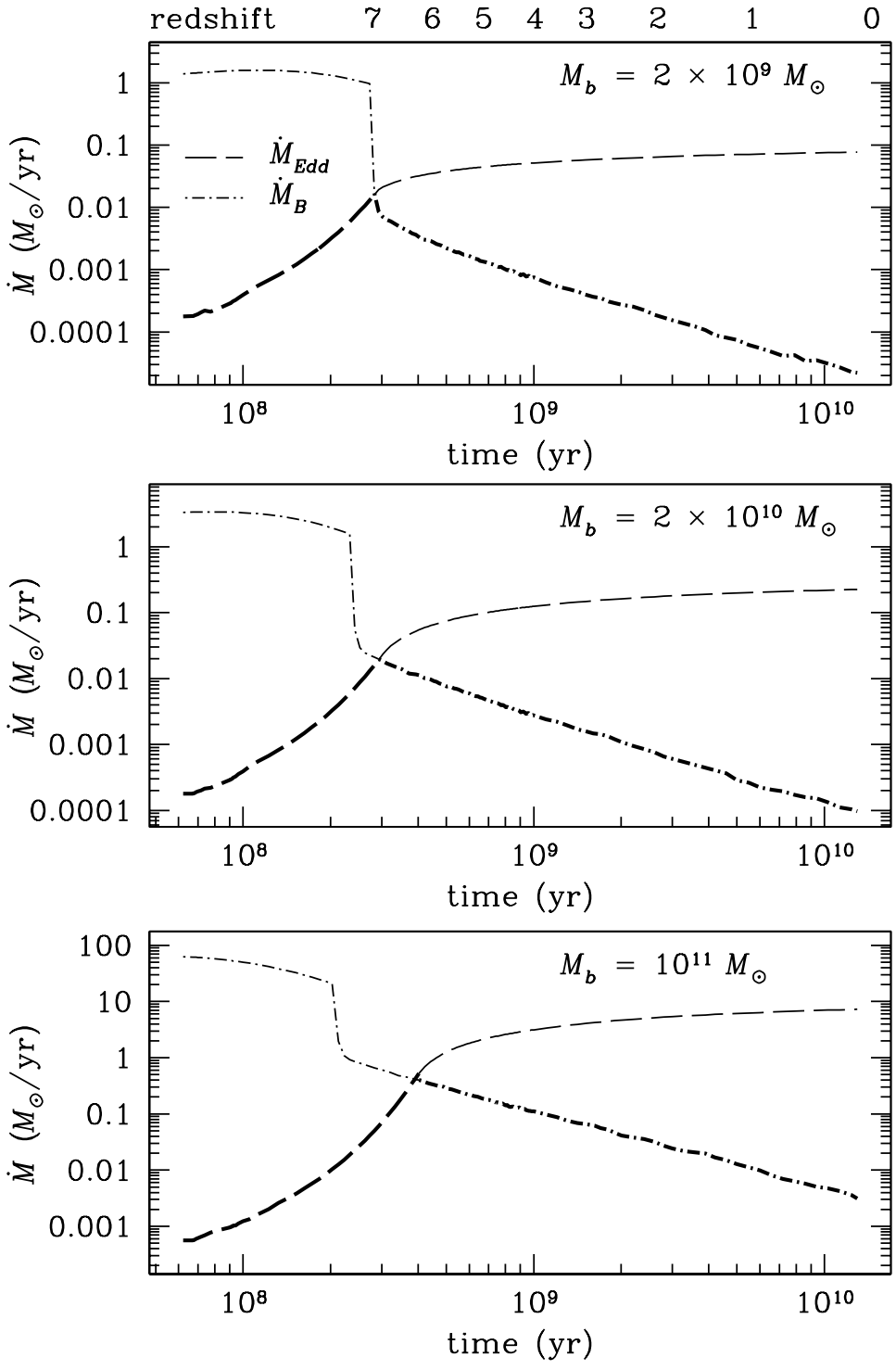

Figure 6.2: Time evolution of the Eddington (dashed line) and Bondi (dot-dashed line) accretion rates for bulges with various masses. The thicker lines indicate the resulting accretion rate, which is assumed to be the minimum between the two. The break in the Bondi rate corresponds to the occurrence of the galactic wind.

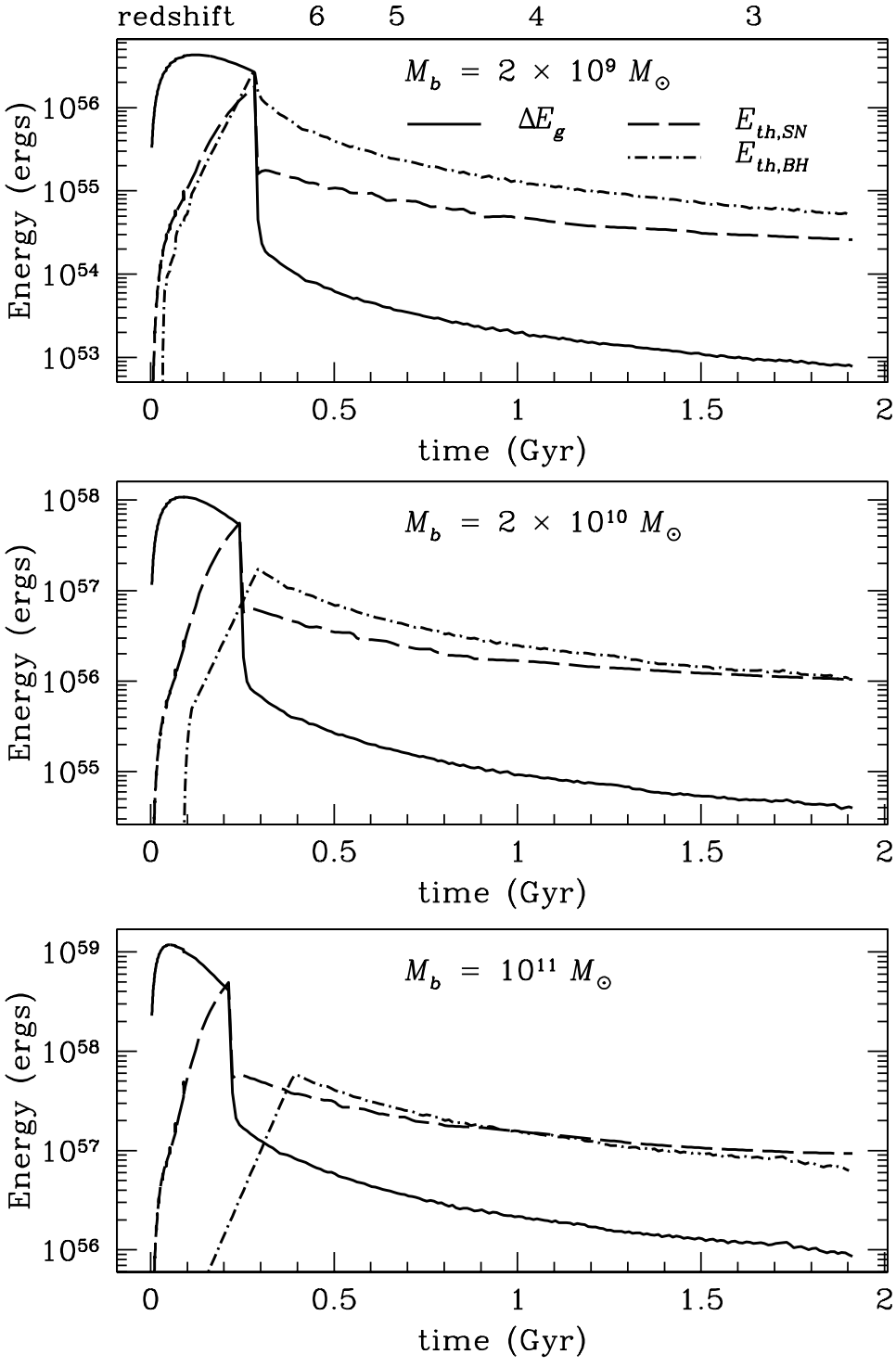

Figure 6.3: Energy balance as a function of time for bulges of various masses. The figure shows the gas binding energy (solid line) compared to the thermal energy released by supernovae (dashed line) and the accreting black hole (dot-dashed line). The break in the binding energy and in the supernova feedback corresponds to the occurrence of the galactic wind.

the first, Eddington-limited, and the second, Bondi-limited. Most of the accretion and fuelling occurs around the period of transition between the two phases, which coincides approximately with the occurrence of the wind, although it extends for some time further in the most massive models. The details of the transition depend on the numerical treatment of the wind; however, since the gas consumption in the bulge is very fast and the Bondi rate depends on the gas density, we can expect that the results would not change significantly even if we modeled the galactic wind as a continuous wind. The black hole mass is essentially accreted, within a factor of two, in a period ranging from 0.3 to 0.8 Gyrs, i.e. 2 to 6% of the bulge lifetime, which we assume to be 13.7 Gyr.

Fig. 6.3 compares the different contributions to the thermal energy, i.e. the feedback from supernovae and from the AGN, with the potential energy. We see that only in the case of $M_b = 2 \times 10^9 M_\odot$ does the black hole feedback provide a thermal energy comparable to what is produced by the supernova explosions before the onset of the wind (note that the Bondi accretion rate does not vanish even if the thermal energy of the interstellar medium is greater than the potential energy, due to the fresh gas provided by the stellar mass losses of the ageing stars in the bulge). Therefore, in the context of chemical and photometrical evolution, the contribution of the black hole feedback is negligible in most cases, unless we assume an unrealistically large fraction of the black hole luminosity is transferred into the interstellar medium. This conclusion is also supported by hydrodynamical simulations specifically designed to study the effects of radiative black hole feedback in elliptical galaxies (Ciotti & Ostriker 1997, 2001, 2007; Ostriker & Ciotti 2005). Also, Di Matteo et al. (2003) show that it is unlikely that black hole accretion plays a crucial role in the general process of galaxy formation, unless there is strong energetic feedback by active QSOs (e.g. in the form of radio jets).

6.6.2 Star formation rate

Fig. 6.4 shows the evolution of the global SFR in the bulge as a function of time and redshift. The break corresponds to the occurrence of the galactic wind. The redshift was calculated assuming a ΛCDM cosmology with $H_0 = 65$ km s^{-1} Mpc^{-1}, $\Omega_M = 0.3$ and $\Omega_\Lambda = 0.7$, and a redshift of formation of $z_f \simeq 10$. It is evident that, in the case of the most massive bulges, it is easy to reach the very high SFRs of a few times $1000 M_\odot$/yr inferred from observations at high redshifts (e.g. Maiolino et al. 2005). It is worth noting that this result matches the statement of Nagao et al. (2006) very well, that the absence of a significant metallicity variation up to $z \simeq 4.5$ implies that the active star

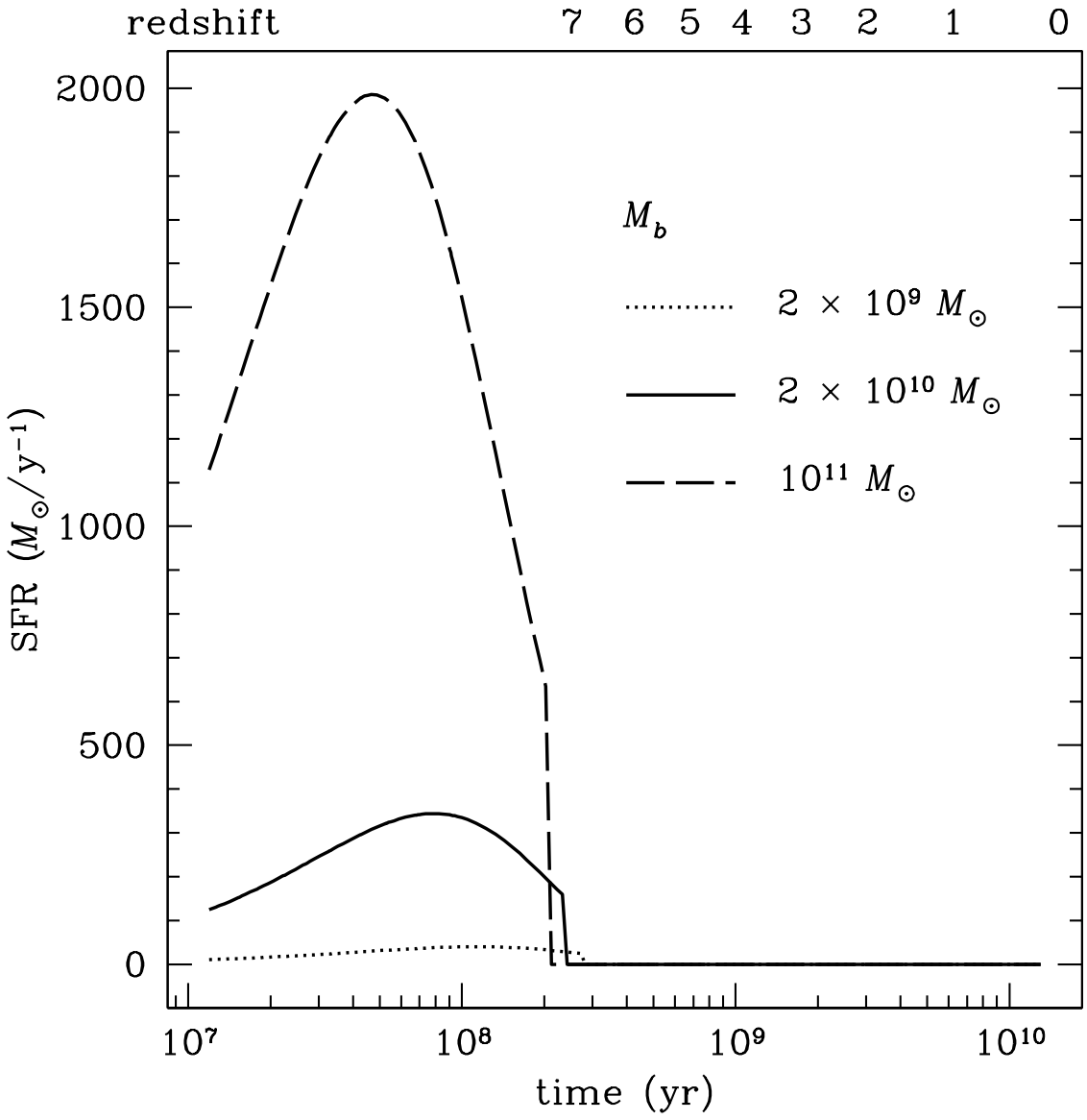

Figure 6.4: Star formation rate as a function of time and redshift for bulges with various masses. The peak value of the $M_b = 2 \times 10^9 M_\odot$ case is $\sim 40 M_\odot$/yr.

formation epoch of QSO host galaxies occurred at $z \gtrsim 7$. There is evidence of some tiny downsizing (star formation ceases at slightly earlier times for larger galaxies; see Table 6.1). We stress that we are making predictions about single galaxies and not about the AGN population, and we only want to show that it is possible to achieve such high rates of star formation in a few Myrs.

6.6.3 Black hole masses and luminosities

In Fig. 6.5 we show the final black hole masses resulting from the accretion as a function of the bulge mass. The predicted black hole masses are in good agreement with measurements of black hole masses inside Seyfert galaxies (Wandel et al. 1999; Kaspi et al. 2000; Peterson 2003). This is a valuable result, given the simplistic assumptions of our model, since in this case we do not have to stop accretion in an artificial way as in Padovani & Matteucci (1993); in fact, the black hole growth at late times is limited by the available amount of gas, as described by Bondi accretion. The figure suggests an approximately linear relation between the bulge and black hole mass, as first measured by Kormendy & Richstone (1995) and Magorrian et al. (1998). Therefore, Seyfert galaxies appear to obey the same relationship as quiescent galaxies and QSOs, as already stated observationally by Nelson et al. (2004).

There were claims for a non-linear relation between spheroid and black hole mass (Laor 2001; Wu & Han 2001); however, measurements of Marconi & Hunt (2003) re-established the direct proportionality between the spheroid mass M_{sph} and M_{BH},

$$M_{BH} \simeq 0.0022 M_{sph}, \tag{6.29}$$

also in good agreement with recent estimates from McLure & Dunlop (2002) and Dunlop et al. (2003)

$$M_{BH} \simeq 0.0012 M_{sph} \tag{6.30}$$

and from Häring & Rix (2004)

$$M_{BH} \simeq 0.0016 M_{sph}. \tag{6.31}$$

The three relations of McLure & Dunlop (2002), Marconi & Hunt (2003) and Häring & Rix (2004) are thus reported in the figure for comparison. The agreement between measurements and predictions is rather good (within a factor of two).

In Fig. 6.6 we plot the predicted bolometric nuclear luminosities L_{bol} for the various masses, compared with luminosity estimates for the Seyfert population (see e.g.

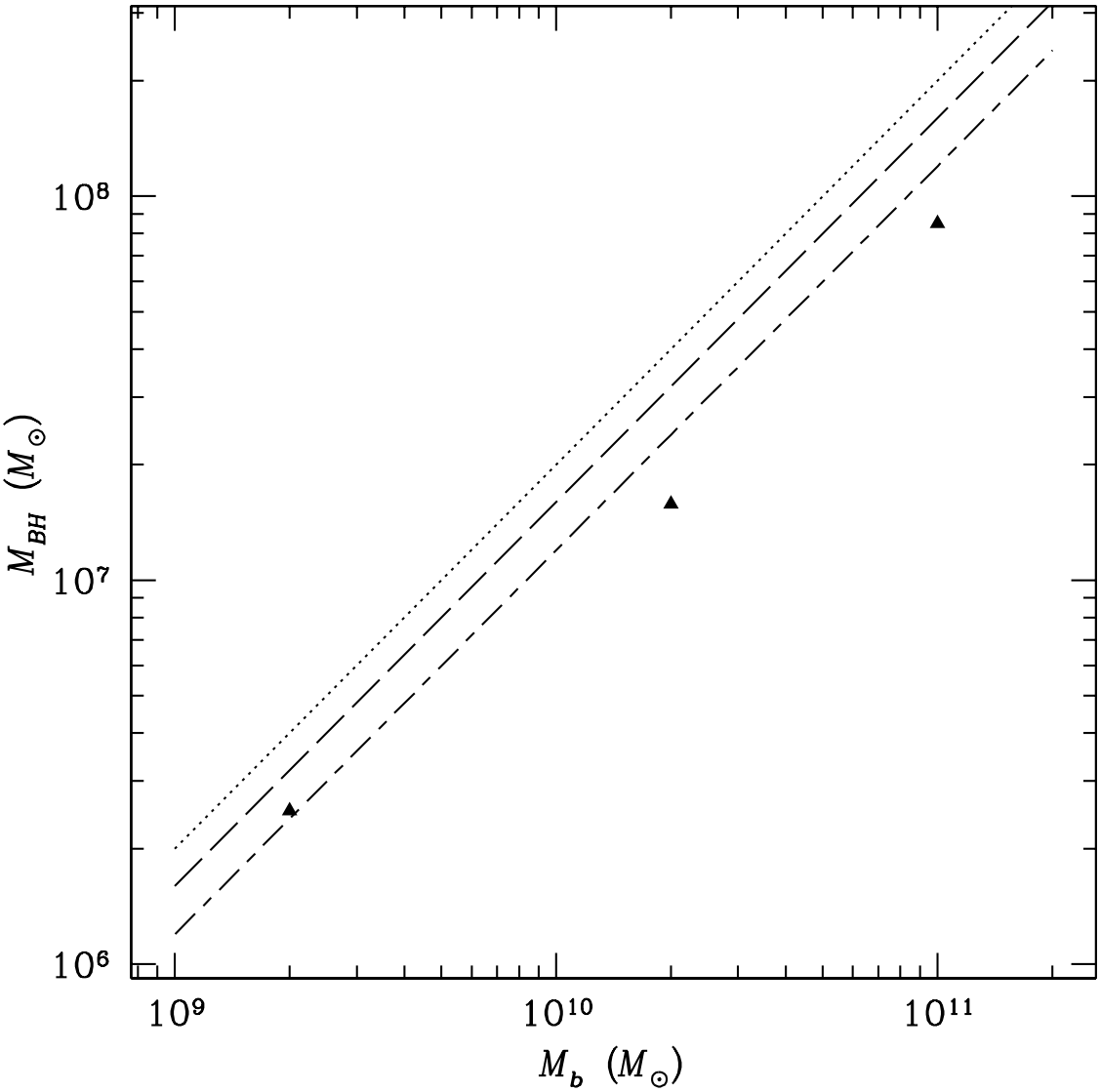

Figure 6.5: Final black hole masses as a function of the bulge mass predicted by our models (triangles). The short dashed-long dashed line represents the measured relation of McLure & Dunlop (2002), the dotted line the one of Marconi & Hunt (2003) and the dashed line the one of Häring & Rix (2004).

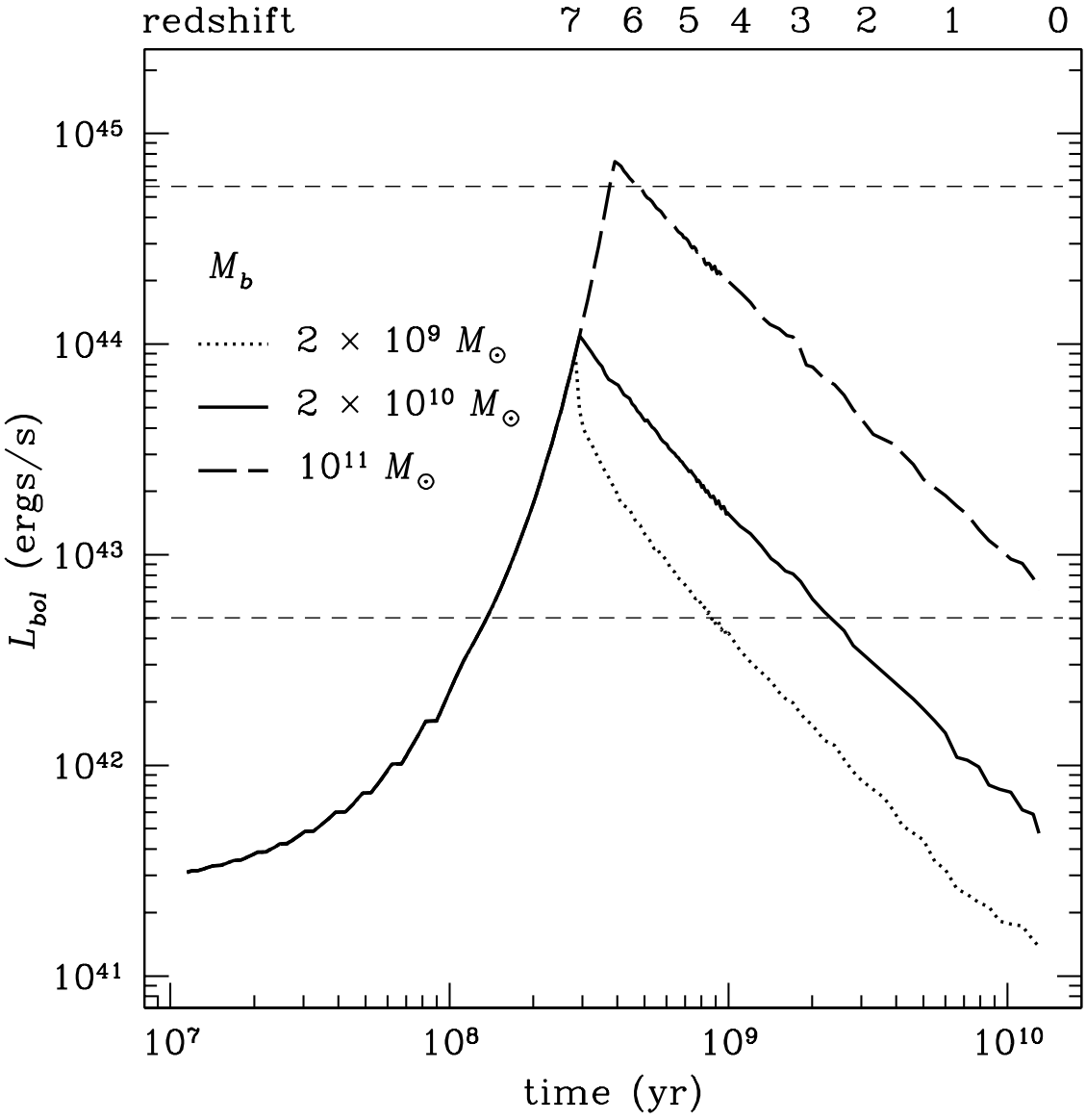

Figure 6.6: Evolution with time and redshift of the bolometric luminosity emitted by the accreting black hole for bulges of various masses. The dotted lines represent the range spanned by observations (see text for details).

González Delgado et al. 1998; Markowitz et al. 2003; Brandt & Hasinger 2005; Wang & Wu 2005; Gu et al. 2006). Of course, L_{bol} is proportional to the calculated mass accretion rate (Fig. 6.2). In the first part, the plots overlap because the Eddington luminosity only depends on the black hole mass, and it is independent of the galaxy mass; on the contrary, the Bondi accretion rate is sensitive to the galaxy features. The break in the plot corresponds to the time when the Bondi accretion rate becomes lower than the Eddington accretion rate (see Eqs. 6.17 and 6.19), and occurs later and later for more massive galaxies, which therefore keep accreting at the Eddington rate on longer timescales. This helps explain why the outcoming final black hole mass is proportional to the adopted bulge mass.

We see that the luminosities near the maximum are reproduced by models of all masses. The same is not true for local ($z \simeq 0$) Seyferts, because only the most massive model yields a bolometric luminosity that lies in the observed range, while for other masses the disagreement reaches a factor of ~ 100. To simply shift the epoch of star formation of the less massive Seyferts would require unrealistically young bulges (with ages $\lesssim 1$ Gyr), whereas one of our main assumptions is that spiral bulges are old systems. Padovani & Matteucci (1993) assumed that the black hole accreted the whole mass lost from evolved stars. If we calculate the fraction $\dot{M}_B/\dot{M}_*$ at any given time, we see that its value is very close to 0.01. This explains why they obtained the correct nuclear bolometric luminosity of local radio-loud QSOs, but severely overestimated the mass of the resulting black hole, which led them to suggest that the accretion phase should last for a period not longer than a few 10^8 years, at variance with the present work. Moreover, it is not physically justified to assume that all the mass expelled from dying stars falls onto the black hole.

One way to overcome this problem is to suppose that the smallest bulges undergo a rejuvenation phase, which is possible because spiral bulges are not isolated systems, but an interaction with their surrounding disks can be triggered in several ways (bar instabilities, minor mergers, fly-by's, and so on). By using models combining recent star formation with a base old population, Thomas & Davies (2006) found that the smallest bulges must have experienced star formation events involving $10 - 30\%$ of their total mass in the past $1 - 2$ Gyr. The same conclusion was also reached on an independent basis by MacArthur et al. (2007), who studied a sample of 137 spiral bulges in the GOODS fields and, by means of photometric techniques, estimated the star formation necessary to reproduce the observed colour range. They concluded that,

while all stellar populations belonging to bulges with $M_B > 10^{11} M_\odot$ are homogeneously old and consistent with a single major burst of star formation at $z > 2$, the colours and mass-to-light ratios of smaller bulges require that they have experienced mass growth since $z \sim 1$, so that a $\sim 10\%$ fraction of stellar mass eventually goes into younger stars.

Secondary accretion/star formation episodes may also help explain the presence of the Galactic bulge Mira population, whose calculated age is $1 - 3$ Gyr (van Loon et al. 2003; Groenewegen & Blommaert 2005) and of young stars and star clusters in the very centre of the Galaxy (Figer et al. 1999; Genzel et al. 2003). Paumard et al. (2006) also studied a population of OB stars in the central parsec of the Galaxy and found an even younger age of $\simeq 6 \pm 2$ Myrs. A small fraction of intermediate-age stellar population was also detected in Seyfert 2 nuclei (Sarzi et al. 2007).

Finally, we note that by means of the present (non-hydrodynamical) modelling of the black hole accretion rate and of the gas budget, a truly realistic accretion cannot be reproduced, whereas in a more realistic treatment, the AGN feedback would cause the luminosity to switch on and off several times at the peaks of luminosity. We also note that at late times, when the accretion is significantly sub-Eddington, a considerable reduction in the emitted AGN luminosity might result as a consequence of a possible radiatively inefficient accretion mode (e.g. Narayan & Yi 1994). This could reproduce the quiescence of black holes at the centre of present-day inactive spiral galaxies in a picture where all spiral galaxies host a Seyfert nucleus at some time of their evolution.

6.6.4 Metallicity and elemental abundances

The mean values attained by the metallicity and the examined abundance ratios for $z \lesssim 6$ are resumed in Table 6.2. Note that all the [α/Fe] ratios are undersolar or solar. Fig. 6.7 shows the evolution with time and redshift of the metallicity Z in solar units (which, we recall, is the abundance of all the elements heavier than ^{4}He), for a standard ΛCDM scenario with $H_0 = 65$ km s^{-1} Mpc^{-1}, $\Omega_M = 0.3$ and $\Omega_\Lambda = 0.7$.

It can be seen that solar metallicities are reached in a very short time, ranging from about 3×10^7 to 10^8 years with decreasing bulge mass (see Table 6.2). We notice that, due to the α-enhancement that is typical of spheroids prior to the wind, solar Z is always reached well before solar [Fe/H] is attained, which occurs at times $\sim (1-3) \times 10^8$ years. Then, Z remains approximately constant for the contribution of Type Ia supernovae and low- and intermediate-mass stars, before declining in the very late phases. The high metallicities inferred from observations (e.g. Hamann et al 2002; Dietrich et al.

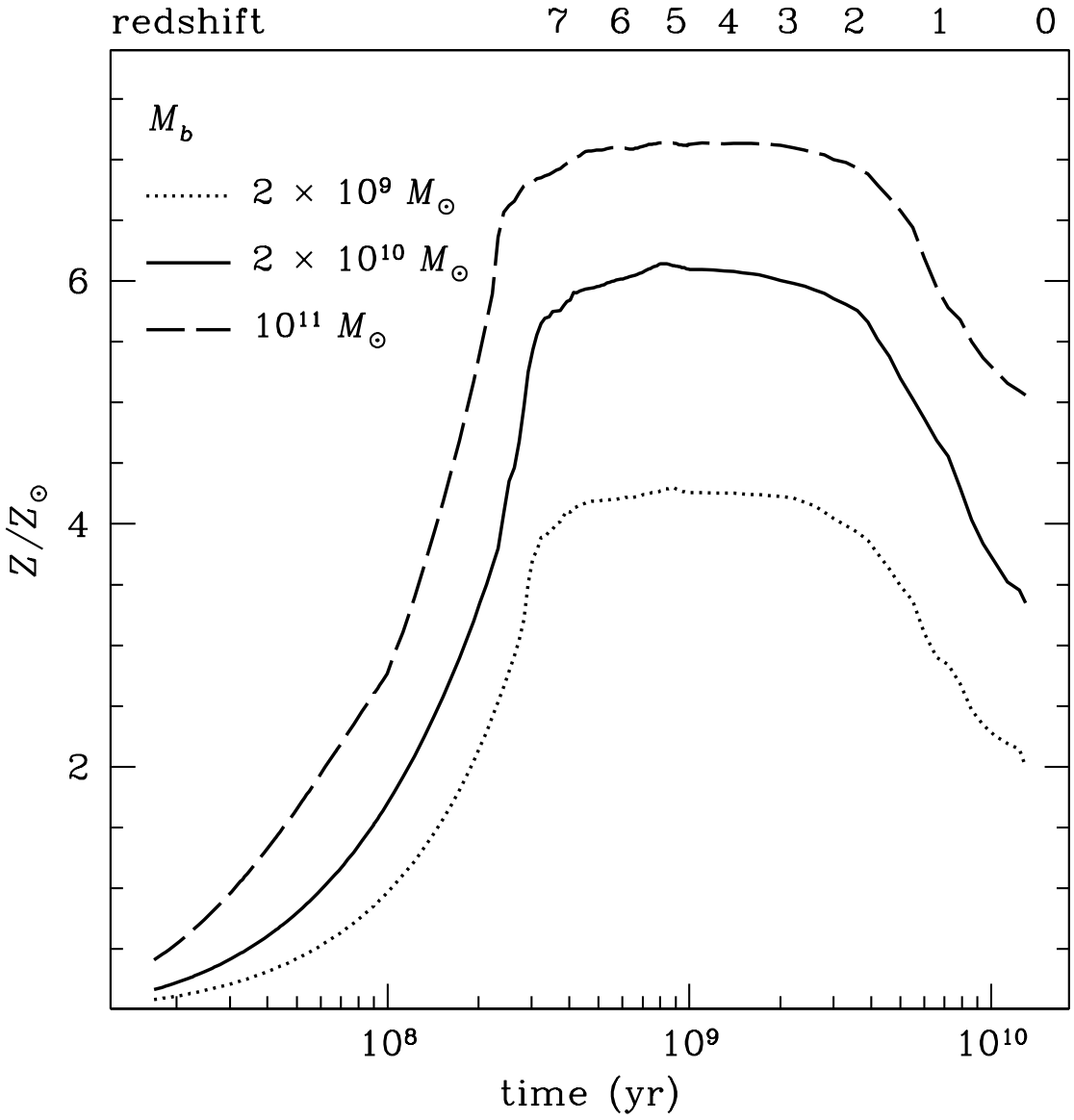

Figure 6.7: Evolution with time (bottom axis) and redshift (top axis) of the metallicity in solar units $Z/Z_\odot$. The different curves denote different bulge masses as indicated in the upper left corner.

Chemical properties of Seyfert nuclei

M_b ($M_\odot$)	2×10^9	2×10^{10}	10^{11}
$Z/Z_\odot$	4.23	6.11	7.22
[Fe/H]	+0.83	+0.96	+1.07
[O/H]	+0.18	+0.36	+0.48
[Mg/H]	+0.38	+0.55	+0.69
[Si/H]	+0.79	+0.98	+1.13
[Ca/H]	+0.63	+0.88	+1.06
[O/Fe]	−0.68	−0.60	−0.59
[Mg/Fe]	−0.45	−0.41	−0.38
[Si/Fe]	−0.04	+0.02	+0.06
[Ca/Fe]	−0.19	−0.07	+0.00
[N/H]	+0.28	+0.63	+0.87
[C/H]	+0.15	+0.24	+0.30
[N/C]	+0.13	+0.40	+0.57
$t(Z_\odot)$ (yr)	10^8	6×10^7	3×10^7

Table 6.2: Values assumed by the chemical abundance ratios and by the metallicity in solar units after the wind by bulges of different masses, and the time by which $Z_\odot$ is reached in the different models (last line), are shown.

2003b, their Figures 5 and 6) are thus very easily achieved. More massive bulges give rise to higher metallicities, which agrees with the statement that more luminous AGNs are more metal rich, if we assume that more massive galaxies are also more luminous. This assumption is supported observationally by e.g. Warner et al. (2003) who find a positive correlation between the mass of the supermassive black hole and the metallicity derived from emission lines involving N V in 578 AGNs spanning a wide range in redshifts.

The time dependencies of the abundances of the elements under study for each mass are shown in the Figs. 6.8 (iron) and 6.9 (α-elements, carbon and nitrogen). A fast increase in the abundances is noticeable at early times, as well as a weak decrease at later times, for all the elements and all masses; after the galactic wind, i.e. for $t \gtrsim 0.2 - 0.3$ Gyr (which corresponds to a redshift $z \simeq 6-7$ in the adopted cosmology) the abundances decrease by a factor smaller than 2. Such a weak decrease occurs over a period of more than 13 Gyr. This can explain the observed constancy of the QSO abundances as a function of redshift (Osmer & Shields 1999).

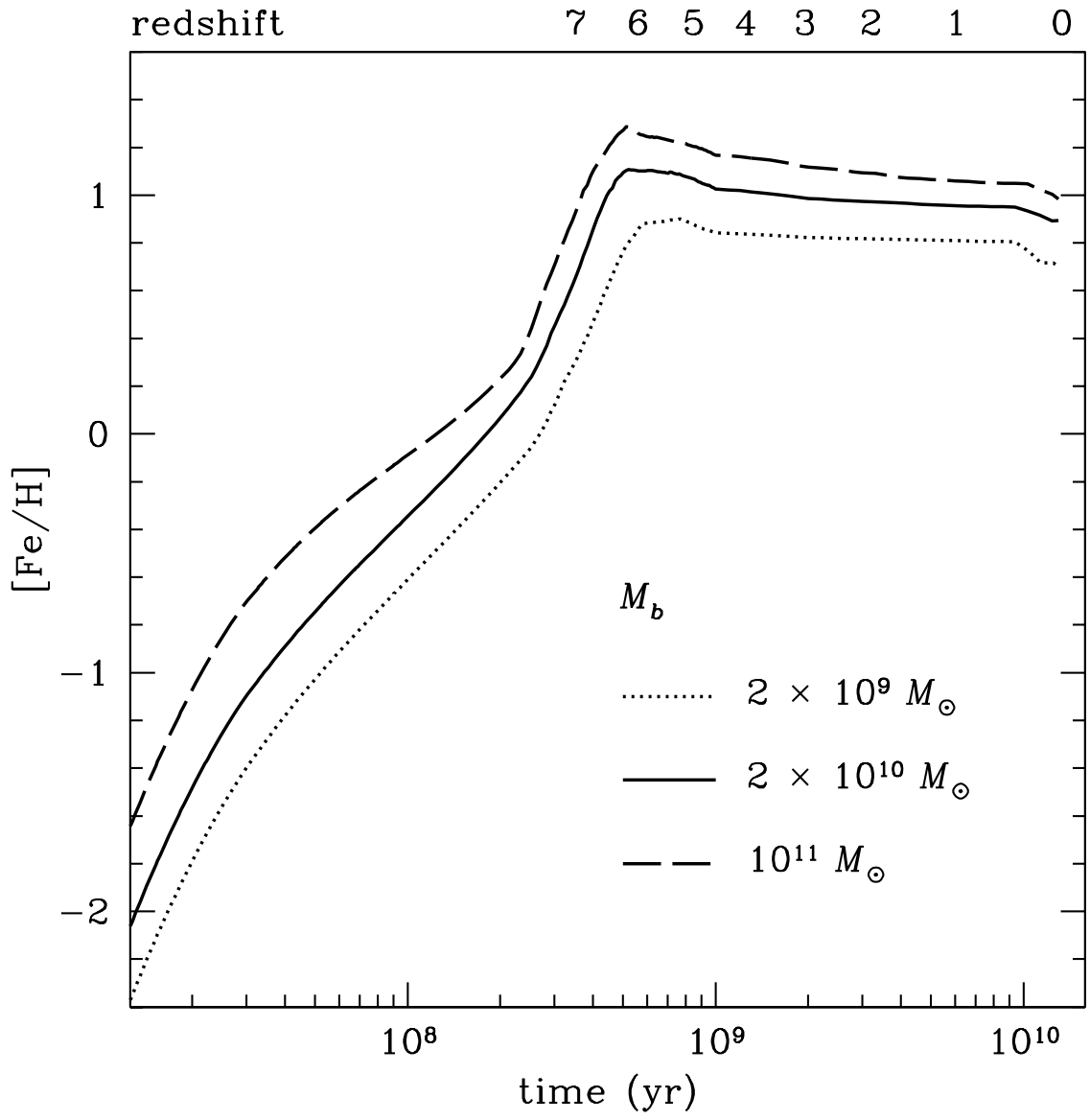

Figure 6.8: Evolution with time (bottom axis) and redshift (top axis) of the [Fe/H] abundance ratio in bulges of various masses, as indicated in the lower right corner.

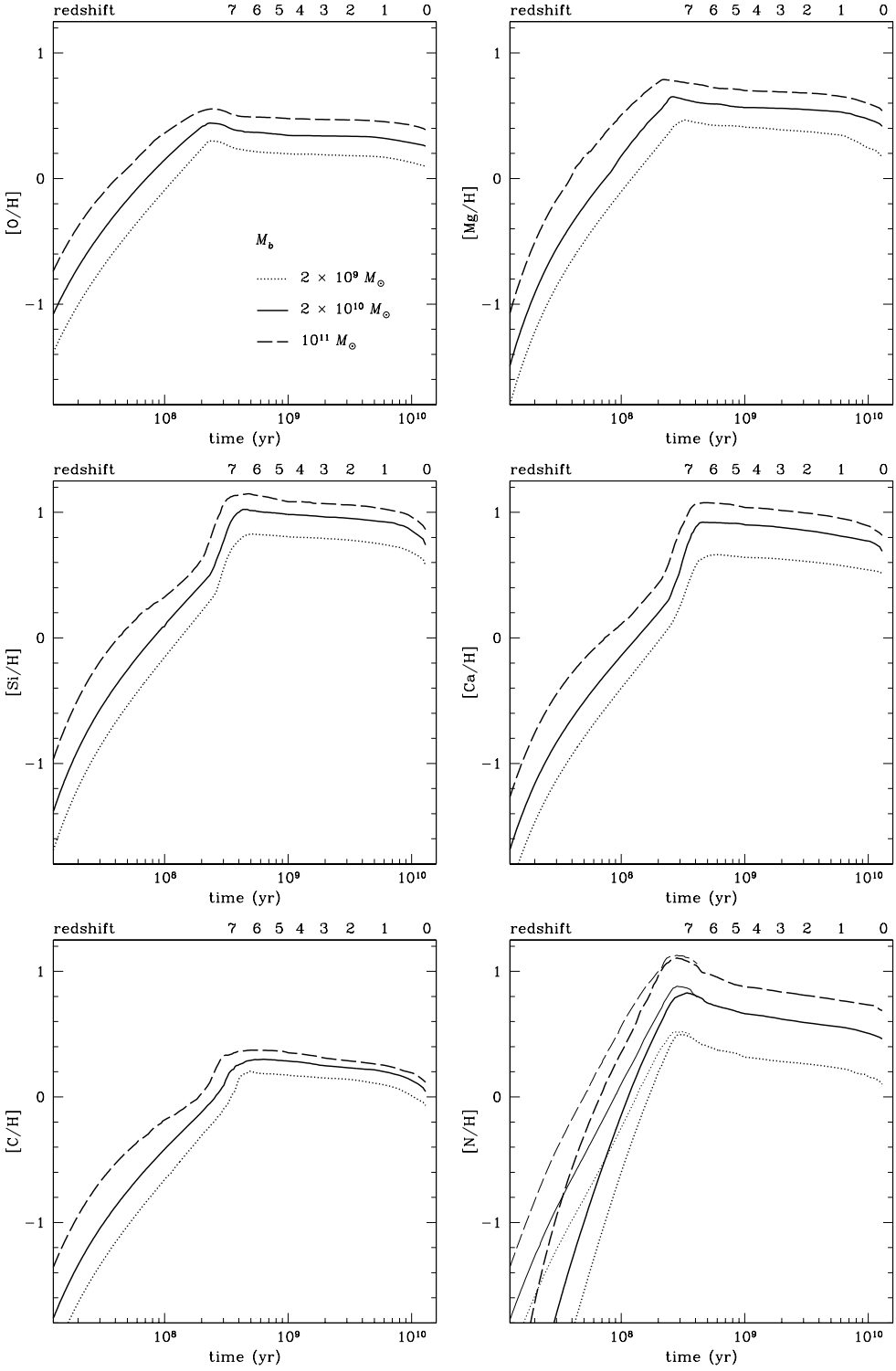

Figure 6.9: Evolution with time and redshift of the [X/H] abundance ratios for O, Mg, Si, Ca, C and N in bulges of various masses. The bump at $\sim 2 \times 10^8$ yr in the [Si/H] and [Ca/H] plots is due to the occurrence of the wind, which shortly precedes the maximum in the Type Ia supernova rate. The thin lines in the [N/H] plot represent the results obtained by adopting primary N in massive stars, as in Matteucci (1986).

The elements can be divided according to their behaviour after the wind:

- O and Mg show moderate overabundances relative to solar. They are produced essentially by massive stars ($M > 8M_{\odot}$) on short timescales ($\lesssim 10^7$ years), i.e. almost in lockstep with the star formation. After the galactic wind, therefore, their abundance cannot increase any more because star formation vanishes. They tend instead to be diluted due to the effect of hydrogen-rich stellar mass loss from dying stars. In our Galactic bulge model, at the time of the onset of the wind, Mg is more abundant than O, since although [O/H] is higher at earlier times, it declines very rapidly due to the dependence on metallicity of the adopted O yields (François et al. 2004)[1]. Therefore, we expect the mean value attained by [O/H] after the wind to be lower than that of [Mg/H], which is what we predict. In fact, the mean [O/H] for $z \lesssim 6$ ranges from +0.18 to +0.48 dex, i.e. oxygen is $\sim$ 1.5 to 3 times solar, in good agreement with observations (Storchi-Bergmann et al. 1996; Fraquelli & Storchi-Bergmann, 2003), and the mean [Mg/H] ranges from +0.38 to +0.69 dex (i.e. 2.5 to 5 times solar), depending on the mass of the host bulge. Finally, we notice that both [O/H] and [Mg/H] reach solar values at times closer to those when $Z = Z_{\odot}$ with respect to [Fe/H] for the different models and are therefore better proxies for the metallicity in the bulge. This is because the metallicity is dominated by O in the bulge.

- Fe, Si and Ca are characterised by a bump immediately after the occurrence of the galactic wind, which leads to a significant increase in their abundance, reaching remarkably higher values than in the previous cases ([Fe/H]: +0.83 to +1.07, i.e. $\sim$7$-$10 times solar; [Si/H]: +0.79 to +1.13, i.e. $\sim$6$-$12 times solar; [Ca/H]: +0.63 to +1.06, i.e. $\sim$4$-$10 times solar). This bump is due to the combined effect of the discontinuity caused by the onset of the galactic wind at times of 0.21 to 0.28 Gyr depending on the model mass, and of the maximum of the Type Ia supernova rate, occurring at $\sim 0.2 - 0.3$ Gyr. In fact, these elements are also produced by Type Ia supernovae (Fe mainly, Si and Ca in part, as they are also produced by Type II supernovae), which derive from progenitors with masses ranging from 0.8 to $8M_{\odot}$. These elements are restored into the interstellar medium on timescales ranging

[1]Although, the Maeder (1992) yields for oxygen have been proved to solve the discrepancy between the abundance evolution of oxygen and other α-elements, in this Chapter we are still using the François (2004) yields as standard since there are still open issues concerning the zero-point of the plots (see Chapter 4).

from $\sim$ 30 Myr to a Hubble time. Thus, their abundances could in principle keep increasing even after the star formation has ceased. However, due to the adopted top-heavy IMF ($x_2 = 0.95$), a relatively small fraction of low- and intermediate-mass stars were produced with respect to what we would expect if we had adopted a steeper IMF (see below for a comparison with the IMF of Salpeter 1955), and therefore what we observe is a decrease of the Si, Fe and Ca abundances after the galactic wind. The estimates for Fe in Seyferts are lower than those calculated here, but we must take several factors into account that would lead to underestimating the Fe produced by stars, e.g. depletion by dust (see Calura et al. 2007a) or dilution of spectra by a dusty torus continuum.

- C, as well as O and Mg, is slightly overabundant ($\sim$1.3 to 2.7 times solar). Although it is mostly produced by low- and intermediate-mass stars, in this same range of masses it is also used up to form N. In this case the bump is less pronounced and is mainly caused by the discontinuity induced by the galactic wind, which enhances the relative contribution of low- and intermediate-mass stars.

- Finally, a behaviour similar to Fe is expected for N, since the bulk of this element originates from stars with $M < 8M_{\odot}$. There are, nonetheless, two significant differences: first, due its secondary nature, its abundance increases much more rapidly than other elements with time (and with metallicity); and second, this very rapid increase hides the bump at the onset of the wind. We also adopt a primary N production in massive stars (Matteucci 1986; see also Chiappini et al. 2006), but the effects of this choice are only visible before t_{GW}, i.e. when nucleosynthesis from massive stars is active; the decrease of the [N/H] ratio towards earlier times (i.e. lower metallicities) is less rapid. Then, after the wind, the plots with and without primary N essentially overlap. This has already been observed in Ballero et al. (2006) and Ballero et al. (2007a). The mean values attained by [N/H] after the galactic wind ranges from +0.28 to +0.87 dex; i.e., nitrogen is $\sim$2 to 8 times overabundant with respect to solar. However, [N/H] reaches overabundances of $\sim$3$-$10 times solar at its peak. These results agree with the estimates for Seyferts (Schmitt et al. 1994; Storchi-Bergmann et al. 1996; Rodríguez-Ardila et al. 2005).

The different behaviour among the α-elements (O, Mg *vs.* Si, Ca) is even more evident in Fig. 6.10, where the correlation with mass of the [α/Fe] abundance ratios after the wind is shown. A net separation is present: whereas [Si/Fe] and [Ca/Fe] are

approximately solar, O and Mg are underabundant with respect to solar, O showing a more pronounced underabundance. This also agrees with the estimates of a slightly supersolar [Fe/Mg] in QSOs and of its weak correlation with luminosity (Dietrich et al. 2003a). Since both [Fe/H] and [Mg/H] are constant within a factor of 2 up to high redshifts ($z \simeq 6$) and follow the same declining trend with time, we expect this relation to hold for most of the bulge lifetime, which is what is observed for QSOs (Thompson et al. 1999; Iwamuro et al. 2002; Freudling et al. 2003; Dietrich et al. 2003a; Barth et al. 2003; Maiolino et al. 2003; Iwamoto et al. 2004). Here, we predict [Fe/Mg] values ranging from +0.38 to +0.45 dex, the highest values corresponding to less massive galaxies where star formation stops later and Type Ia supernovae have more time to pollute the bulge interstellar medium.

Fig. 6.11 shows the variation with mass in the [N/C] abundance ratio. The figure illustrates well that this ratio is remarkably sensitive to the galaxy mass, which, as we have seen in Fig. 6.7, is correlated with the galaxy metallicity. This happens because of the secondary nature of N, which is produced at the expense of C in a fashion proportional to the metallicity of the interstellar medium. The mean [N/C] ratio for $z \lesssim 6$ ranges from +0.13 to +0.57 dex depending on the bulge mass; i.e., the N/C ratio is $\sim$ 1.4 to 3.7 times solar. If we consider the amount of variation in the two abundances, these values are consistent with the estimates of Fields et al. (2005a).

Finally, we briefly compare the results obtained with the top-heavy IMF ($x_2 = 0.95$) with those we obtain if instead we adopt $x_2 = 1.35$ (Salpeter 1955). In Ballero et al. (2007a) this IMF was excluded on the basis of the stellar metallicity distribution, since with our model the Salpeter index for massive stars gives rise to a distribution that is too metal-poor with respect to the observed ones (Zoccali et al. 2003; Fulbright et al. 2006), and Ballero et al. (2007b) seem to further confirm this point. However, Pipino et al. (2007b) showed that the multi-zone hydrodynamical model for ellipticals of Pipino et al. (2007a), where the spheroids form "outside-in", can be adapted to the galactic bulge and, by means of internal gas flows that funnel metals to the centre, it reproduces the above-mentioned metallicity distributions with a Salpeter IMF (although the top-heavy IMF with is still considered a viable solution). Furthermore, as we shall show (see §6.6.5), the $(B-I)$ colours and bulge K-band luminosity are better reproduced by a Salpeter IMF above $1M_{\odot}$. Therefore a brief comparison is useful.

In Fig. 6.12 we show the evolution with time and redshift of the abundance ratios relative to hydrogen for some of the elements considered, namely Fe, O and N. We find

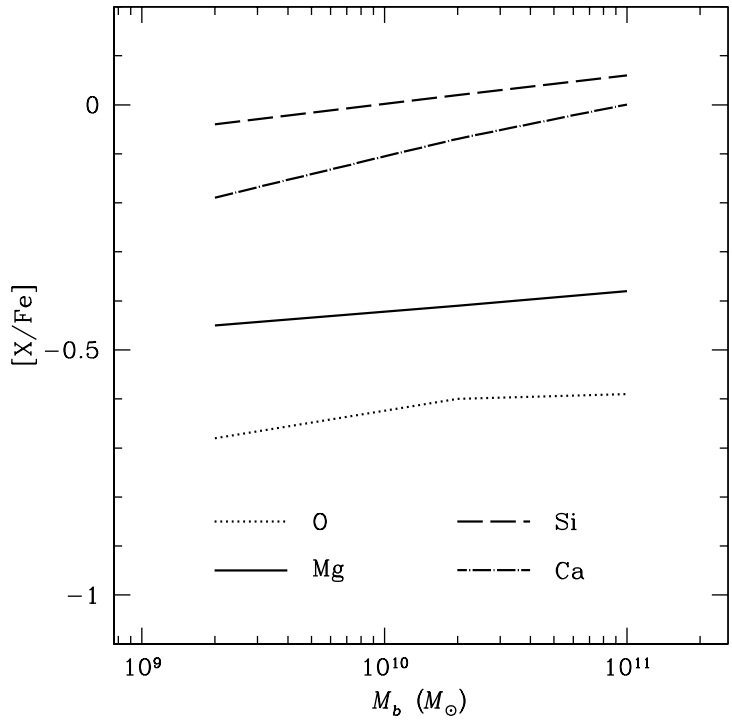

Figure 6.10: Correlation with bulge mass of the [α/Fe] abundance ratios for $z \lesssim 6$.

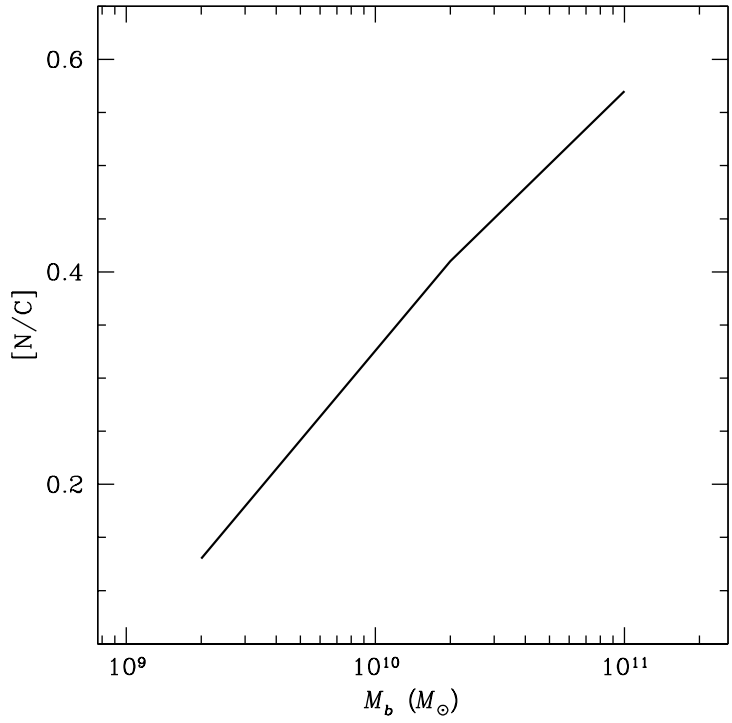

Figure 6.11: Correlation with bulge mass of the [N/C] abundance ratio for $z \lesssim 6$.

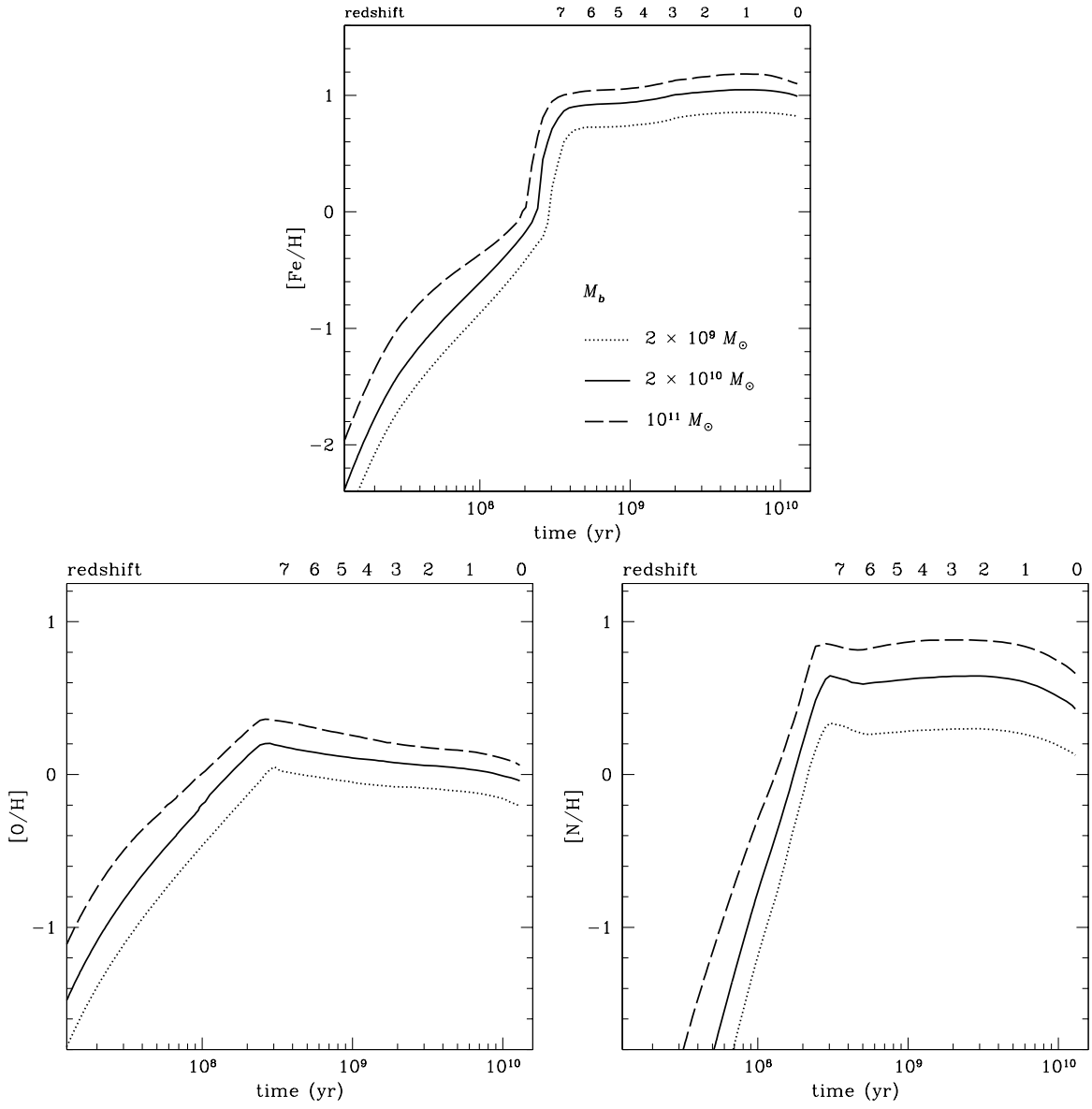

Figure 6.12: Evolution with time and redshift of the [X/H] abundance ratios for Fe, O and N in bulges of various masses and the adoption of a Salpeter (1955) IMF above $1M_\odot$. The discontinuity at $\sim 3 \times 10^8$ yr in the [Fe/H] plot is due to the occurrence of the galactic wind, which shortly precedes the maximum in the Type Ia supernova rate.

similar trends for all the elements. However, in the Salpeter case, the abundances at the wind are lower than with a top-heavy IMF, because the enrichment from massive stars is lower. Then, those elements that are produced mainly by low- and intermediate-mass stars (in this case, Fe and N) keep increasing after the wind until they reach a maximum value, which is generally slightly higher than what is obtained with the top-heavy IMF, and their abundance stops increasing. The bump in the [Fe/H] ratio is ~ 0.1 dex larger because the production of Type Ia supernova progenitors is favoured in this case. In contrast, oxygen abundance decreases steadily after the wind because it is essentially produced by massive stars and its value remains below the one calculated with the top-heavy IMF. The abundance ratios are still almost constant for $z \lesssim 6$, and their mean values are, respectively,

- [Fe/H] = +0.79 to +1.08 dex, i.e. 6 to 12 times solar;
- [O/H] = −0.09 to +0.27 dex, i.e. 0.8 to 2 times solar;
- [N/H] = +0.29 to +0.84 dex, i.e. 2 to 7 times solar.

The values for Fe are thus again overestimated with respect to observations, but as said, the latter are not corrected for Fe depletion by dust or dilution by dusty torus continuum (Ivanov et al. 2003). The total metallicity Z ranges from about 3.5 to 6.5 solar, i.e. slightly less than in the top-heavy IMF case, but still in agreement with observational estimates, as well as the N and O abundances.

We point out that the adoption of a Salpeter (1955) IMF only results into small changes in the quantities calculated previously, i.e. mass accretion rate, luminosity, energetics and final black hole mass. The accretion rates of Eddington and Bondi do not depend directly on the adopted IMF. A steeper IMF only slightly shifts the time of occurrence of the wind of a few tens Myrs ahead, thus prolonging the Eddington-limited accretion phase that, as we said, is the phase when most of accretion and shining occurs. This will lead to a higher black hole mass; however, the final black hole masses increase by only about 10%.

6.6.5 Bulge colours and colour-magnitude relation

In this section, we present our results for the spectro-photometric evolution of the three bulge models we studied.

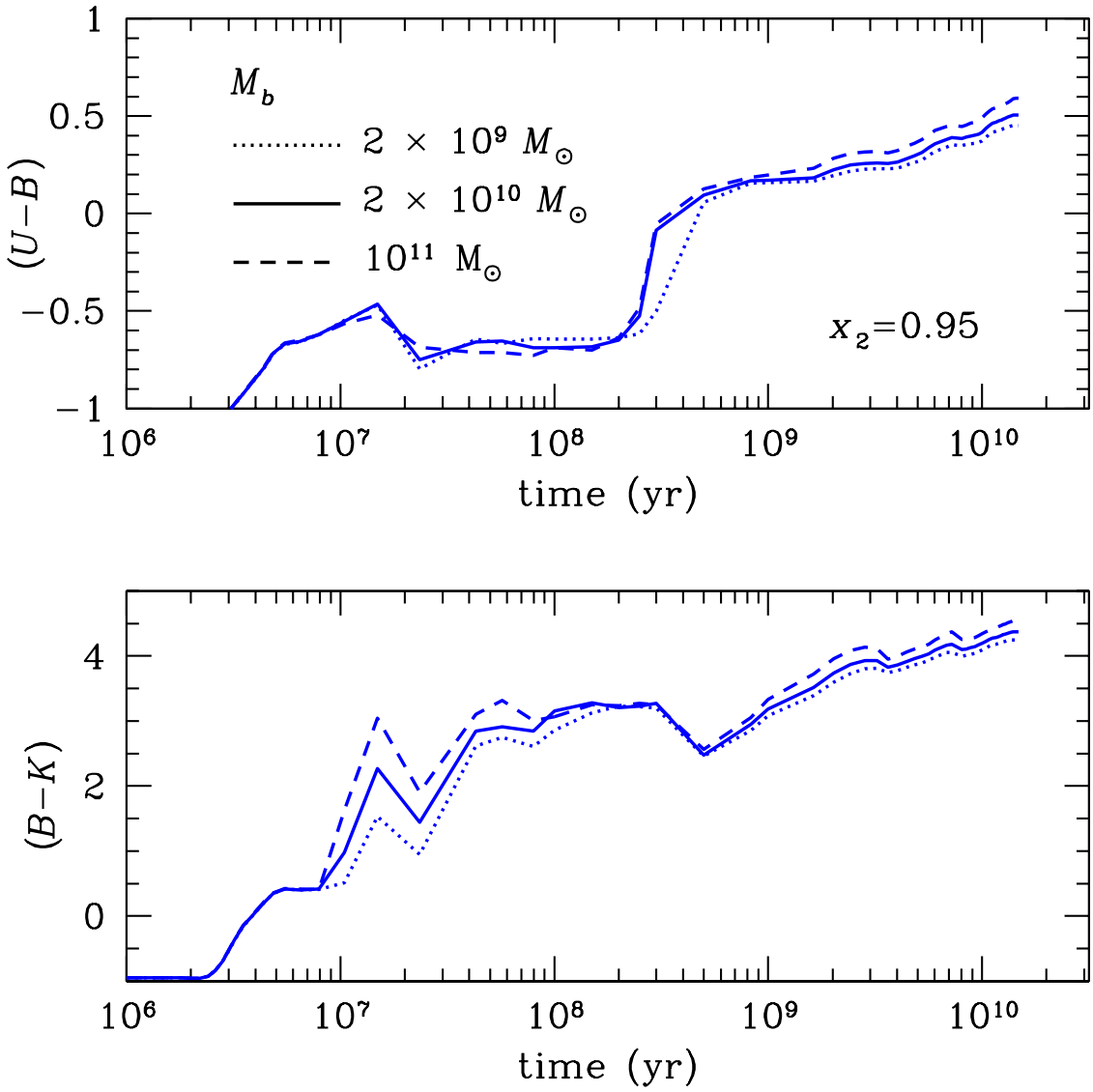

Figure 6.13: Evolution of the predicted $(U-B)$ (upper panel) and $(B-K)$ (lower panel) colours for bulge models of three different masses (*dotted line:* $M_b = 2 \times 10^9 M_\odot$; *solid line:* $M_b = 2 \times 10^{10} M_\odot$; *dashed line:* $M_b = 10^{11} M_\odot$), assuming an IMF with $x_2 = 0.95$.

In Fig. 6.13, we show the predicted time evolution of the $(U-B)$ and $(B-K)$ colours for the three bulge models studied in this work. We assume an IMF with $x_1 = 0.33$ for stars with masses m in the range $0.1 \leq m/M_{\odot} \leq 1$ and $x_2 = 0.95$ for $m > 1M_{\odot}$, i.e. our reference IMF. At all times, higher bulge masses correspond to redder colours, owing both to a higher metallicity and to an older age. This is consistent with the popular downsizing picture of galaxy evolution, according to which the most massive galaxies have evolved faster than the less massive ones (Matteucci 1994; Calura et al. 2007c).

In Fig. 6.14, we show how the assumption of two different IMFs affects the predicted evolution of the $(U-B)$ and $(B-K)$ colours, for a bulge of mass $M_b = 2 \times 10^{10} M_{\odot}$. We compare the colours calculated with the reference IMF with the ones calculated by assuming $x_1 = 0.33$ for stars with masses m in the range $0.1 \leq m/M_{\odot} \leq 1$ and $x_2 = 1.35$ for $m > 1M_{\odot}$, i.e. a Salpeter (1955) index for x_2. It is interesting to note how, at most of the times, the assumption of a flatter IMF for stars with masses $m > 1M_{\odot}$ implies redder colours. This is due primarily to a metallicity effect, since a flatter IMF gives rise to a larger number of massive stars and a larger fraction of O (the element that dominates the metal content) restored into the interstellar medium at all times.

In Figure 6.15, we show the colour-magnitude relation predicted for our bulge models and compared to the data from Itoh & Ichikawa (1998, panel *a*), and Peletier & Balcells (1996, panels *b* and *c*). Itoh & Ichikawa (1998) measured the colours of 9 bulges in a fan-shaped aperture opened along the minor axis, in order to minimise the effects of dust extinction. In panel *a* of Fig. 6.15 we show the linear regression to the data observed by Itoh & Ichikawa (1998) and the dispersion.

Peletier & Balcells (1996) determined the colours for a sample of local bulges, for which they estimated that the effect of dust reddening is negligible. Of the sample studied by Peletier & Balcells (1996), we consider a subsample of 17 bulges here, for which Balcells & Peletier (1994) have published the absolute R magnitudes. This allows us to plot an observational colour-magnitude relation.

The predicted colour-magnitude relation has been calculated by adopting two different IMFs, i.e. with $x_2 = 0.95$ and $x_2 = 1.35$, represented in Fig. 6.15 by solid circles and solid squares respectively. From the analysis of the I *vs.* $(B-I)$ plot, we note that the adoption of a flatter IMF leads to an overestimation of the predicted $(B-I)$ colours; in fact, the predictions for the flatter IMF lie above the upper dotted lines, representing the upper limits for the data observed by Itoh & Ichikawa (1998). On the other hand, the predictions computed with an IMF with $x_2 = 1.35$ are consistent with the available

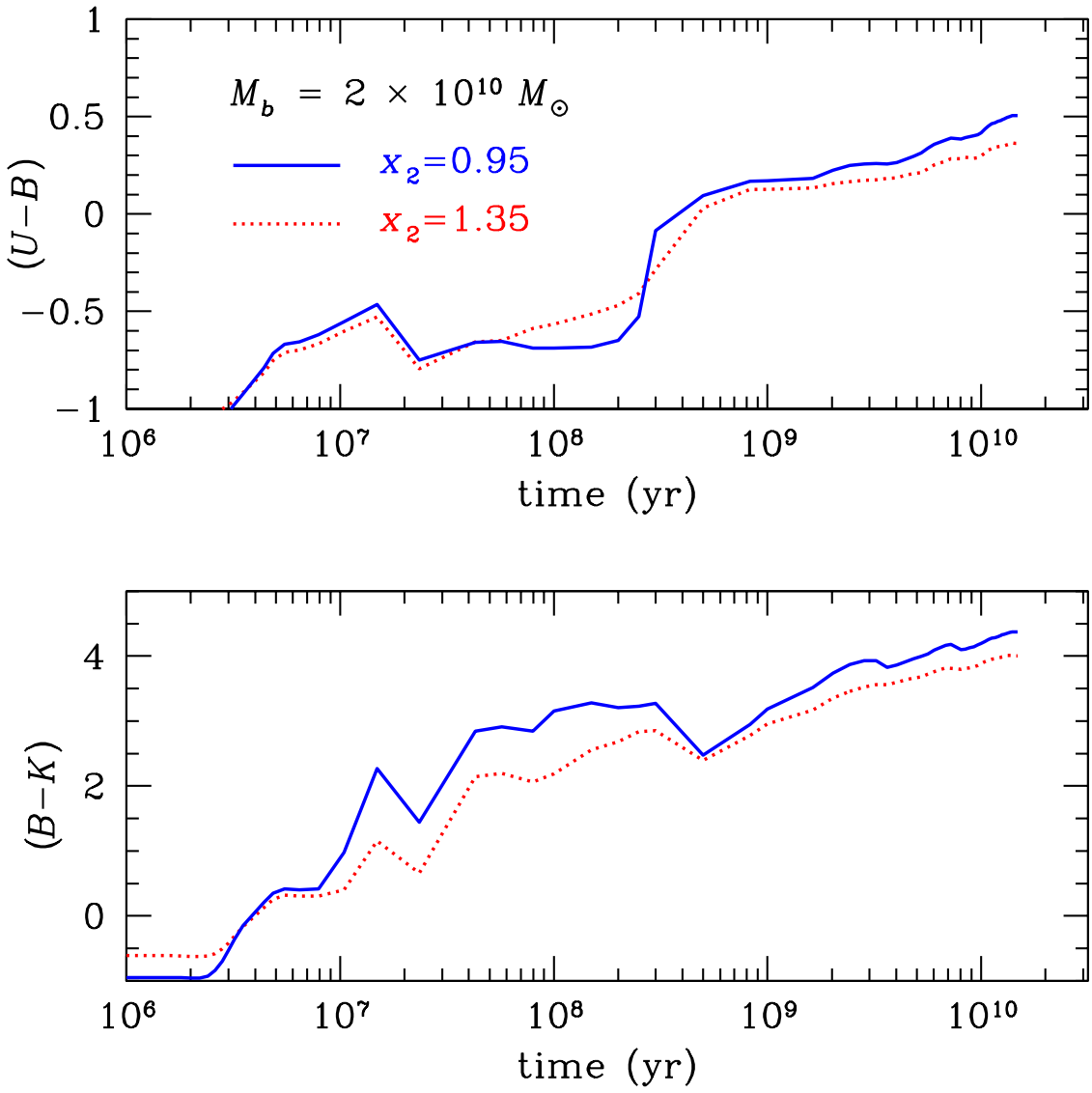

Figure 6.14: Evolution of the predicted $(U-B)$ (upper panel) and $(B-K)$ (lower panel) colours for a bulge model of mass $M_b = 2 \times 10^{10} M_\odot$ assuming two different IMFs. The solid lines represent the colours computed by assuming $x_2 = 0.95$, whereas the dotted lines are computed assuming $x_2 = 1.35$.

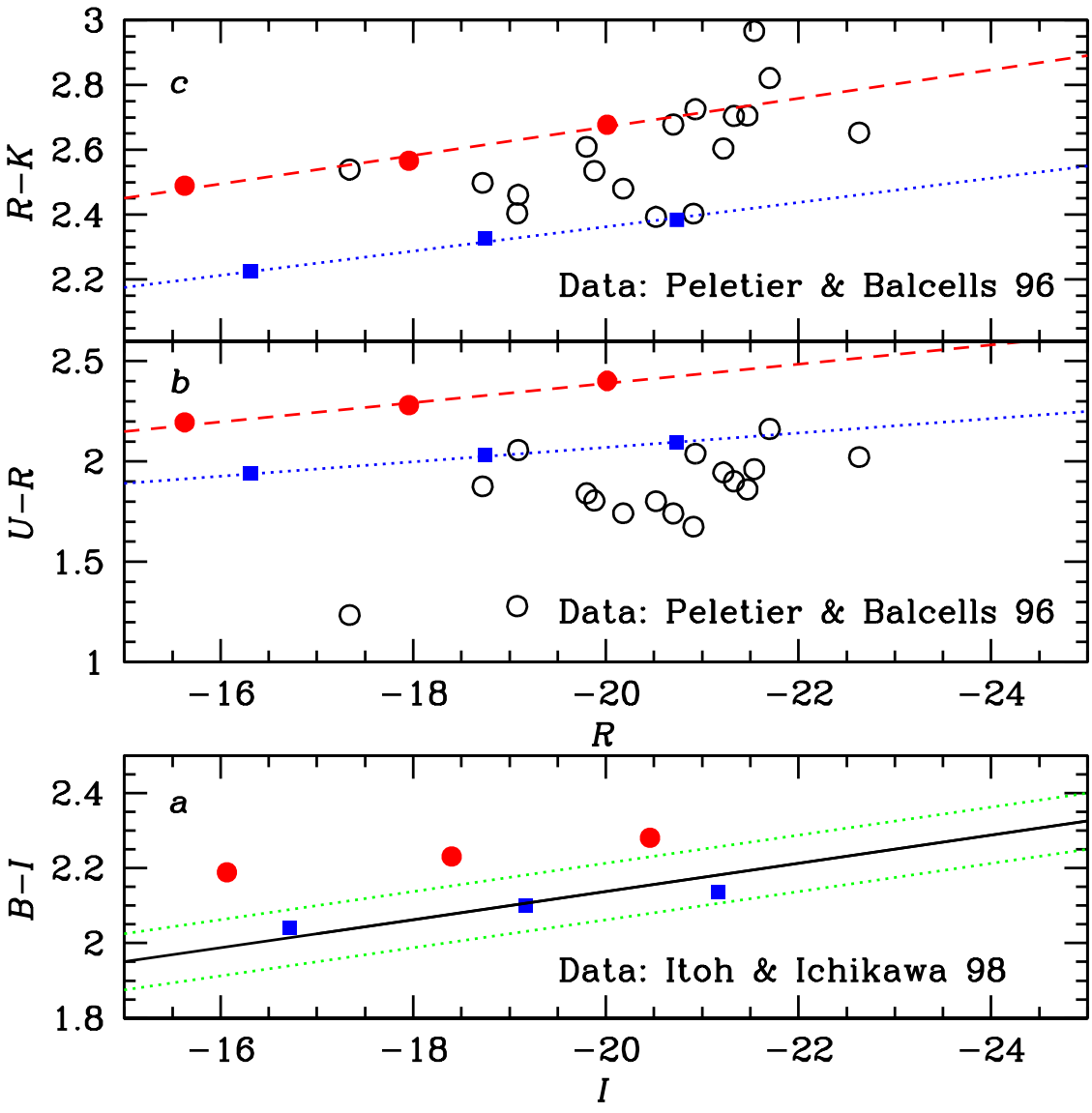

Figure 6.15: Predicted and observed colour-magnitude relation for bulges. The solid line and the dotted lines in panel *a* are the regression and the dispersion of colour-magnitude relation observed by Itoh & Ichikawa (1998), respectively. The solid circles and solid squares are our predictions for the three bulge models investigated, computed by assuming for the IMF $x_2 = 0.95$ and $x_2 = 1.35$, respectively. Panel *b*: *R vs.* $(U - R)$ diagram. The open circles are the data by Peletier & Balcells (1996). Solid circles and solid squares as in panel *a*. Panel *c*: *R vs.* $(R - K)$ diagram. Open circles, solid circles and solid squares as in panel *b*. The dotted and dashed lines in panels *b* and *c* are the best fitting lines for our predictions obtained by assuming $x_2 = 0.95$ and $x_2 = 1.35$ as IMF indexes, respectively.

Photometric properties of the galactic bulges

		$(B-R)$	$(U-R)$	$(R-K)$
Observed	(a)	$1.27-1.6$	$1.24-2.16$	$2.39-2.97$
	(b)	$0.5-2.18$		
Predicted	$(x=1.35)$	$1.64-1.71$	$1.94-2.09$	$2.22-2.38$
	$(x=0.95)$	$1.75-1.83$	$2.20-2.40$	$2.49-2.68$

Table 6.3: Predicted colours for galactic bulges assuming two different IMFs, compared to observational values of local bulges from various sources (a: Balcells & Peletier 1994; b: Galaz et al. 2006.)

observations.

From the analysis of the R *vs.* $(U-R)$ diagram, we note that our predictions computed assuming $x_2 = 1.35$ are consistent with the observations, in particular for the bulge models of masses $2\times10^{10}M_{\odot}$ and $10^{11}M_{\odot}$. For the lowest-mass bulge, corresponding to the highest absolute R magnitude, the $(U-R)$ colour seems to be overestimated. In Table 6.3, we present our results for the predicted present-day colours for the bulge model of mass $2\times10^{10}M_{\odot}$, computed for two different IMFs, compared to observational values for local bulges derived by various authors. The present-day values are computed at 13.7 Gyr. Note that, for each colour, the observational values represent the lowest and highest observed values reported by the authors. The values we predict are compatible with the observations of local bulges, which show a considerable spread. However, the sample of bulges considered here seems to be skewed towards high-mass bulges, making it difficult to infer the trend of the R *vs.* $(U-R)$ for magnitudes $R<-16$ mag. On the other hand, the predictions computed by assuming $x_2 = 0.95$ seem to produce $(U-R)$ colours that are much too high with respect to the observations. Finally, the R *vs.* $(R-K)$ diagram does not allow us to draw any firm conclusion on the slope of the IMF.

From the combined study of the I *vs.* $(B-I)$, R *vs.* $(U-R)$ and R *vs.* $(R-K)$ diagrams, we conclude that the observational data for local bulges seem to disfavour IMFs flatter than $x_2 = 1.35$ in the stellar mass range $1 \leq m/M_{\odot} \leq 80$. In Table 6.3, we present our results for the predicted present-day colours for the three bulge models presented, computed for two different IMFs. The present-day values are computed at 13.7 Gyr. Still in Table 6.3, we also show the observational data of Peletier & Balcells (1996) and of Galaz et al. (2006), who estimate that dust effects should be small

for their sample, with an upper limit on the extinction of 0.3 mag. For each colour, the observational values again represent the lowest and highest values reported by the authors.

For the model with mass comparable to the one of the bulge of the Milky Way galaxy, i.e. the one with a total mass $M = 2 \times 10^{10} M_{\odot}$, with the assumption of an IMF with $x_2 = 0.95$, we predict a present K-band luminosity $L_{Bul,K} = 4.5 \times 10^{9} L_{\odot}$. Existing observational estimates of the K-band luminosity of the bulge indicate values $0.96 \times 10^{10} \leq L_{Bul,K,obs} \leq 1.8 \times 10^{10} L_{\odot}$ (Dwek et al. 1995, Launhardt et al. 2002), i.e. at least a factor of 2 higher than the estimate obtained with our model. By adopting an IMF with $x_2 = 1.35$, we obtain $L_{Bul,K}^{x=1.35} = 7.6 \times 10^{9} L_{\odot}$, in better agreement with the observed range of values.

6.7 Summary and conclusions

We made use of our self-consistent model of galactic evolution which reproduces the main observational features of the Galactic bulge (Ballero et al. 2007a) to study the fuelling and the luminous output of the central supermassive black hole in spiral bulges, as fed by the stellar mass loss and cosmological infall, at a rate given by the minimum between the Eddington and Bondi accretion rates in order to make predictions about the evolution of Seyfert nuclei. A realistic galaxy model was adopted to estimate the gas binding energy in the bulge, and the combined effect of AGN and supernova feedback was taken into account as contributing to the thermal energy of the interstellar medium. We also investigated the chemical composition of the gas restored by stars to the interstellar medium. Assuming that the gas emitting the broad and narrow lines observed in Seyfert spectra is well mixed with the bulge interstellar medium, we have made specific predictions regarding Seyfert metallicities and abundances of several chemical species (Fe, O, Mg, Si, Ca, C and N), and their redshift evolution. Finally, we calculated the evolution of the $(B-K)$ and $(U-B)$ colours, the present-day bulge colours and K-band luminosity and the colour-magnitude relation, and discussed their dependence on the adopted IMF.

Our main results can be summarised as follows:

1. The AGN goes through a first phase of Eddington-limited accretion and a second phase of Bondi-limited accretion. Most of the fuelling (and of the shining) of the AGN occurs at the transition between the two phases, which approximately

coincides with the occurrence of the wind. Within a factor of two, the final black hole mass is reached in a fraction of the bulge lifetime ranging from 2 to 6%.

2. Since, like in Ballero et al. (2007a), the galactic wind occurs after the bulk of star formation, it does not have considerable effects on the chemical abundances. It only plays a part in regulating the final black hole mass.

3. The peak bolometric luminosities predicted for AGNs residing in the bulge of spiral galaxies are in good agreement with those observed in Seyfert galaxies ($\simeq 10^{42} - 10^{44}$ erg s^{-1}). At late times, the model nuclear luminosities (produced by accretion of the mass return from the passively ageing stellar populations) are $< 10^{42}$ erg s^{-1}, and would be further reduced by a factor ~ 0.01 when considering advection-dominated accretion flow regimes or its variants. To recover an agreement with the luminosities of local Seyferts, it is necessary to assume a rejuvenation event in the past $1 - 2$ Gyrs.

4. The feedback from the central AGN is not in any case the main one responsible for triggering the galactic wind, since its contribution to the thermal energy is at most comparable to that of the supernova feedback.

5. The proportionality between the mass of the host bulge and that of the central black hole is reproduced very well without the need to switch off the accretion *ad hoc*. We derived an approximate relation of $M_{BH} \approx 0.0009 M_b$, consistent with recent estimates (McLure & Dunlop 2002; Marconi & Hunt 2003; Häring & Rix 2004).

6. The huge star formation rates (several thousands solar masses a year) needed to produce the observed line strengths, dust content and metallicities of Seyfert galaxies are easily attained. Due to such a high star formation rate, solar metallicity is reached in less than 10^8 yr, and solar abundances for the elements we considered are reached in a few hundred million years. This naturally explains the high metallicities and abundances inferred for Seyfert galaxies in analogy with QSOs.

7. After the first ∼300 million years, the interstellar medium in the bulge reaches overabundances of up to one order of magnitude for N, Fe, Si, Ca, up to 5 times solar for Mg and 3 times solar for C and O. This is roughly consistent with the

estimates for Fe, N and O in the broad and intrinsic narrow line regions of Seyfert galaxies. The slightly supersolar [Fe/Mg] and its weak dependence on the galaxy luminosity (mass) are recovered. These results remain essentially unchanged if we adopt a Salpeter (1955) stellar IMF.

8. The mean value assumed by the [N/C] abundance ratio is very sensitive to the galaxy mass, due to the sensitivity of N to metallicity. The calculated values are consistent with recent estimates (Fields et al. 2005a).

9. Higher bulge masses imply redder colours, in agreement with the downsizing picture of galaxy evolution. A flatter IMF gives rise to a redder bulge. While the present-day bulge colours are well fitted both by a top-heavy ($x_2 = 0.95$) and a Salpeter ($x_2 = 1.35$) IMF, the latter is required in order to achieve a better agreement with the colour-magnitude relation and the present-day K-band luminosity of the bulge.

Chapter 7

Concluding remarks

"There was a point to this story, but it has temporarily escaped the chronicler's mind."
(Douglas Adams)

7.1 Summary

In this thesis, we undertook the task of updating the existing models of chemical evolution of the Galactic bulge, based on the most recent high-quality datasets of abundances in bulge evolved stars, and to begin investigating the link between supermassive black holes residing in spiral galaxies and the host galaxies themselves, in a framework where bulges are old stellar systems formed by a fast collapse of gas at a very early epoch. A variety of independent observables helped us carry out a consistent picture where we derived information about the processes of galactic formation and evolution, stellar nucleosynthesis and about the relative rôle played by supernova and black hole feedback.

The conclusions achieved in this investigation can be shortly summarised as follows:

- We confirm that a short formation timescale combined with a high star formation efficiency (the value we suggest is 20 Gyr^{-1}) fits the observed metallicity distribution and naturally explain the α-enhancements detected in bulge stars up to $\sim$solar metallicities. The star formation history of the Galactic bulge can thus be assimilated to that of an elliptical, with a strong burst of star formation at the beginning which vanishes very soon thereafter. A finite, though small, accretion time (of the order of 0.1 Gyr) prevents the formation of an excessive amount of low-metallicity stars, although this phenomenon is much less serious than in the solar neighbourhood (G-dwarf problem). Values of τ longer than 0.1 Gyr can

combine with values of ν lower than 20 Gyr^{-1} and match the observed metallicity distribution. However, such a "degeneracy" is broken when we consider also the evolution of [O/Fe] *vs.* [Fe/H].

- The observations of nitrogen in the giants and planetary nebulae of the bulge cannot give us a strong constraint on the nucleosynthesis of nitrogen in massive stars, since nitrogen in evolved stars is generally self-enriched. However, a primary contribution of this element from massive stars seems to be required if we suppose that the average trend of the [N/O] *vs.* [O/H] abundance ratio reflects the pristine one. Clearly, measurements performed in less evolved environments would help settle this point.

- Results concerning the stellar initial mass function (IMF) are contradictory. A Scalo (1986) or Weidner & Kroupa (2005) IMF are robustly excluded by observations. Considerations on the metallicity distribution of giants in the Galactic bulge and in the bulge of M31 seem to favour a rather flat IMF, with an index $x \sim 1$ for masses above $1M_{\odot}$, instead of a Salpeter (1955) index ($x \simeq 1.35$); in general, a variation of the IMF among the various environment is suggested. The [α/Fe] *vs.* [Fe/H] plots do not provide a strong constraint on this point. On the contrary, the photometric features of local bulges (colour-magnitude relation, present K-band luminosity) can only be reproduced by means of a Salpeter IMF. The specific predictions we have made represent a challenge to observe essential data in order to test these predictions. We suggest to extend the photometric measurements to a larger sample of bulges, and to carefully investigate the presence and effects of any observational biases.

- Mass loss from massive stars and its effects on the chemical yields, which depend on metallicity, provide a natural mechanism to solve the long-standing discrepancy between the trend of [O/Fe] at high [Fe/H] and the other [α/Fe] trends in the Galactic disk and bulge, and to significantly improve the agreement between predicted and observed [O/Mg] ratios in the bulge and disk above solar metallicity. A small zero-point normalisation problem remains, which could imply either that the yields of François et al. (2004) need adjustment, or that the bulge IMF is steeper than the reference one ($x = 0.95$). The former explanation is preferred, since preliminary results obtained with a Salpeter (1955) IMF show that the slope of [O/Mg] for supersolar metallicities is poorly reproduced. A combination of the

two factors may explain this offset as well.

- Simple recipes for black hole accretion and feedback, based on Eddington-limited accretion, can account for the peak bolometric luminosity and for the observed relation between bulge mass and black hole mass in Seyfert galaxies. The radiative feedback from the black hole is not important in the energy budget, since it is at most comparable to the supernova feedback. Taking into account the Bondi rate allows to reproduce the final black hole masses without forcing the accretion phase to stop at a determined time. However, the predicted bolometric luminosities of local Seyfert nuclei hosted by bulges with $M < 10^{11} M_{\odot}$ fall below the observations by about the same factor. Therefore, these bulges must experience a secondary accretion episode at low ($z < 1$) redshift turning $10 - 30\%$ of their mass into stars, as also suggested by other independent observations.

- The occurrence of the galactic wind is of secondary importance in determining the chemical properties of both active and inactive bulges, since it occurs after the bulk of gas has already been turned into stars; it only helps reproduce the high-metallicity tail in the [Fe/H] distribution. Since the Bondi accretion rate depends on the gas density, its sharp decrease induced by the one-step wind may play some part in determining the exact final black hole mass in Seyferts; however since the gas consumption in the bulge is very fast, we expect that the adoption of a continuous wind would not change the results significantly.

- The chemical properties of Seyfert galaxies and AGN in general, such as the high metallicities and the constancy of chemical abundances up to very high redshifts ($z \sim 6 - 7$), as well as the huge star formation rates inferred from line strengths, dust content and metallicities, are consistent with a star formation history typical of old bulges, where a strong major episode of star formation occurs in the first few hundred million years of bulge lifetime and then gets switched off quickly. The underlying model for the Galactic bulge also explains fairly well the overabundances of certain elements (Fe, N, O) observed in the broad and intrinsic narrow line regions of Seyfert galaxies.

7.2 Future perspectives

We briefly outline some of the future investigations which may be carried out as a natural consequence of the work presented in this thesis:

1. As stated in Chapter 3, carbon and nitrogen in evolved stars are likely to be self-processed, so that the abundances of these elements measured in giants are not in general the pristine ones. In particular, carbon is consumed to form nitrogen. It is thus probable that the (C+N) abundance is less affected by stellar evolution. A study of the evolution of the [C+N/Fe] abundance ratio with metallicity is underway and confirms that a certain amount of primary nitrogen from massive stars is necessary.

2. The inclusion of sodium and aluminium nucleosynthesis in chemical evolution models will allow the comparison with the most recent measurements of these two elementary abundances in the solar neighbourhood and Galactic bulge.

3. The oxygen yields of Meynet & Maeder (2000, 2002) and Hirschi (2007), which take rotation and mass loss into account, should be tested in the solar neighbourhood and bulge to see if they can reproduce the [O/Fe] and [O/Mg] trends as discussed in Chapter 4.

4. The effects of primordial nucleosynthesis from zero-metal stars (Population III stars) on the chemical evolution of the bulge can be investigated.

5. The spectral energy distribution of an accreting supermassive black hole and of a dusty torus can be calculated so that predictions about the spectro-photometric properties of actual Seyfert 1 and Seyfert 2 galaxies can be made.

6. The calculations carried here for the black hole feedback can be integrated into multi-zone models for elliptical galaxies, so that the chemical evolution of QSOs hosted by ellipticals can be studied.

Appendix A

The disk gravitational energy contributions

In Chapter 6, we assumed spherical symmetry for the bulge gas distribution in order to estimate the binding energy of the gas itself. Thus, the contribute of the spherical stellar bulge and the spherical dark matter halo are given by the elementary expressions in Eqs. 6.13 and 6.14.

A more complicate case is represented by the disk-gas interaction. In fact, one could suppose that a two-dimensional integral, involving special functions must be evaluated, because of the disk geometry. However, this is not the case: in fact, if each gas element is displaced radially from r to r_t, then

$$\begin{aligned} \Delta E_{gd} &= \int_0^{r_t} \rho_g(r) r^2 dr \int_{4\pi} d\Omega [\phi_d(\mathbf{e}_r r_t) - \phi_d(\mathbf{e}_r r)] = \\ &= 4\pi \int_0^{r_t} \rho_g(r) r^2 [\bar{\phi}_d(r_t) - \bar{\phi}_d(r)] dr \end{aligned} \tag{A.1}$$

where

$$\bar{\phi}_d(r) = \frac{1}{4\pi} \int_{4\pi} \phi_d(\mathbf{e}_r r) d\Omega \tag{A.2}$$

is the angular averaged potential, and $\mathbf{e}_r$ the radial unit vector. It is trivial to prove by direct evaluation that the angular mean of the potential of a generic density distribution is also the (spherical) potential of the angular averaged density. Of course, this result can also be obtained in a more elegant way by considering the angular mean of the expansion of the potential in spherical harmonics (e.g., Binney & Tremaine 1987), so that all the terms vanish, except the monopole. An identical argument also holds in the

case of the computation of the virial trace. In fact, from $\mathbf{x} = \mathbf{e}_r r$ it follows that

$$W_{bd} = -\int \rho_g < \mathbf{x}, \nabla\phi_d > d^3\mathbf{x} = -4\pi \int \rho_g(r) \frac{d\bar{\phi}_d(r)}{dr} r^3 dr. \tag{A.3}$$

The surface density of a razor-thin axisymmetric disk in spherical coordinates is

$$\Sigma(r, \vartheta, \varphi) = \frac{\Sigma_d(r \sin\vartheta)\delta(\cos\vartheta)}{r}, \tag{A.4}$$

so that

$$\bar{\rho}_d(r) = \frac{1}{4\pi} \int_{4\pi} \Sigma(r, \vartheta, \varphi) d\Omega = \frac{\Sigma_d(r)}{2r} \tag{A.5}$$

For the exponential disk in Eq. 6.10 we then obtain

$$\bar{\phi}_d(r) = -\frac{GM_d}{r} \left(1 - e^{-r/R_d}\right), \tag{A.6}$$

so that integrations in Eqs. A.1 and A.3 reduce to

$$\begin{aligned} \widetilde{\Delta E_{gd}} &= \frac{\delta + (1-h)(1-e^{-\delta/h})}{1+\delta} + \\ &+ \frac{e^{1/h}}{h} \left[\mathrm{E_i}\left(-\frac{1}{h}\right) - \mathrm{E_i}\left(-\frac{1}{h} - \frac{1}{\delta}\right) \right] \end{aligned} \tag{A.7}$$

and

$$\widetilde{W_{bd}} = -\frac{1}{h} - \frac{e^{1/h}(1+h)}{h^2} \mathrm{E_i}\left(-\frac{1}{h}\right) \tag{A.8}$$

where $h \equiv R_d/r_b$, $\delta \equiv r_t/r_b$, and $\mathrm{E_i}(-x) = -\int_r^\infty e^{-t} t^{-1} dt$ is the exponential integral.

Bibliography

[1] Adams, T.F., 1977, ApJS 33, 19

[2] Aguerri, J.A.L., Balcells, M., Peletier, R.F., 2001, A&A 373, 786

[3] Alard, C., 1996, PhD thesis, University of Paris VI

[4] Angeletti, L., Giannone, P., 1990, A&A 234, 53

[5] Antonucci, R., 1993, ARA&A 31, 473

[6] Arimoto, N., Yoshii, Y., 1986, A&A 164, 260

[7] Arimoto, N., Yoshii, Y, 1987, A&A 173, 23

[8] Arnett, D., 1991, in "Frontiers of Stellar Evolution", ed. D.L. Lambert, ASP Conf. Series 20, 389

[9] Asplund, M., Grevesse, N., Sauval, A.J., 2005, in "Cosmic Abundances as Records of Stellar Evolution and Nucleosynthesis", eds. Thomas G. Barnes III & Frank N. Bash, ASP Conf. Series 336, 25

[10] Balcells, M., Peletier, R.F., 1994, AJ 107, 135

[11] Baldwin, J.A., Ferland, G.J., Korista, K.T., Hamann, F., LaCluyzé, A., 2004, ApJ 615, 610

[12] Ballero, S.K., Kroupa, P., Matteucci, F., 2007b, A&A 467, 117

[13] Ballero, S.K., Matteucci, F., Chiappini, C., 2006, NewA 11, 306

[14] Ballero, S.K., Matteucci, F., Ciotti, L., Calura, F., Padovani, P., 2008, A&A, in press (*arXiv:0710.4129*)

[15] Ballero, S.K., Matteucci, F., Origlia, L., Rich, R.M., 2007a, A&A 467, 124

[16] Barbuy, B., 1999, Ap&SS 265, 319

[17] Barth, A.J., Martini, P., Nelson, C.H., Ho, L.C., 2003, ApJ 594, L95

[18] Baugh, C.M., Lacey, C.G., Frenk, C.S., Granato, G.L., Silva, L., Bressan, A., Benson, A.J., Cole, S., 2005, MNRAS 356, 1191

[19] Baumgardt, H., Makino, J., 2003, MNRAS 340, 227

[20] Bender, R., Burstein, D., Faber, S.M., 1992, ApJ 399, 462

[21] Bensby, T., Feltzing, S., Lundström, I., 2004, A&A 415, 155

[22] Bensby, T., Feltzing, S., Lundström, I., Ilyn, I., 2005, A&A 433, 185

[23] Bentz, M.C., Hall, P.B., Osmer, P.S., 2004, AJ 128, 561

[24] Bertin, G., Saglia, R.P., Stiavelli, M., 1992, ApJ 384, 423

[25] Bertola, F., Vietri, M., Zeilinger, W.W., 1991, ApJ 374, L13

[26] Binney, J., Tremaine, S., 1987, "Galactic Dynamics", Princeton University Press, Princeton, NJ

[27] Blain, A.W., Smail, I., Ivison, R.J., Kneib, J.P., Frayer, D.T., 2002, Physic Reports 369, 111

[28] Bondi, H., 1952, MNRAS 112, 195

[29] Brandt, W.N., Hasinger, G., 2005, ARA&A 43, 827

[30] Bromm, V., Larson, R.B., 2004, ARA&A 42, 79

[31] Brown, J.A., Wallerstein, G., Zucker, D., 1997, AJ 114, 180

[32] Burstein D., Bender, R., Faber, S.M., Nolthenius, R., 1997, AJ 114, 1365

[33] Calura, F., Jimenez, R., Panter, B., Matteucci, F., Heavens, A. F., 2007a, MNRAS submitted (*arXiv:0707.1345v2*)

[34] Calura, F., Matteucci, F., 2003, ApJ 596, 734

[35] Calura, F., Matteucci, F., 2006, ApJ 652, 889

[36] Calura, F., Matteucci, F., Menci, N., 2004, MNRAS 353, 500

[37] Calura, F., Matteucci, F., Tozzi, P., 2007b, MNRAS 378, L11

[38] Calura, F., Pipino, A., Matteucci, F., 2007c, A&A accepted (*arXiv:0706.2197v1*)

[39] Carretta, E., Cohen, J., Gratton, R.G., Behr, B. 2001, AJ, 122, 1469

[40] Castro, S., Rich, R.M., Grenon, M., Barbuy, B., McCarthy, J.K., 1997, AJ 114, 376

[41] Cavaliere, A., Vittorini, V., 1998, in "The Young Universe: Galaxy Formation and Evolution at Intermediate and High Redshift", eds. S. D'Odorico, A. Fontana & E. Giallongo, ASP Conf. Series 146, 26

[42] Chabrier, G., 2003, PASP 115, Issue 809, 763

[43] Chiappini, C., Hirschi, R., Meynet, G., Elström, S., Maeder, A., Matteucci, F., 2006, A&A 449, L27

[44] Chiappini, C., Matteucci, F., Ballero, S.K., 2005, A&A 437, 429

[45] Chiappini, C., Matteucci, F., Gratton, R., 1997, ApJ 477, 765

[46] Chiappini, C., Matteucci, F., Meynet, G., 2003a, A&A 410, 257

[47] Chiappini, C., Matteucci, F., Romano, D., 2003b, ApJ 554, 1044

[48] Chiappini, C., Romano, D., Matteucci, F., 2003c, MNRAS 339, 63

[49] Cimatti, A., Pozzetti. L., Mignoli, M., Daddi, E., Menci, N., Poli, F., Fontana, A., Renzini, A., Zamorani, G., Broadhurst, T., Cristiani, S., D'Odorico, S., Giallongo, E., Gilmozzi, R., 2002, A&A 391, L1

[50] Cioffi, D.F., McKee, C.F., Bertschinger, E., 1988, ApJ 334, 252

[51] Ciotti, L., Ostriker, J.P., 1997, ApJ 487, L105

[52] Ciotti, L., Ostriker, J.P., 2001, ApJ 551, 131

[53] Ciotti, L., Ostriker, J.P., 2007, ApJ 665, 1038

[54] Collin, S., Joly, M., 2000, NewAR 44, 531

[55] Combes, F., Sanders, R.H., 1981, A&A 96, 164

[56] Costa, R.D.D., Escudero, A.V., Maciel, W.J., 2005, in "Planetary Nebulae as Astronomical Tools", AIP Conference Proceedings, Volume 804, p. 252

[57] Cox, D.P., 1972, ApJ 178, 143

[58] Cox, P., Omont, A., Djorgovski, S.G., Bertoldi, F., Pety, J., Carilli, C.L., Isaak, K.G., Beelen, A., McMahon, R.G., Castro, S., 2002, A&A 387, 406

[59] Cuisinier, F., Maciel., W.J., Köppen, J., Acker, A., Stenholm, B., 2000, A&A 353, 543

[60] Dietrich, M., Hamann, F., Appenzeller, I., Vestergaard, M., 2003a, ApJ 596, 817

[61] Dietrich, M., Hamann, F., Shields, J.C., Constantin, A., Heidt, J., Jäger, K., Vestergaard, M., Wagner, S.J., 2003b, ApJ 589, 722

[62] Di Matteo, T., Croft, R.A.C., Springel, V., Hernquist, L., 2003, ApJ 593, 56

[63] Di Matteo, T., Springel, V., Hernquist, L., 2005, Nature 433, 604

[64] Djorgovski, S., Davis, M., 1987, ApJ 313, 59

[65] D'Odorico, V., Cristiani, S., Romano, D., Granato, G.L., Danese, L., 2004, MNRAS 351, 976

[66] Dopita, M.A., Ryder, S.D., 1994, ApJ 430, 163

[67] Dunlop, J.S., McLure, R.J., Kukula, M.J., Baum, S.A., O'Dea, C.P., Hughes, D.H., 2003, MNRAS 340, 1095

[68] Dwek, E., Arendt, R.G., Hauser, M.G., Kelsall, T., Lisse, C.M., Moseley, S.H., Silverberg, R.F., Sodroski, T.J., Weiland, J.L., 1995, ApJ 445, 716

[69] Edvardsson, B., Andersen, J., Gustafsson, B., Lambert, D. L., Nissen, P. E., Tomkin, J., 1993, A&AS 102, 603

[70] Eggen, O.J., Lynden-Bell, D., Sandage, A.R., 1962, ApJ 136, 748

[71] Elmegreen, B., 1999, ApJ 517, 103

[72] Escudero, A.V., Costa, R.D.D., 2001, A&A 380, 300

[73] Escudero, A.V., Costa, R.D.D., Maciel, W.J., 2004, A&A 414, 211

[74] Fabian, A.C., Iwasawa, K., 2000, AdSpR 25, 471

[75] Falcon-Barroso, J., Peletier, R.F., Balcells, M., 2002, MNRAS 335, 741

[76] Feltzing, S., Gustafsson, B., 1998, A&AS 129, 237

[77] Ferrarese, L., Merritt, D., 2000, ApJ 539, L9

[78] Ferrarese, L., Pogge, R.W., Peterson, B.M., Merritt, D., Wandel, A., Joseph, C.L., 2001, ApJ 555, L79

[79] Ferreras, I., Wyse, R.F.G., Silk, J., 2003, MNRAS 345, 1381

[80] Fields, D.L., Mathur, S., Pogge, R.W., Nicastro, F., Komossa, S., 2005a, ApJ 620, 183

[81] Fields, D.L., Mathur, S., Pogge, R.W., Nicastro, F., Komossa, S., Krongold, Y., 2005b, ApJ 634, 928

[82] Figer, D.F., 2005, Nature 434, 192

[83] Figer, D.F., Kim, S.S., Morris, M., Serabyn, E., Rich, R.M., McLean, I.S., 1999, ApJ 525, 750

[84] Ford, H.C., Tsvetanov, Z.I., Ferrarese, L., Jaffe, W., 1998, in "The Central Regions of the Galaxy and galaxies", ed. Y. Sofue, IAU Symp. 184, 377

[85] Fraquelli, H.A., Storchi-Bergmann, T., 2003, BASBr 23, 150

[86] Freudling, W., Corbin, M.R., Korista, K.T., 2003, ApJ 587, L67

[87] François , P., Matteucci, F., Cayrel, R., Spite, M., Spite, F., Chiappini, C., 2004, A&A 421, 613

[88] Friaça, A.C.S., Terlevich, R.J., 1998, MNRAS 298, 399

[89] Friedli, D., Benz, W., 1993, A&A 268, 65

[90] Friedli, D., Benz, W., 1995, A&A 301, 649

[91] Fryer, C.L., Young, P.A., Hungerford, A.L., 2006, ApJ 650, 1028

[92] Fulbright, J.P., McWilliam, A., Rich, R.M., 2006, ApJ 636, 821

[93] Fulbright, J.P., McWilliam, A., Rich, R.M., 2007, ApJ 661, 1152

[94] Galaz, G., Villalobos, A., Infante, L., Donzelli, C., 2006, AJ 131, 2035

[95] Gebhardt, K., Bender, R., Bower, G., Dressler, A., Faber, S.M., Filippenko, A.V., Green, R., Grillmair, C., Ho, L.C., Kormendy, J., Lauer, T., Magorrian, J., Pinkney, J., Richstone, D., Tremaine, S., 2000a, ApJ 539, L13

[96] Gebhardt, K., Kormendy, J., Ho, L.C., Bender, R., Bower, G., Dressler, A., Faber, S.M., Filippenko, A.V., Green, R., Grillmair, C., Lauer, T., Magorrian, J., Pinkney, J., Richstone, D., Tremaine, S., 2000b, ApJ 543, L5

[97] Geisler, D., Smith, V.V., Wallerstein, G., Gonzalez, G., Charbonnel, C., 2005, AJ 129, 1428

[98] Genzel, R., Baker, A.J., Tacconi, L.J., Lutz, D., Cox, P., Guilloteau, S., Omont, A., 2003, ApJ 584, 633

[99] González Delgado, R.M., Heckman, T., Leitherer, C., Meurer, G., Krolik, J., Wilson, A.S., Kinney, A., Koratkar, A., 1998, ApJ 505, 174

[100] Górny, S. K., Stasińska, G., Escudero, A. V., Costa, R. D. D., 2004, A&A 427, 231

[101] Granato, G.L., De Zotti, G., Silva, L., Bressan, A., Danese, L., 2004, ApJ 600, 580

[102] Greggio, L., Renzini, A., 1983, A&A 118, 217

[103] Grevesse, N., Sauval, A.J., 1998, SSRv 85, 161

[104] Groenewegen, M.A.T., Blommaert, J.A.D.L., 2005, A&A 443, 143

[105] Gu, Q., Melnick, J., Cid Fernandes, R., Kunth, D., Terlevich, E., Terlevich, R., 2006, MNRAS 366, 480

[106] Haehnelt, M.G., Natarajan, P., Rees, M.J., 1998, MNRAS 300, 817

[107] Haiman, Z., Ciotti, L., Ostriker, J.P., 2004, ApJ 606, 763

[108] Hamann, F., Dietrich, M., Sabra, B.M., Warner, C., 2004, in "Origin and Evolution of the Elements", eds. A. McWilliam & M. Rauch, Carnegie Observatories Astrophysics Series 4, 443

[109] Hamann, F., Dietrich, M., Sabra, B., Warner, C., Barlow, T., Chaffee, F., Junkkarinen, V., 2003, in "CNO in the Universe", eds. C. Charbonnel, D. Schaerer & G. Meynet, ASP Conf. Series 304, 236

[110] Hamann, F., Ferland, G., 1993, ApJ 418, 11

[111] Hamann, F., Ferland, G., 1999, ARA&A 37, 487

[112] Hamann, F., Korista, K.T., Ferland, G.J., Warner, C., Baldwin, J., 2002, ApJ 564, 592

[113] Häring, N., Rix, H.W., 2004, ApJ 604, L89

[114] Harmon, R., Gilmore, G., 1988, MNRAS 235, 1025

[115] Hasan, H., Pfenniger, D., Norman, C., 1993, ApJ 409, 91

[116] Hernquist, L., 1990, ApJ 356, 359

[117] Hill, V., 1997, A&A 324, 435

[118] Hirschi, R., 2007, A&A 461, 571

[119] Ho, L.C., 1999, ApJ 516, 672

[120] Ho, L.C., Filippenko, A.V., Sargent, W.L.W., 1997, ApJ 487, 568

[121] Holtzman, J.A., Light, R.M., Baum, W.A., Worthey, G., Faber, S.M., Hunter, D.A., O'Neil Jr., E.J., Kreidl, T.J., Groth, E.J., Westphal, J.A., 1993, AJ 106, 1826

[122] Hou, J., Chang, R., Fu C., 1998, Annals of Shanghai Observatory, Academia Sinica No. 19, 96

[123] Ibata, R.A., Gilmore, G.F., 1995, MNRAS 275, 591

[124] Immeli, A., Samland, M., Gerhard, O., Westera, P., 2004, A&A 413, 547

[125] Itoh, N., Ichikawa, T., 1998, IAU Symp. 184, 55

[126] Ivanov, V.D., Alonso-Herrero, A., Rieke, M.J., 2003, in "Star Formation through Time", eds. E. Pérez, R.M. González Delgado, G. Tenorio-Tagle, ASP Conf. Series 297, 165

[127] Iwamoto, K., Brachwitz, F., Nomoto, K., Kishimoto, N., Umeda, H., Hix, W.R., Thielemann, F.K., 1999, ApJS 125, 439

[128] Iwamuro, F., Kimura, M., Eto, S., Maihara, T., Motohara, K., Yoshii, Y., Doi, M., 2004, ApJ 614, 69

[129] Iwamuro, F., Motohara, K., Maihara, T., Kimura, M., Yoshii, Y., Doi, M., 2002, ApJ 565, 63

[130] Jiang, L., Fan, X., Vestergaard, M., Kurk, J.D., Walter, F., Kelly, B.C., Strauss, M.A., 2007, AJ 134, 1150

[131] Jimenez, R., MacDonald, J., Dunlop, J.S., Padoan, P., Peacock, J.A., 2004, MNRAS 349, 240

[132] Jimenez, R., Padoan, P., Matteucci, F., Heavens, A.F., 1998, MNRAS 299, 123

[133] Kaspi, S., Smith, P.S., Netzer, H., Maoz, D., Jannuzi, B.T., Giveon, U., 2000, ApJ 533, 631

[134] Kauffmann, G., 1996, MNRAS 281, 487

[135] Kennicutt Jr., R.C., 1998, ApJ 498, 541

[136] Kim, S.S., Figer, D.F., Kudritzki, R.P., Najarro, F., 2006, ApJ 653, L113

[137] Kobayashi, C., Umeda, H., Nomoto, K., Tominaga, N., Ohkubo, T., 2006, ApJ 653, 1145

[138] Kodama, T., 1997, PhD thesis, Institute of Astronomy, University of Tokyo

[139] Koen, C., 2006, MNRAS 365, 590

[140] Komossa, S., Mathur, S., 2001, A&A 374, 914

[141] Korista, K., Kodituwakku, N., Corbin, M., Freudling, W., 2004, in "AGN Physics with the SDSS", eds. G.T. Richards & P.B. Hall, ASP Conf. Series 311, 415

[142] Kormendy, J., 1982, ApJ 256, 460

[143] Kormendy, J., Kennicutt, Jr., R.C., 2004, ARA&A 42, 603

[144] Kormendy, J., Richstone, D., 1995, ARA&A 33, 581

[145] Kroupa, P., 2001, MNRAS 332, 231

[146] Kroupa, P., Tout, C.A., Gilmore, G. 1993, MNRAS, 262, 545

[147] Kroupa, P., Weidner, C., 2003, ApJ 598, 1076

[148] Kuijken, K., Rich, R.M., 2002, AJ 124, 2054

[149] Kurk, J.D., Walter, F., Fan, X., Jiang, L., Riechers, D.A., Rix, H.W., Pentericci, L., Strauss, M.A., Carilli, C., Wagner, S., 2007, ApJ, in press (*arXiv:0707.1662*)

[150] Kurucz, R.L., 1992, IAU Symp. 149, 225

[151] Lanfranchi, G.A., Matteucci, F., 2004, MNRAS 351, 1338

[152] Langer, N., Henkel, C., 1995, Space Science Rev. 74, 343

[153] Laor, A., 2001, ApJ 553, 677

[154] Larson, R.B., 1998, MNRAS 301, 569

[155] Launhardt, R., Zylka, R., Mezger, P.G, 2002, A&A 384, 112

[156] Lecureur, A., Hill, V., Zoccali, M., Barbuy, B., Gómez, A., Minniti, D., Ortolani, S., Renzini, A., 2007, A&A 465, 799

[157] Lee, Y.W., 1992, AJ 104, 1780

[158] Lee, J.C., Fabian, A.C., Brandt, W.N., Reynolds, C.S., Iwasawa, K., 1999, MNRAS 310, 973

[159] Limongi, M., Chieffi, A., 2003, ApJ 592, 404

[160] Liu, X.W., Luo, S.G., Barlow, M.J., Danziger, I.J., Storey, P.J., 2001, MNRAS 327, 141

[161] Lucy, L.B., Solomon, P.M., 1970 ApJ 159, 879

[162] Luna, G.J.M., Costa, R.D.D., 2005, A&A 435, 1087

[163] MacKenty, J.W., 1990, ApJS 72, 231

[164] Maeder, A., 1992, A&A 264, 105

[165] Maeder, A., Meynet, G. 1989, A&A, 210, 155

[166] Magorrian, J., Tremaine, S., Richstone, D., Bender, R., Bower, G., Dressler, A., Faber, S.M., Gebhardt, K., Green, R., Grillmair, C., Kormendy, J., Lauer, T.R., 1998, AJ 115, 2285

[167] Maiolino, R., Cox, P., Caselli, P., Beelen, A., Bertoldi, F., Kaufman, M.J., Nagao, T., Omont, A., Weiß, A., Walmsley, M., 2005, A&A 440, L51

[168] Maiolino, R., Juarez, Y., Mujica, R., Nagar, N.M., Oliva, E., 2003, ApJ 596, L155

[169] Mannucci, F., Della Valle, M., Panagia, N., Cappellaro, E., Cresci, G., Maiolino, R., Petrosian, A., Turatto, M., 2005, A&A 433, 807

[170] Maraston, C., Greggio, L., Renzini, A., Ortolani, S., Saglia, R.P., Puzia, T.H., Kissler-Patig, M., 2003, A&A 400, 823

[171] Marconi, A., Hunt, L., 2003, ApJ 589, 21

[172] Markowitz, A., Edelson, R., Vaughan, S., Uttley, P., George, I.M., Griffiths, R.E., Kaspi, S., Lawrence, A., McHardy, I., Nandra, K., Pounds, K., Reeves, J., Schurch, N., Warwick, R., 2003, ApJ 593, 96

[173] Massey, P., 1998, in "The Stellar Initial Mass Function", eds. G. Gilmore & Debbie Howell, ASP Conf. Series 142, 17

[174] Massey, P., 2003, ARA&A 41, 15

[175] Massey, P., Hunter, D.A., 1998, ApJ 493, 180

[176] Mathur, S., 2000, NewAR 22, 469

[177] Matteucci, F., 1986, MNRAS 221, 911

[178] Matteucci, F., 1992, ApJ 397, 32

[179] Matteucci, F., 1994, A&A 288, 57

[180] Matteucci, F., 2000, in "The Evolution of the Milky Way: Stars versus Clusters", eds. F. Matteucci & F. Giovannelli, ASSL vol. 255, Kluwer Academic Publishers, p. 3

[181] Matteucci, F., Brocato, E., 1990, ApJ 365, 539

[182] Matteucci, F., Greggio, L., 1986, A&A 154, 279

[183] Matteucci, F., Padovani, P., 1993, ApJ 419, 485

[184] Matteucci, F., Recchi, S., 2001, ApJ 558, 351

[185] Matteucci, F., Romano, D., Molaro, P., 1999, A&A 341, 458, MRM99

[186] Matteucci, F., Tornambè, A., 1987, A&A 185, 51

[187] MacArthur, L.A., Ellis, R.S., Treu, T., U, V., Bundy, K., Moran, S., 2007, submitted to ApJ (*arXiv:0711.0238*)

[188] McLure, R.J., Dunlop, J.S., 2002, MNRAS 331, 795

[189] McWilliam, A., Matteucci, F., Ballero, S.K., Rich, R.M., Fulbright, J.P., Cescutti, G., 2008, ApJ accepted (*arXiv:0708.4026*)

[190] McWilliam, A., Rich, R.M., 1994, ApJS 91, 749, MR94

[191] McWilliam, A., Rich, R.M., 2004, in "Origin and Evolution of the Elements", from the Carnegie Observatories Centennial Symposia, Carnegie Observatories Astrophysics Series, eds. A. McWilliam & M. Rauch, p. 38

[192] McWilliam, A., Rich, R.M., Smecker-Hane, T.A., 2003, ApJ 592, L21

[193] McWilliam, A., Smecker-Hane, T.A., 2005, "Cosmic Abundances as Records of Stellar Evolution and Nucleosynthesis in honor of David Lambert", eds. Thomas G. Barnes III & Frank N. Bash, ASP Conference Series 336, 221

[194] Melèndez, J., Barbuy, B., Bica, E., Zoccali, M., Ortolani, S., Renzini, A., Hill, V. 2003, A&A, 411, 417

[195] Meynet, G., Maeder, A., 2002, A&A 390, 561

[196] Meynet, G., Maeder, A., 2003, A&A 404, 975

[197] Meynet, G., Maeder, A., 2005, A&A 429, 581

[198] Minniti, D., Olzsewski, E.W., Liebert, J., White, S.D.M., Hill, J.M., Irwin, M.J., 1995, MNRAS 277, 1293

[199] Minniti, D., Zoccali, M., 2007, to appear in "Formation and Evolution of Galaxy Bulges", eds. M. Bureau, E. Athanassoula & B. Barbuy, IAU Symp. 245 (*arXiv:0710.3104*)

[200] Mollá, M., Ferrini, F., Gozzi, G., 2000, MNRAS 316, 345

[201] Monaco, L., Bellazzini, M., Bonifacio, P., Buzzoni, A., Ferraro, F.R., Marconi, G., Sbordone, L., Zaggia, S., 2007, A&A 464, 201

[202] Monaco, P., Salucci, P., Danese, L., 2000, MNRAS 311, 279

[203] Nagao, T., Marconi, A., Maiolino, R., 2006, A&A 447, 157

[204] Nagao, T., Murayama, T., Shioya, Y., Taniguchi, Y., 2002, ApJ 575, 721

[205] Nagashima, M., Lacey, C.G., Baugh, C.M., Frenk, C.S., Cole, S., MNRAS 358, 1247

[206] Nakamura, F., Umemura, M., 2001, ApJ 548, 19

[207] Narayan, R., Yi, I. 1994, ApJ 428, L13

[208] Nelson, C.H., Green, R.F., Bower, G., Gebhardt, K., Weistrop, D., 2004, ApJ 615, 652

[209] Nissen, P.E., Schuster, W.J., 1997, A&A 326, 751

[210] Noguchi, M., 1999, ApJ 514, 77

[211] Nomoto, K., Thielemann, F.K., Yokoi, K., 1984, ApJ 286, 644

[212] Norman, C.A., Sellwood, J.A., Hasan, H., 1996, ApJ 462, 114

[213] Nugis, T., Lamers, H.J.G.L.N., 2000, A&A 360, 227

[214] Nussbaumer, H., Schmid, H.M., Vogel, M., Schild, H., 1988, A&A 198, 179

[215] Oey, M.S., Clarke, C.J., 2005, ApJ 620, L430

[216] Okamoto, T., Eke, V.R., Frenk, C.S., Jenkins, A., 2005, MNRAS 363, 1299

[217] Onken, C.A., Ferrarese, L., Merritt, D., Peterson, B.M., Pogge, R.W., Vestergaard, M., Wandel, A., 2004, ApJ 615, 645

[218] Origlia, L., Ferraro, F.R., Bellazzini, M., Pancino, E., 2003, ApJ, 591, 916

[219] Origlia, L., Rich, R.M., 2004, AJ 127, 3422

[220] Origlia, L., Rich, R.M., Castro, S., 2002 AJ 123, 1559

[221] Origlia, L., Valenti, E., Rich, R.M., 2005, MNRAS 256, 127

[222] Ortolani, S., Renzini, A., Gilmozzi, R., Marconi, G., Barbuy, B., Bica, E., Rich, R.M., 1995, Nature 377, 701

[223] Osmer, P.S., Shields, J.C., 1999, in "Quasars and Cosmology", eds. G. Ferland & J. Baldwin, ASP Conf. Series 162, 235

[224] Ostriker, J.P., Ciotti, L., 2005, Philosophical Transactions of the Royal Society Part A, 363, 1828, 667

[225] Padoan, P., Nordlund, Å., Jones, B.J.T., 1997, MNRAS 288, 145

[226] Padovani, P., Matteucci, F., 1993, ApJ 416, 26

[227] Paresce, F., de Marchi, G., 2000, ApJ 534, 870

[228] Paumard, T., Genzel, R., Martins, F., Nayakshin, S., Beloborodov, A.M., Levin, Y., Trippe, S., Eisenhauer, F., Ott, T., Gillessen, S., Abuter, R., Cuadra, J., Alexander, T., Sternberg, A., 2006, ApJ 643, 1011

[229] Peimbert, M., Serrano, A., 1980, RMxAA 5, 9

[230] Peletier, R.F., Balcells, M., 1996, AJ 111, 2238

[231] Peletier, R.F., Balcells, M., Davies, R.L., Andredakis, Y., Vazdekis, A., Burkert, A., Prada, F., 1999, MNRAS 310, 703

[232] Peterson, B.M., 2003, in "Active Galactic Nuclei: from central engine to host galaxy", eds. S. Collin, F. Combes & I. Shlosman, ASP Conf. Series 290, 43

[233] Petitjean, P., Srianand, R., 1999, A&A 345, 73

[234] Pfenniger, D., Norman, C.A., 1990, ApJ 363, 391

[235] Piotto, G., Zoccali, M., 1999, A&A 345, 485

[236] Pipino, A., D'Ercole, A., Matteucci, F., 2007a, submitted to A&A (*arXiv:0706.2932*)

[237] Pipino, A., Matteucci, F., Borgani, S., Biviano, A., 2002, NewA 7, 227

[238] Pipino, A., Matteucci, F., D'Ercole, A., 2007b, to appear in "Formation and Evolution of Galaxy Bulges", eds. M. Bureau, E. Athanassoula & B. Barbuy, IAU Symp. 245 (*arXiv:0709.0658*)

[239] Pompéia, L., Barbuy, B., Grenon, M., 2003, ApJ 592, 1173

[240] Prantzos, N., Aubert, O., Audouze, J., 1996, A&A 309, 760

[241] Ramírez, S.V., Stephens, A.W., Frogel, J.A., DePoy, D.L., 2000, AJ 120, 833

[242] Reddy, B.E., Lambert, D.L., Allende Prieto, C., 2006, MNRAS 367, 1329

[243] Renzini, A., 1993, in "Galactic Bulges", IAU Symp. 153, eds. H. DeJonghe & H.J. Habing (Kluwer Academic Publishers, Dordrecht), 151

[244] Renzini, A., 1999, Ap&SS 267, 357

[245] Renzini, A., Voli, M., 1981, A&A 94, 175

[246] Rich, R.M., 1988, AJ 95, 828

[247] Rich, R.M., Origlia, L., 2005, ApJ 634, 1293

[248] Rodríguez-Ardila, A., Contini, M., Viegas, S.M., 2005, MNRAS 357, 220

[249] Romano, D., Silva, L., Matteucci, F., Danese, L., 2002, MNRAS 334, 444

[250] Sadler, E.M., Rich, R.M., Terndrup, D.M., 1996, AJ 112, 171

[251] Salaris, M., Weiss, A., Percival, S.M., 2004, A&A 414, 163

[252] Salpeter, E.E., 1955, ApJ 121, 161

[253] Salpeter, E.E., 1964, ApJ 140, 796

[254] Samland, M., Hensler, G., Theis, C., 1997, ApJ 476, 544

[255] Sarajedini, A., Jablonka, P., 2005, AJ 130, 1627

[256] Sarzi, M., Shields, J.C., Pogge, R.W., Martini, P., 2007, to appear in "Stellar Populations as Building Blocks of Galaxies", IAU Symp. 241, eds. R.F. Peletier & A. Vazdekis (*arXiv:astro-ph/0703794*)

[257] Sazonov, S.Y., Ostriker, J.P., Ciotti, L., Sunyaev, R.A., 2005, MNRAS 358, 168

[258] Scalo, J., 1986, FCPh 11, 1

[259] Scannapieco, E., Silk, J., Bouwens, R., 2005, ApJ 635, L13

[260] Schaerer, D., 2002, A&A 382, 28

[261] Schmidt, M., 1959, ApJ 129, 243

[262] Schmidt, M., Green, R.F., 1983, ApJ 269, 352

[263] Schmitt, H.R., Storchi-Bergmann, T., Baldwin, J.A., 1994, ApJ 423, 237

[264] Schwarzschild, M., Härm, R., 1959, ApJ 129, 637

[265] Schweizer, F., Seitzer, P., 1988, ApJ 328, 88

[266] Searle, L., Zinn, R., 1978, ApJ 225, 357

[267] Seyfert, C.K., 1943, ApJ 97, 28

[268] Shetrone, M.D., Côté, P., Sargent, W.L.W., 2001, ApJ 548, 592

[269] Shields, G.A., Gebhardt, K., Salviander, S., Wills, B.J., Xie, B., Brotherton, M.S., Yuan, J., Dietrich, M., 2003, ApJ 583, 124

[270] Stasińska, G., Tylenda, R., Acker, A., Stenholm, B., 1991, A&A 247, 173

[271] Storchi-Bergmann, T., 1991, MNRAS 249, 404

[272] Storchi-Bergmann, T., Bica, E., Pastoriza, M.G., 1990, MNRAS 245, 749

[273] Storchi-Bergmann, T., Pastoriza, M.G., 1989, ApJ 347, 195

[274] Storchi-Bergmann, T., Wilson, A.S., Baldwin, J.A., 1996, ApJ 460, 252

[275] Terndrup, D.M., 1988, AJ 96, 884

[276] Thielemann, F.K., Nomoto, K., Hashimoto, M., 1993, in "Origin and Evolution of the Elements", eds. N. Prantzos, E. Vangioni-Flam & M. Casse, Cambridge University Press, Cambridge, p. 297

[277] Thomas, D., Davies, R.L., 2006, MNRAS 366, 510

[278] Thomas, D., Greggio, L. Bender, R., 1998, MNRAS 296, 119

[279] Thomas, D., Maraston, C., Bender, R., 2002, Ap&SS, 281, 371

[280] Thompson, K.L., Hill, G.J., Elston, R., 1999, ApJ 515, 487

[281] Tinsley, B.M., 1979, ApJ 229, 1046

[282] Tinsley, B.M., 1980, FCPh 5, 287

[283] Tolstoy, E., Venn, K.A., Shetrone, M.D., Primas, F., Hill, V., Kaufer, A., Thomas, S., 2003, AJ 125, 707

[284] Tosi M., Steigman G., Matteucci F., Chiappini C., 1998, ApJ 498, 226

[285] Tremaine, S., Gebhardt, K., Bender, R., Bower, G., Dressler, A., Faber, S.M., Filippenko, A.M., Green, R., Grillmair, C., Ho, L.C., Kormendy, J., Lauer, T.R., Magorrian, J., Pinkey, J., Richstone, D., 2002, ApJ 574, 740

[286] Tsujimoto, T., Nomoto, K., Yoshii, Y., Hashimoto, M., Yanagida, S., Thielemann, F.K., 1995, MNRAS 277, 945

[287] Turner, T.J., George, I., Netzer, H., 1999, ApJ 526, 52

[288] Ulrich, M.H., Comastri, A., Komossa, S., Crane, P., 1999, A&A 350, 816

[289] Van den Hoek, L.B., Groenewegen, M.A.T., 1997, A&AS 123, 305

[290] Van Loon, J.T., Gilmore, G.F., Omont, A., Blommaert, J.A.D.L., Glass, I.S., Messineo, M., Schuller, F., Schultheis, M., Yamamura, I., Zhao, H.S, 2003, MNRAS 338, 857

[291] Venn, K.,A., Irwin, M., Shetrone, M.D., Tout, C.A., Hill, V., Tolstoy, E., 2004, AJ 128, 1177

[292] Verner, E., Bruhweiler, F., Verner, D., Johansson, S., Gull, T., 2003, ApJ 592, L59

[293] Vink, J.S., Koter, A., Lamers, H.J.G.L.M., 2000, A&A 362, 295

[294] Wainscoat, R.J., Freeman, K.C., Hyland, A.R., 1989, ApJ 337, 163

[295] Walton, N.A., Barlow, M.J., Clegg, R.E.S., 1993, in "Galactic Bulges", IAU Symp. 153, eds. H. DeJonghe & H.J. Habing (Kluwer Academic Publishers, Dordrecht), 337

[296] Wandel, A., 1999, ApJ 519, L39

[297] Wandel, A., Peterson, B.M., Malkan, M.A., 1999, ApJ 526, 579

[298] Wang, R., Wu, X.B., 2005, ChJAA 5, 299

[299] Warner, C., Hamann, F., Dietrich, M., 2003, ApJ 596, 72

[300] Webster, B.L., 1984, ASAu Proceedings vol. 5, 535

[301] Weidner, C., Kroupa, P., 2004, MNRAS 348, 187

[302] Weidner, C., Kroupa, P., 2005, ApJ 625, 754

[303] Whitford, A.E., 1978, ApJ 226, 777

[304] Wills, B.J., Shang, Z., Yuan, J.M., 2000, NewAR 44, 511

[305] Woosley, S.E., Weaver, T.A., 1995, ApJS 101, 181

[306] Wu, X.B., Han, J.L., 2001, A&A 380, 31

[307] Wyse, R.F.G., 1998, MNRAS 293, 429

[308] Wyse, R.F.G., 1999, Ap&SS 267, 145

[309] Yee, H.K.C., 1983, ApJ 473, 713

[310] Yu, Q., Tremaine, S., 2002, MNRAS 335, 965

[311] Zoccali, M., Barbuy, B., Hill, V., Ortolani, S., Renzini, A., Bica, E., Momany, Y., Pasquini, L., Minniti, D., Rich, R.M. 2004, A&A, 423, 507

[312] Zoccali, M., Cassisi, S., Frogel, J.A., Gould, A., Ortolani, S., Renzini, A., Rich, R.M., Stephens, A.W., 2000, ApJ 530, 418

[313] Zoccali, M., Lecureur, A., Barbuy, B., Hill, V., Renzini, A., Minniti, D., Momany, Y., Gómez, A., Ortolani, S., 2006, A&A 457, L1

[314] Zoccali, M., Renzini, A., Ortolani, S., Greggio, L., Saviane, I., Cassisi, S., Rejkuba, M., Barbuy, B., Rich, R.M., Bica, E., 2003, A&A 399, 931

Acknowledgements

It is not for tradition or whatever else that I begin with my tutor Francesca Matteucci, for being available most of the times, for listening, suggesting, correcting, encouraging me, shedding light here and there, pushing me forward and bringing me back to my way hundreds of times.

Since he is acknowledged in all of my papers, I cannot omit Pipino – a bit pedant at times, but he often helped me handle some physical problems and topics with a certain care. And sorry for waking you up in Oxford. Many thanks to Calura, the silent night host of the Department, for his kindness. Thanks to Cescutti for his availability and – well, nothing else. Thanks to Spito, Saro, Teschio for giving a surreal hue to my afternoons.

Thanks to my precious co-authors: Livia Origlia, Mike Rich, Pavel Kroupa, Andrew McWilliam, Luca Ciotti, Paolo Padovani and Cristina Chiappini. Thanks to Manuela Zoccali, who kindly provided me with unpublished material, private communications and very clear and useful explanations. Thanks to Paolo Ventura and Franca D'Antona, and all the people I happened to meet in Monte Porzio. Thanks to Aurélie, Vanessa Hill and the Meudon people, who critically discussed my bulge model. Thanks to Mathias Dietrich.

Thanks to my parents who support me and tolerate me no matter what I do – it must be tough. Thanks to my family down to the little monsters Salif and Lorenzo. Thanks to Johnny.

Thanks to the SISSA side: to Lucio, to his housemates, and to the all-girls.

Thanks to Grifo for listening to my useless chats, I'm sure that was painful. Thanks to Satyajit, Debarathi and their families for introducing me to their amazing country in the least traumatic way. And for the coconuts. Thanks to Valentina & Andrea.

Thanks to the TNers: everyone who hosted me, everyone I argued with, all those who made me laugh, get angry, and stop to think for a while. Special thanks to the PM, Ka', Moana, Insane, Coldie, Frankie, Chop, Nausy, sFrancy, Bredo, the Naives, Gu^Lk!, Tyreal... I stop here for now.

I am sincerely grateful to all the "Windtalkers", real & virtual: you never learn enough.

And thanks to both my "small" hosts (the cat one and the redneck® one).


LA MIA PUNTATA
C'E' QUALCUNO AL CENTRO DI TUTTO QUESTO?
E SE C'E', CHI E'?
BRAVO STELLO! DICCELO TU!
CONTINUA


CAPITO? CAZZO, PARLARE DI DONNE... E CHI LO FA PIU'?
E NOIA SI SCOPA, NOIA SI SCOPA...
PASSAMI IL FILTRO. AH! LAVA STELLA! CAPITO? E I VECCHI, CIOA SI SCOPA? MACCHI?
IO NO. VECCHIO SCONVOLTO CHE SGNO. MAH!
CAZZO.
OH, IL FILTRO...


PAPERS
PAPERS
PAPEHRS